Creep Buckling of Shells of Revolution Loaded Under Uniform External Pressure

by

Paul Francis Sullivan,
Lieutenant, United States Navy

B.S. United States Naval Academy
(1970)

Submitted In Partial Fulfillment of the
Requirements for the Degree of

Ocean Engineer

at the

Woods Hole Oceanographic Institution

and the

Massachusetts Institute of Technology

and for the degree of

Master of Science in Ocean Engineering

at the

Massachusetts Institute of Technology

January, 1975

Signature of Author.....
Joint Program in Ocean Engineering, Woods Hole Oceanographic Institution - Massachusetts Institute of Technology, and the Department of Ocean Engineering, Massachusetts Institute of Technology, January 1975.

Certified by.....
Thesis Supervisor

.....
Thesis Supervisor

Accepted by.....
Chairman, Joint Committee on Ocean Engineering, Woods Hole Oceanographic Institution - Massachusetts Institute of Technology

Creep Buckling of Shells of Revolution
Loaded Under Uniform External Pressure

by

Paul Francis Sullivan

Submitted to the Department of Ocean Engineering in partial fulfillment of the requirements for the degrees of Ocean Engineer and Master of Science in Ocean Engineering.

Abstract

A theoretical investigation is undertaken into the creep instability of two common shells of revolution, the infinitely long cylinder and the complete sphere. The linear and non-linear visco-elastic material idealizations are used in the various theoretical procedures. The critical buckling time is greatly influenced by the parameter a/h ratio, magnitude of initial imperfections and material selection. The spherical shell has a lifetime longer than the cylindrical shell having the same a/h ratio, initial imperfections and material constants, while the critical mode numbers are the same.

Thesis Supervisor: Norman Jones
Title: Associate Professor of Ocean Engineering at Massachusetts Institute of Technology

Thesis Supervisor: James W. Mavor, Jr.
Title: Mechanical Engineer at Woods Hole Oceanographic Institution

ACKNOWLEDGMENTS

The list of individuals that need to be recognized for their help and support for a large project, such as this thesis, is lengthy.

First, I would like to thank the United States Navy, which gave me the opportunity to pursue a graduate education.

Second, I am in debt to Professor Norman Jones for his continuing advice, instruction and unwavering enthusiasm during the preparation of this thesis.

Third, I am grateful to Mr. James Mavor, who provided me with the initial idea for the project and the much-needed monetary support.

Fourth, a special thanks to a large contingency from Woods Hole Oceanographic Institution whose assistance was essential to the successful completion of this thesis, Dr. A.J. Williams 3rd, Mr. James Sullivan, Mrs. Karen Pires, Mr. Arnold Sharp, Mr. Patrick O'Malley, Mr. Kenneth Doherty, Mr. William Shultz and the entire ALVIN group.

Finally, I wish to express a deep appreciation to my family, Anne, Shane Francis and Irish Morn, for their patience, support, and understanding over these past months.

NOTATION

w	transverse displacement, positive outwards.
u	displacement in η_1 direction.
v	displacement in η_2 direction.
M_1, M_2, M_{21}, M_{12}	moments per unit length as defined in Figure 2.
N_1, N_2, N_{21}, N_{12}	forces per unit length as defined in Figure 2.
$e_{11}, e_{22}, e_{21}, e_{12}$	total strains.
P_1, P_2, P_3	external loads per unit area as defined in Figure 2.
x_1, x_2, x_3	orthogonal coordinates as defined in Figure 1.
Q_1, Q_2	transverse shear forces per unit length as defined in Figure 2.
R_1, R_2	Principle radii of curvature of a shell and radii of curvature of the coordinate curves η_1, η_2.
a	cylindrical shell mean radius.
a^*	out--of-roundness parameter defined by equation (4.19).
h	cylindrical shell mean thickness.
S	arc length.
A, B	defined in equations (2.5 b-c).
Z	distance measured along a normal from the middle surface of a shell.
E	Youngs Modulus of Elasticity.
C, K	material viscous coefficients.
M	creep exponent defined by equation (3.4).
R	spherical shell mean radius
R^*	out--of-roundness parameter of spherical shell.

NOTATION (cont.)

H	spherical shell mean thickness.
A_n	amplification function (cylinder).
t	time.
t_{cr}	critical time.
B_{mn}	amplification function (sphere).
C_n/D_{mn}	maximum initial imperfection; cylinder/sphere.
n	harmonic in circumferential (θ) direction.
m	harmonic in circumpolar (ϕ) direction.
η_1, η_2	lines of principle curvature.
κ_1, κ_2	change of curvature.
κ_{12}	half total change of curvature in twist.
$\overset{*}{\kappa}_1 \overset{*}{\kappa}_2$	principle curvatures $= \frac{1}{R_{1,2}}$.
$\varepsilon_1, \varepsilon_2$	membrane strains.
γ_0	shear strain.
υ	poisson's ratio.
σ^*	effective stress defined in equation (3.5b).
α	$\frac{4}{3}$ Ch or $\frac{4}{3}$ CH.
θ, x	circumferential and axial coordinates in cylindrical shell.
ϕ, θ	circumpolar and circumferential coordinates in spherical shell.
Ω	$\frac{4}{3}$ kh or $\frac{4}{3}$ kH.
ξ	$\frac{Ch^3}{9}$ or $\frac{CH^3}{9}$.
ζ	$\frac{Kh^3}{9}$ or $\frac{KH^3}{9}$.

NOTATION (cont.)

χ	$-a\alpha\dot{\bar{w}}/\xi$ (time constant linear viscous cylinder).
χ	$-a\Omega\dot{\bar{w}}/\zeta$ (time constant non-linear viscous cylinder).
Φ	$-3R\alpha\dot{\bar{w}}/2\xi$ (time constant linear viscous sphere).
Λ	$-3R\Omega\dot{\bar{w}}/2\zeta$ (time constant non-linear viscous sphere).
$\hat{\tau}_c$	χt (non-dimensional time linear viscous cylinder).
τ_c	Xt (non-dimensional time non-linear viscous cylinder).
$\hat{\tau}_s$	Φt (non-dimensional time linear viscous sphere).
τ_s	Λt (non-dimensional time non-linear viscous sphere).
λ_n	$n(n+1)$
∇^2	defined by equation (5.12c).
ψ	σ^*/σ^*_0 .
S_{ij}	stress deviator.
$(\ )_0$	initial value of ( ).
$(\ )_{,i}$	$\frac{\partial(\ )}{\partial i}$.
$(\dot{\ })$	$\frac{\partial(\ )}{\partial t}$.
$(\bar{\ })$	dominant part of ( ).
$(\ )'$	perturbation part of ( ).

TABLE OF CONTENTS

TABLE OF CONTENTS (cont.) Page

TABLE OF CONTENTS (cont.) Page

1. INTRODUCTION

1.1 Preface

The problems of creep deformation and buckling of structural members while often addressed in aerospace and chemical engineering have, until recently, been aphonic design considerations in ocean engineering. The rationale being that the ocean, itself, offers an environment very unaccommodating to creep with its relatively low temperatures. Further, the general use of creep resistive materials for relatively short periods of loading made creep insignificant in the design of ocean shell structures. Recently, the escalating demand man and his society have placed on the ocean in pursuit of its understanding and resources has resulted in a rapid advancement in ocean technology. This new technology has generated an increased interest in the creep of shell structures. This manifestation of interest has been stimulated by many events, the greater use of creep prone materials, aluminum and titanium, the longer duration structures are required to withstand compelling hydrostatic pressures, and the need to predict volumetric changes due to creep of shells which have stringent volumetric design constraints, such as the neutrally buoyant and compressible, free floating, current measuring SOFAR floats of the Woods Hole Oceanographic Institution.

In the past, the ocean engineer was perplexed with a two part dilemma when asked to predict the creep performance of his design, first, find an acceptable analytical model for creep deformation of shells and second, locate accurate material constants for low temperature creep.

The purpose of this paper is to solve the first dilemma of developing a simple analytic technique to predict creep deformation of two common shells of revolution, the cylinder and complete sphere, suitable to oceanic applications and which will be useful in preliminary stages of design and may be adequate for final design. Finally, to discover if creep buckling is a phenomenon that needs to be actively considered in the design of long term ocean shell structures.

1.2 Historical Review

A literary search of the existing literature reveals that few published works have been transcribed which are directly applicable to conditions experienced in the ocean. Most papers deal with columns, plates or cylindrical shells loaded in axial compression. A number of investigators have attempted solutions for the creep behavior of thin cylindrical shells loaded under uniform external pressure. To the best knowledge of this author, no paper has been published dealing with the creep performance of a complete spherical shell loaded under external pressure.

The author's dealing with cylindrical shells use a variety of simplifications, but do have an assemblage of assumptions common to all their analyses. These similar assumptions include:

(a) thin shell assumption, so that the radial stress component is negligible in comparison to the in-plane stress components

(b) only the effect of secondary creep, according to Odquist's law (1937) are considered

(c) buckling is not defined in the bifurcation sense, but rather as a state of progressive accelerated growth rate of the displacement

field, creating unfavorable strain distribution and leading to full structural failure.

(d) initial imperfections of a shell cause eccentricity of loading, thus serving as a lever arm for compressive in-plane forces, which in turn increases the bending moment, which in turn, increases the rate of curvature change

(e) an assumed solution of an infinite trigonometric series, either a complete or partial Fourier series.

Hoff, et al (1959) used a sandwich model, in which the outer skins support membrane and bending stresses and the core supports shear without deformation. The sandwich model avoids complications in the superposition of compressive and bending stresses due to the non-linearity of the creep law. Further, a quasi-elliptical initial imperfection was assumed. Samuelson (1970) developed a numerical solution for non-uniform external loads. Sankaranarayan (1969) generated a solution for creep deformation of cylindrical shells under combined lateral and axial pressures for a material that adheres to the Tresca criterion. Berman, et al (1974) presented a numerical analysis for a cylindrical shell infinitely long, so that, a state of generalized plane strain exists. As did Hoff, Berman assumed that the initial imperfection is quasi-elliptical.

Penny and Marriott (1969) have carried out the only known, but rather special analysis of creep deformation of a spherical shell. They explored snap through of a spherical boss point loaded.

All analyses emphasize the fact that initial imperfections play a most important role in creep buckling. That, buckling stems

from the accelerated growth of these initial imperfections in an otherwise uniform initial displacement field.

1.3 Method of Analysis

The conviction that creep buckling stems from the growth of small imperfections in the otherwise uniform initial displacement field suggests the use of a perturbation method of solution as first developed by Abrahamson and Goodier (1962) for dynamic plastic problems. The method assumes an axisymmetric dominant solution in which buckling does not occur and a perturbation solution in which the influence of bending is significantly greater than the in-plane forces thereby giving rise to inextensible buckling.

Due to the axisymmetry of the dominant displacement field of the shell of revolution, only the transverse displacement field consists of a dominant and perturbation part, while the in-plane displacements have only a perturbation part so that

$$w(\eta_1, \eta_2, t) = \bar{w}(t) + w'(\eta_1, \eta_2, t) \tag{1.1a}$$

$$u(\eta_1, \eta_2, t) = u'(\eta_1, \eta_2, t) \tag{1.1b}$$

and

$$v(\eta_1, \eta_2, t) = v'(\eta_1, \eta_2, t) \tag{1.1c}$$

respectively, with perturbation parts delineated by primes and dominant parts by bars.

In turn, to remain consistent, the shear strain and twisting curvature change have only perturbation parts while the membrane strains and bending curvature changes have both dominant and perturbation parts.

Similarly, the shear forces and twisting moments have just perturbation parts while normal forces and bending moments have both dominant and perturbation parts

$$N_1(\eta_1, \eta_2, t) = \bar{N}_1(t) + N'_1(\eta_1, \eta_2, t) \tag{1.2a}$$

$$N_2(\eta_1, \eta_2, t) = \bar{N}_2(t) + N'_2(\eta_1, \eta_2, t) \tag{1.2b}$$

$$N_{12}(\eta_1, \eta_2, t) = N''_{12}(\eta_1, \eta_2, t) = N_{21}(\eta_1, \eta_2, t) \tag{1.2c}$$

$$M_1(\eta_1, \eta_2, t) = \bar{M}_1(t) + M'_1(\eta_1, \eta_2, t) \tag{1.2d}$$

$$M_2(\eta_1, \eta_2, t) = \bar{M}_2(t) + M'_2(\eta_1, \eta_2, t) \tag{1.2e}$$

and

$$M_{12}(\eta_1, \eta_2, t) = M''_{12}(\eta_1, \eta_2, t) = -M_{21}(\eta_1, \eta_2, t) \tag{1.2f}$$

The material comprising the shell is isotropic, incompressible and homogeneous. The initial elastic response is considered to be infinitesimal. No initial shape of imperfections is inferred. Further, the assemblage of assumptions common to past analysis, (a) - (e) on page 11 is assumed.

The analysis will present non-linear equilibrium, strain-curvature relations and constitutive equations for linear and non-linear visco-elastic materials for an arbitrary shaped shell. The reduction of these relations will be carried out for the infinite cylinder and the complete sphere.

2. BASIC RELATIONS FOR THIN SHELLS

2.1 Introduction

The succeeding relations were developed by Walters and Jones (1972). They were derived with the aid of differential geometry as discussed in Kraus (1967) and are valid for any thin arbitrary shell which has lines of principle curvature aligned with the parametric lines.

2.2 Shell Coordinates - Differential Geometry

The coordinates of point P on the middle surface of a shell, the reference surface, are defined in Figure 1. $\bar{r}$ is the position vector which is a function of parametric lines η_1, η_2. $\hat{n}$ is the unit normal vector. The position vector can be expressed as

$$\bar{r} = x_1 \hat{i} + x_2 \hat{j} + x_3 \hat{k} \tag{2.1}$$

where $\hat{i}$, $\hat{j}$, and $\hat{k}$ are the unit vectors in the x_1, x_2, x_3 directions, respectively.

As demonstrated in Kraus (1967), the magnitude of the principle curvatures are the roots of the following quadratic equation

$$H^2\kappa^2 - (EN-2MF-GL)\kappa + (LN-M^2) = 0 \tag{2.2}$$

where

$$E = \bar{r}_{,1} \cdot \bar{r}_{,1} \tag{2.3a}$$

$$F = \bar{r}_{,1}\ \bar{r}_{,2} \tag{2.3b}$$

(equal to zero when η_1 is orthogonal to η_2)

$$G = \bar{r}_{,2} \cdot \bar{r}_{,2} \tag{2.3c}$$

$$H = (EG-F^2)^{\frac{1}{2}} \tag{2.3d}$$

$$L = \hat{n} \cdot \bar{r}_{,11} \tag{2.3e}$$

$$M = \hat{n} \cdot \bar{r}_{,12} \tag{2.3f}$$

(equal to zero when η_1 and η_2 coincide with the lines of curvature)

$$N = \hat{n} \cdot r_{,22} \tag{2.3g}$$

with

$$\hat{n} = \frac{\bar{r}_{,1} X \bar{r}_{,12}}{H} \tag{2.4}$$

Equations 5(a-d) are referred to as the first fundamental magnitudes while equations 5(e-g) are called the second fundamental magnitudes.

If η_1 and η_2 are orthogonal, then F equals zero, the elemental area can be expressed as

$$ds^2 = A^2 d^2\eta_1 + B^2 d^2\eta_1 \tag{2.5a}$$

where

$$A = (E)^{\frac{1}{2}} \tag{2.5b}$$

and

$$B = (G)^{\frac{1}{2}} \tag{2.5c}$$

2.3 Strain-Curvature Relations

A tensor formulation and the usual assumptions of shell theory, (eg. Kraus (1967)) have been employed by Walters and Jones (1972) to show that the strains in the thin shell may be written

$$e_{11} = \varepsilon_1 + z\kappa_1 \tag{2.6a}$$

$$e_{22} = \varepsilon_2 + z\kappa_2 \tag{2.6b}$$

and

$$e_{12} + e_{21} = \gamma_0 + 2z\kappa_{12} \tag{2.6c}$$

where the membrane strains are

$$\varepsilon_1 = \frac{u_{,1}}{A} + \frac{A_{,2}v}{AB} + \frac{w}{R_1} + \frac{(w_{,1})^2}{2A^2} \tag{2.7a}$$

$$\varepsilon_2 = \frac{v_{,2}}{B} + \frac{B_{,1}u}{AB} + \frac{w}{R_2} + \frac{(w_{,2})^2}{2B^2} \tag{2.7b}$$

and

$$\gamma_0 = \frac{A}{B}\left(\frac{u}{A}\right)_{,2} + \frac{B}{A}\left(\frac{v}{B}\right)_{,1} + \frac{w_{,1}w_{,2}}{AB} \tag{2.7c}$$

and the curvature changes are

$$\kappa_1 = \frac{1}{A}\left(\frac{u}{R_1} - \frac{w_{,1}}{A}\right)_{,1} + \frac{A_{,2}}{AB}\left(\frac{v}{R_2} - \frac{w_{,2}}{B}\right) \tag{2.7d}$$

$$\kappa_2 = \frac{1}{B}\left(\frac{v}{R_2} - \frac{w_{,2}}{B}\right) + \frac{B_{,1}}{AB}\left(\frac{u}{R_1} - \frac{w_{,1}}{A}\right) \tag{2.7e}$$

and

$$2\kappa_{12} = \frac{A}{B}\left(\frac{u}{AR_1} - \frac{w_{,1}}{A^2}\right)_{,2} + \frac{B}{A}\left(\frac{v}{BR_2} - \frac{w_{,2}}{B^2}\right)_{,1} \tag{2.7f}$$

Note that γ_0 is the total shear strain while κ_{12} is one-half the total twist curvature change

The Love-Kirchhoff assumption has been invoked in the derivation of these equations.

2.4 Equilibrium Equations

The typical shell differential element illustrated in Figure 2 will have a rate of internal energy dissipation.

$$W_{int} = \int_S \left[N_1 \dot{\varepsilon}_1 + N_2 \dot{\varepsilon}_2 + N_{12} \dot{\gamma}_0 + M_1 \dot{\kappa}_1 + M_2 \dot{\kappa}_2 + 2M_{12} \dot{\kappa}_{12} \right] ds \qquad (2.8)$$

where s is the total undeformed area of the middle surface of the arbitrary thin shell. Now, equating the rate of internal energy dissipation to the rate of external work (i.e., using the principle of virtual velocities), a consistent set of equations of equilibrium is obtained.

$$ABp_1 - N_{2,1} + (N_{12})_{,2} + (N_1)_{,1} + N_{12,2} + \frac{(M_1)_{,1}}{R_1} - \frac{M_{2,1}}{R_1} + \frac{(M_{12})_{,2}}{R_1} + \frac{M_{12,2}}{R_1} = 0 \qquad (2.9a)$$

$$ABp_2 - N_{1,2} + (N_{12})_{,1} + (N_2)_{,2} + N_{12,1} + \frac{(M_2)_{,2}}{R_2} - \frac{M_{1,2}}{R_2} + \frac{(M_{12})_{,1}}{R_2} + \frac{M_{12,1}}{R_2} = 0 \qquad (2.9b)$$

and

$$ABp_3 - \frac{N_1 AB}{R_1} - \frac{N_2 AB}{R_2} + \left(\frac{N_1 Bw_{,1}}{A}\right)_{,1} + \left(\frac{N_2 Aw_{,2}}{B}\right)_{,2} + (N_{12} w_{,2})_{,1} + (N_{12} w_{,1})_{,2} + \left[\frac{(M_1 B)_{,1}}{A}\right]_{,1}$$

$$+\left[\frac{(M_{2}A),_{2}}{B}\right],_{2}+2\left(\frac{M_{12}A,_{2}}{A}\right),_{1}+2\left(\frac{M_{12}B,_{1}}{B}\right),_{2}$$

$$+2M_{12,12}-\left(\frac{M_{1}A,_{2}}{B}\right),_{2}-\left(\frac{M_{2}B,_{1}}{A}\right),_{1}=0 \qquad (2.9c)$$

Inertia terms are disregarded since creep is assumed to be a very protracted deformation process

3. CONSTITUTIVE RELATIONS

3.1 Linear Visco-elastic Material

The appropriate model to simulate secondary creep during the application of a step function load is the Maxwell model illustrated in Figure 3a. The strain at all times is the sum of the elastic strain component, and viscous strain component. The stress in the viscous and elastic elements are always equal. Thus, from the equation of equilibrium the following expression for strain rate is found, (eg., Drucker 1967)

$$\dot{e}=\frac{\dot{\sigma}}{E}+\frac{\sigma}{C} \qquad (3.1)$$

During application of the step function load, the motion of the dashpot is negligible. Hence, the initial strain is the elastic stretch of the spring. As time procedes, the model will continue to creep steadily at the rate of σ/C as shown in Figure 3b.

The relation for the linear Maxwell model can be written in tensor notation as, (eg., Drucker 1967)

$$\dot{e}_{ij}=\frac{1+\nu}{E}\dot{S}_{ij}+\frac{(1-2\nu)}{E}\frac{\dot{\sigma}_{kk}}{3}\delta_{ij}+\frac{3}{2}\frac{S_{ij}}{C} \qquad (3.2a)$$

where

$$\sigma_{\kappa\kappa} = \sigma_{11} + \sigma_{22} + \sigma_{33}$$

$$S_{ij} = \sigma_{ij} - \frac{\sigma_{kk}}{3}\delta_{ij}$$

δ_{ij} = kronecker delta

and E, C are material elastic and viscous constants respectively. Since superposition of hydrostatic stresses is assumed to cause no further straining, equation (3.2a) reduces to

$$\dot{e}_{ij} = \frac{1+\nu}{E}\dot{S}_{ij} + \frac{3}{2}\frac{S_{ij}}{C} \qquad (3.2b)$$

Inverting equation (3.2b) and performing the proper intergration reveals the linear viscous constitutive equations, after the initial elastic response, that is, disregarding the elastic behavior, for a thin shell as

$$N_1 = \alpha(\dot{\varepsilon}_1 + \frac{1}{2}\dot{\varepsilon}_2) \qquad (3.3a)$$

$$N_2 = \alpha(\dot{\varepsilon}_2 + \frac{1}{2}\dot{\varepsilon}_1) \qquad (3.3b)$$

$$N_{12} = N_{21} = \frac{\alpha}{3}\dot{\gamma}_0 \qquad (3.3c)$$

$$M_1 = \xi(\dot{\kappa}_1 + \frac{1}{2}\dot{\kappa}_2) \qquad (3.3d)$$

$$M_2 = \xi(\dot{\kappa}_2 + \frac{1}{2}\dot{\kappa}_1) \qquad (3.3e)$$

and

$$M_{12} = -M_{21} = \xi\dot{\kappa}_{12} \qquad (3.3f)$$

where

$$\alpha = \frac{4}{3}Ch$$

and

$$\xi = \frac{Ch^3}{9}$$

3.2 Non-Linear Visco-Elastic Material

Secondary creep for the non-linear visco-elastic material can be, as in the linear case, represented by a Maxwell model where

$$\dot{e} = \frac{\dot{\sigma}}{E} + \left(\frac{\sigma}{K}\right)^M \tag{3.4}$$

This model does not simulate primary creep and has a poor response to variable stress conditions.

Assuming that the creep strains are dependent on loading history, the Prandtl-Reuss Incremental relations can be used for the non-elastic part

$$de_{ij} = \frac{3}{2}\frac{de^*}{\sigma^*}S_{ij} \tag{3.5a}$$

where

σ^* and e^* are effective stress and strain based on Von Mises criterion

where

$$\sigma^* = \frac{1}{\sqrt{2}}\left[(\sigma_{11}-\sigma_{22})^2 + (\sigma_{22}-\sigma_{33})^2 + (\sigma_{33}-\sigma_{11})^2 + 6(\tau_{12}^2+\tau_{23}^2+\tau_{31}^2)\right]^{\frac{1}{2}} \tag{3.5b}$$

$$e^* = \frac{1}{\sqrt{2}}\left[(e_{11}-e_{22})^2 + (e_{22}-e_{33})^2 + (e_{33}-e_{11})^2 + 6(\gamma_{12}^2+\gamma_{23}^2+\gamma_{31}^2)\right]^{\frac{1}{2}} \tag{3.5c}$$

Norton's Law for secondary creep under a uniform constant load is expressed as

$$de^* = \frac{\sigma^{*M}}{K}\,dt, \tag{3.6}$$

Hence, one can substitute (3.6) into equation (3.5) and find

$$\dot{e}_{ij} = \frac{3}{2} \frac{\sigma^{*M-1}}{K} S_{ij} \tag{3.7}$$

which is Odquist's Law for secondary creep, (eg., Odquist (1956)).

By assuming that the effective stress remains constant across the shell thickness, equation (3.7) can be inverted and intergrated to yield the non-linear constitutive relations while neglecting the elastic effects (Penney and Mariott 1971)

$$N_1 = \Omega\sigma^{*(1-M)} (\dot{\varepsilon}_{11} + \frac{1}{2} \dot{\varepsilon}_{22}) \tag{3.8a}$$

$$N_2 = \Omega\sigma^{*(1-M)} (\dot{\varepsilon}_{22} + \frac{1}{2} \dot{\varepsilon}_{11}) \tag{3.8b}$$

$$N_{12} = N_{21} = \frac{\Omega\sigma^{*(1-M)}}{3} \gamma_0 \tag{3.8c}$$

$$M_1 = \zeta\sigma^{*(1-M)} (\dot{\kappa}_{11} + \frac{1}{2} \dot{\kappa}_{22}) \tag{3.8d}$$

$$M_2 = \zeta\sigma^{*(1-M)} (\dot{\kappa}_{22} + \frac{1}{2} \dot{\kappa}_{11}) \tag{3.8e}$$

$$M_{12} = -M_{21} = \zeta\sigma^{*(1-M)} \dot{\kappa}_{12} \tag{3.8f}$$

where

$$\Omega = \frac{4}{3} Kh$$

$$\zeta = \frac{Kh^3}{9}$$

Note, that if M equals one, the linear case, these constitutive relations reduce to the linear relations, equation (3.3).

4. INFINITELY LONG CYLINDRICAL SHELL

4.1 Introduction

The objective of the following section is to reduce the general equations for an arbitrary shaped shell to the particular case of an infinitely long, thin cylinder. The perturbation solution for transverse deflection is assumed to be a Fourier cosine series

$$w' = \sum_{n=0}^{\infty} A_n(t)\cos n\theta \tag{4.1}$$

4.2 Basic Cylindrical Shell Equations

4.2.1 Differential Geometry

Defining x as η_1 and θ as η_2, as illustrated in Figure 4, the position vector equals

$$\bar{r} = x\hat{i} + a\sin\theta\hat{j} + a\cos\theta\hat{k} \quad . \tag{4.2a}$$

The principle curvature magnitudes are

$$\overset{*}{\kappa}_x = 0 \tag{4.2b}$$

and

$$\overset{*}{\kappa}_\theta = 1/a \tag{4.2c}$$

and the differential area is

$$ds^2 = dx^2 + a^2 d\theta^2 \tag{4.2d}$$

where,

$$A = 1$$

and

$$B = a$$

4.2.2 Strain Curvature Relations

Equations (2.7 a-f) reduce to

$$\varepsilon_x = u_{,x} + \frac{1}{2} w_{,x}^2 \tag{4.3a}$$

$$\varepsilon_\theta = \frac{1}{a} (v_{,\theta} + w + \frac{w_{,\theta}^2}{2a}) \tag{4.3b}$$

$$\gamma_0 = \frac{u_{,\theta}}{a} + v_{,x} + \frac{w_{,x} w_{,\theta}}{a} \tag{4.3c}$$

$$\kappa_x = -w_{,xx} \tag{4.3d}$$

$$\kappa_\theta = \frac{1}{a^2} (v_{,\theta} - w_{,\theta\theta}) \tag{4.3e}$$

and

$$2\kappa_{x\theta} = \frac{1}{a} (v_{,x} - 2w_{,x\theta}) \tag{4.3f}$$

The time derivatives of (4.3a-f) are

$$\dot{\varepsilon}_x = \dot{u}_{,x} + w_{,x} \dot{w}_{,x} \tag{4.4a}$$

$$\dot{\varepsilon}_\theta = \frac{1}{a} (\dot{v}_{,\theta} + \dot{w} + \frac{1}{a} w_{,\theta} \dot{w}_{,\theta}) \tag{4.4b}$$

$$\dot{\gamma}_0 = \frac{1}{a} \dot{u}_{,\theta} + \dot{v}_{,x} + \frac{1}{a} (\dot{w}_{,x} w_{,\theta} + \dot{w}_{,\theta} w_{,x}) \tag{4.4c}$$

$$\dot{\kappa}_x = -\dot{w}_{,xx} \tag{4.4d}$$

$$\dot{\kappa}_\theta = \frac{1}{a^2} (\dot{v}_{,\theta} - \dot{w}_{,\theta\theta}) \tag{4.4e}$$

and

$$2\dot{\kappa}_{x\theta} = \frac{1}{a} (\dot{v}_{,x} - 2\dot{w}_{,\theta x}) \tag{4.4f}$$

4.2.3 Equilibrium Equations

Equations (2.9 a-c) yield in-plane equations

$$ap_x + N_{x\theta,\theta} + aN_{x,x} = 0 \tag{4.5a}$$

and

$$ap_\theta + aN_{x\theta,x} + N_{\theta,\theta} + \frac{1}{a} M_{\theta,\theta} + M_{x\theta,x} = 0 \qquad (4.5b)$$

and transverse equation

$$ap_z - N_\theta + a(N_x w_{,xx} + N_{x,x} w_{,x})$$

$$+ \frac{1}{a}(N_\theta w_{,\theta\theta} + N_{\theta,\theta} w_{,\theta}) + 2N_{x\theta} w_{,x\theta}$$

$$+ N_{x\theta,x} w_{,\theta} + N_{x\theta,\theta} w_{,x} + aM_{x,xx}$$

$$+ \frac{M_{\theta,\theta\theta}}{a} + 2M_{x\theta,x\theta} = 0 \qquad (4.5c)$$

4.3 Buckling Solution

For the axisymmetric loading of an infinitely long cylinder, the following assumptions are stipulated:

(1) loading is axisymmetric, thus the dominant solution has no θ dependence and $p_\theta = p_x = 0$

(2) plane strain conditions exist, $N_x = \frac{N_\theta}{2}$

(3) transverse displacement, forces and moments do not vary significantly with the longitudinal, x, direction, hence both the dominant and perturbation solutions are independent of x.

The equilibrium equations simplify to dominant equation of

$$p_z - \frac{\overline{N_\theta}}{a} = 0 \qquad (4.6a)$$

and perturbation equation of

$$\overline{N}_\theta w'_{,\theta\theta} + M'_{\theta,\theta\theta} = 0 \qquad (4.6b)$$

The dominant rates of membrane strains are

$$\dot{\overline{\varepsilon}}_x = 0 \qquad (4.7a)$$

$$\dot{\varepsilon}_\theta = \frac{\dot{w}}{a} \tag{4.7b}$$

and

$$\dot{\gamma}_0 = 0 \tag{4.7c}$$

and the rate of curvature change become

$$\dot{\kappa}_x = 0 \qquad \dot{\kappa}_\theta = 0 \qquad \dot{\kappa}_{x\theta} = 0$$

Assuming inextensible buckling the perturbation membrane strains are zero and the curvature changes are simplified to

$$\dot{\kappa}'_x = 0 \tag{4.7d}$$

$$\dot{\kappa}'_\theta = -\frac{1}{a^2}(\dot{w}' - \dot{w}'_{,\theta\theta}) \tag{4.7e}$$

$$\dot{\kappa}'_{x\theta} = 0 \tag{4.7f}$$

4.3.1 Linear Visco-Elastic Case

Substituting the constitutive relations (3.3 a-f) into (4.6a) reveals a dominant transverse displacement rate of

$$\dot{w} = \frac{a^2 p_z}{\alpha} \tag{4.8}$$

The perturbation solution (4.6b), with the assumption of inextensible buckling ($\varepsilon'_x = \varepsilon'_\theta = \varepsilon'_{x\theta} = 0$), becomes

$$\dot{\alpha}ww'_{,\theta\theta} - \xi/a(\dot{w}'_{,\theta\theta} + \dot{w}'_{,\theta\theta\theta\theta}) = 0 \tag{4.9}$$

Substituting the assumed solution for w', (4.1), into equation (4.9) yields a first order, ordinary differential equation of constant coefficients.

$$\chi A_n + (n^2-1)\dot{A}_n = 0 \tag{4.10a}$$

where

A_n = amplification function

$$\chi = \frac{-a\alpha\dot{\bar{w}}}{\xi} \quad . \tag{4.10b}$$

Thus:

$$A_n = C_n \exp\left(\frac{\chi t}{(n^2-1)}\right) \tag{4.11}$$

where

C_n = an arbitrary constant dependent on the initial imperfections.

Defining

$$\hat{\tau}_c = \chi t$$

one can plot A_n/C_n versus $\hat{\tau}_c$ to discover the critical mode (n_{crit}). Figure 5 reveals that the elliptical mode, n equal to 2, is the critical mode. The growth of the critical amplification function is displayed in Figure 6.

4.3.2 Non-Linear Visco-Elastic Case

Combining the equilibrium equation (4.6 a-b) and the non-linear constitutive equations (3.8 a-f) generates a dominant transverse displacement rate of

$$\dot{\bar{w}} = \frac{a^2 p_z \sigma^{*(M-1)}}{\Omega} \tag{4.12}$$

The perturbation equation is transformed to

$$\dot{\bar{\Omega}}\bar{w}w'_{,\theta\theta} - \zeta/a(\dot{w}'_{,\theta\theta} + \dot{w}'_{,\theta\theta\theta\theta}) = 0 \tag{4.13}$$

Note, if creep exponent M equals one, equation (4.13) reduces to the linear equation (4.8).

Substituting the assumed solution for w', equation (4.1), into equation (4.13) yields a first order ordinary differential equation of

constant coefficients.

$$XA_n + (n^2+1)\dot{A}_n = 0 \tag{4.14a}$$

where

A_n = amplification function

and

$$X = \frac{-a\Omega\dot{\bar{w}}}{\zeta} \tag{4.14b}$$

hence

$$A_n = C_n \exp\left(\frac{\tau_c}{(n^2-1)}\right) \tag{4.15}$$

where C_n is an arbitrary constant dependent on initial imperfections and

$$\tau_c = Xt \quad .$$

As in the linear case, the elliptical mode is critical.

In the formulation of the analysis, it was assumed that the effective stress remained constant, however, as the perturbation solution of transverse displacement grows, the effective stress increases. To overcome this problem one can divide the deformation process into a finite number of time segments in which the effective stress is considered constant. This operation generates a piecewise approximation of the transverse deflection.

Plane strain conditions allows the effective stress to be expressed as

$$\sigma^* = 0.866\ (\bar{\sigma}_\theta + \sigma'_\theta) \tag{4.16}$$

where

$$\bar{\sigma}_\theta = \frac{p_z a}{h} \qquad (4.17a)$$

$$\sigma'_\theta = \frac{4}{3} K \sigma^{*(1-M)} (\dot{e}'_\theta)$$

which reduces to

$$\sigma'_\theta = 2 \frac{Kh}{a^2} \sigma^{*(1-M)} \dot{w}' \quad . \qquad (4.17b)$$

Defining

$$\psi = \frac{\sigma^*}{\sigma^*_0}$$

the perturbation solution becomes

$$w' = C_n \exp\left(\frac{\tau_c}{3} \psi^{(M-1)}\right) \cos 2\theta \qquad (4.18a)$$

and

$$\dot{w}' = \frac{\psi^{(M-1)}}{3} \frac{\tau_c}{t} w' \quad . \qquad (4.18b)$$

The effective stress becomes

$$\sigma^* = .866 \frac{p_z a}{h} \left(1 + 6\psi^{(M-1)} \left(\frac{a}{h}\right) a^* \exp\left(\frac{\tau_c}{3} \psi^{(M-1)}\right)\right) \qquad (4.19)$$

where

$a^* = C_n/a$ (initial out of roundness parameter $<< 1$).

The initial effective stress is

$$\tau_c = X_0 t$$

X_0 = initial value of X

$$\sigma^*_0 = .866 \frac{p_z a}{h} \left(1 + 6 \left(\frac{a}{h}\right) a^*\right) \qquad (4.20)$$

The duration of the time segment is dictated by the growth of effective stress. When the effective stress increases by a given percent, i.e. ten percent ($\psi = 1.1$), a new time segment using the new value of σ^* is initiated.

As an example, taking (a/h) equal to 10 and a^* equal to .005, the amplification function's accelerated growth causes buckling at τ_c equal to 2.59, as graphically portrayed in Figure 7. Inspection of Figure 7 shows that the amplification function growth is very slow. It is only over the final 10 percent of the total lifetime that the amplification function becomes substantial, indicating catastrophic buckling.

5. COMPLETE SPHERICAL SHELL

5.1 Introduction

The succeeding chapter presents the creep response for the complete spherical shell. The perturbation solution for transverse deflection is assumed to be

$$w' = \sum_{n=0}^{\infty} \left(B_{on}(t) P_n(\cos\phi) + \sum_{m=1}^{n} B_{mn}(t) P_n^m(\cos\phi) \cos m\theta \right) \tag{5.1}$$

where P_n and P_n^m are Legendre and associated Legendre polynomials of degree n and order m.

5.2 Basic Spherical Shell Equations

5.2.1 Differential Geometry

Stipulating ϕ as η_1 and θ as η_2, as exhibited in Figure 8, defines the position vector equal to

$$\bar{r} = R(\sin\phi \cos\theta \hat{i} + \cos\phi \sin\theta \hat{j} - \sin\phi \hat{k}), \tag{5.2a}$$

the principle curvature magnatudes equal to

$$\overset{*}{\kappa}_{\phi} = \frac{1}{R} \tag{5.2b}$$

and

$$\overset{*}{\kappa}_{\theta} = \frac{1}{R} , \tag{5.2c}$$

and the differential area equal to

$$ds^2 = R^2 d\phi^2 + R^2 \sin^2\phi d\theta^2 \tag{5.2d}$$

where,

$$A = R$$

and

$$B = R \sin\phi$$

5.2.2 Strain Curvature Relations

Equations (2.7 a-f) simplify to membrane strains

$$\varepsilon_\phi = \frac{1}{R}\left(u_{,\phi} + w + \frac{(w_{,\phi})^2}{2R}\right) \tag{5.3a}$$

$$\varepsilon_\theta = \frac{1}{R}\left(v_{,\theta}\csc\phi + u\cot\phi + w + \frac{(w_{,\theta})^2}{2R}\csc^2\phi\right) \tag{5.3b}$$

and

$$\gamma_0 = \frac{1}{R}\left(u_{,\theta}\csc\phi + v_{,\phi} - v\cot\phi + \frac{w_{,\phi}w_{,\theta}}{R}\csc^2\phi\right) \tag{5.3c}$$

and curvature changes

$$\kappa_\phi = \frac{1}{R^2}(u_{,\phi} - w_{,\phi\phi}) \tag{5.3d}$$

$$\kappa_\theta = \frac{\csc\phi}{R^2}(v_{,\theta} - w_{,\theta\theta}\csc\phi) + \frac{\cot\phi}{R^2}(u - w_{,\phi}) \tag{5.3e}$$

and

$$2\kappa_{\phi\theta} = \frac{\csc\phi}{R^2}(u_{,\theta} - w_{,\phi\theta}) + \frac{1}{R^2}(v_{,\phi} - v\cot\phi - w_{,\theta\phi}\csc\phi + 2w_{,\theta}\csc\phi\cot\phi). \tag{5.3f}$$

The time derivatives of (5.3 a-f) are

$$\dot{\varepsilon}_\phi = \frac{1}{R}(\dot{u}_{,\phi} + \dot{w} + \frac{1}{R}w_{,\phi}\dot{w}_{,\phi}) \tag{5.4a}$$

$$\dot{\varepsilon}_\theta = \frac{1}{R}(\dot{v}_{,\theta}\csc\phi + \dot{u}\cot\phi + \dot{w} + \frac{\csc^2\phi}{R}w_{,\theta}\dot{w}_{,\theta}) \tag{5.4b}$$

$$\dot{\gamma}_0 = \frac{1}{R}\left(\csc\phi\,\dot{u}_{,\theta} - \dot{v}_{,\phi} + \dot{v}\cot\phi + \frac{\csc^2\phi}{R}(\dot{w}_{,\phi}w_{,\theta} + w_{,\phi}\dot{w}_{,\theta})\right) \tag{5.4c}$$

$$\dot{\kappa}_{\phi} = \frac{1}{R^2}\,(\dot{u}_{,\phi} - \dot{w}_{,\phi\phi}) \tag{5.4d}$$

$$\dot{\kappa}_{\theta} = \frac{\csc\phi}{R^2}\,(\dot{v}_{,\theta} - \dot{w}_{,\theta\theta}\csc\phi) + \frac{\cot\phi}{R^2}\,(\dot{u}-\dot{w}_{,\phi}) \tag{5.4e}$$

and

$$2\dot{\kappa}_{\phi\theta} = \frac{\csc\phi}{R^2}\,(\dot{u}_{,\phi} - \dot{w}_{,\phi\phi}) + \frac{1}{R^2}\,(\dot{v}_{,\phi} - \dot{v}\cot\phi$$

$$- \dot{w}_{,\phi\theta}\csc\phi + 2\dot{w}_{,\theta}\csc\phi\cot\phi) \tag{5.4f}$$

5.2.3 Equilibrium Equations

Equations (2.9 a-c) simplify into in-plane equations

$$Rp_{\phi} - N_{\theta}\cot\phi + N_{\phi\theta,\theta}\csc\phi + N_{\phi,\phi} + N_{\phi}\cot\phi$$

$$+ \frac{1}{R}\,(M_{\phi,\phi} + M_{\phi}\cot\phi - M_{\theta}\cot\phi + M_{\phi\theta,\theta}\csc\phi) = 0 \tag{5.5a}$$

$$Rp_{\theta} + N_{\phi\theta,\phi} + 2\cot\phi N_{\phi\theta} + \csc\phi N_{\theta,\theta}$$

$$+ \frac{1}{R}\,(\csc\phi M_{\theta,\theta} + M_{\phi\theta,\phi} + 2M_{\phi\theta}\cot\phi) = 0 \tag{5.5b}$$

and transverse equation

$$R^2 p_z + N_{\phi}(w_{,\phi}\cot\phi + w_{,\phi\phi}) + N_{\theta}w_{,\theta\theta}\csc^2\phi$$

$$- R(N_{\phi} + N_{\theta}) + 2\csc\phi N_{\phi\theta}w_{,\theta\phi} + N_{\phi,\phi}w_{,\phi}$$

$$+ \csc^2\phi N_{\theta,\theta}w_{,\theta} + \csc\phi(N_{\phi\theta,\phi}w_{,\theta} + N_{\phi\theta,\theta}w_{,\phi})$$

$$+ M_{\phi,\phi\phi} + 2\cot\phi M_{\phi,\phi} - M_{\phi} + \csc^2\phi M_{\theta,\theta\theta}$$

$$+ 2M_{\phi\theta,\theta}\cot\phi\csc\phi + 2M_{\phi\theta,\phi\theta}\csc\phi - M_{\theta,\phi}\cot\phi$$

$$+ M_{\theta} = 0 \tag{5.5c}$$

5.3 Buckling Solution

In the analysis of the complete sphere, it is assumed the dominant solution has point symmetry, loaded in a uniform pressure field. As a consequence, there is no dominant θ or ϕ dependence, $p\theta = p\phi = 0$, $\bar{M}_{,\phi\theta} = 0$, $\bar{M}_{\phi} = \bar{M}_{\theta}$, and $\bar{N}_{\theta} = \bar{N}_{\phi}$. The dominant transverse equilibrium equation simplifies to

$$Rp_z - 2\bar{N}_{\phi} = 0 \qquad (5.6a)$$

The in-plane perturbation equilibrium equations reduce to

$$M'_{\phi,\phi} + \cot\phi M'_{\phi} - \cot\phi M'_{\theta} + \csc\phi M'_{\phi\theta,\theta} = 0 \qquad (5.6b)$$

and

$$\csc\phi M'_{\theta,\theta} + M_{\phi\theta,\phi} + 2\cot\phi M'_{\phi\theta} = 0 \qquad (5.6c)$$

The transverse perturbation equilibrium equation becomes

$$\bar{N}_{\phi}(w'_{,\phi\phi} + \cot\phi w'_{,\phi} + \csc^2\phi w'_{,\theta\theta}) + M_{\phi,\phi\phi}$$

$$+ 2\cot\phi M'_{\phi,\phi} - M'_{\phi} + \csc^2\phi M'_{\theta,\theta\theta} + 2\cot\phi\csc\phi M'_{\phi\theta,\theta}$$

$$+ 2\csc\phi M'_{\phi\theta,\phi\theta} - \cot\phi M'_{\theta,\phi} + M'_{\theta} = 0 \qquad (5.6d)$$

The dominant rates of membrane strains and curvatures changes are

$$\dot{\bar{\varepsilon}}_{\phi} = \dot{\bar{\varepsilon}}_{\theta} = \frac{\dot{\bar{W}}}{R} \quad , \quad \dot{\bar{\varepsilon}}_{\phi\theta} = 0 \qquad (5.7a\text{-}c)$$

and

$$\dot{\bar{\kappa}}_{\phi} = \dot{\bar{\kappa}}_{\theta} = 0 \quad , \quad \dot{\bar{\kappa}}_{\phi\theta} = 0 \qquad (5.7d\text{-}f)$$

Assuming inextensible buckling the perturbation rates of membrane strains are zero and the rates of curvature changes can be expressed as

$$\dot{\kappa}'_{\phi} = -\frac{1}{R^2}\left(\dot{w}' + \dot{w}'_{,\phi\phi}\right) \tag{5.8a}$$

$$\dot{\kappa}'_{\theta} = -\frac{1}{R^2}\left(\dot{w}' + \csc^2\phi\dot{w}'_{,\theta\theta} + \cot\phi\dot{w}'_{,\phi}\right) \tag{5.8b}$$

and

$$2\dot{\kappa}'_{\phi\theta} = \frac{2}{R^2}\left(\csc\phi\cot\phi\dot{w}'_{,\theta} - \csc\phi\dot{w}'_{,\phi\theta}\right) \tag{5.8c}$$

If one examines the perturbation expressions derived for curvature changes when inextensible buckling is assumed (equations 5.8a - 5.8c), one discovers that they are identical to the curvature change expressions derived by Jones and Ahn (1974). By comparing the formulation of the transverse equilibrium equations of Walters and Jones and Ahn, it is found that Walters and Jones assumed the $\frac{W}{R^2}$ term to be negligible in the curvature change expressions, while Jones and Ahn include it. The curvature change expressions are assumed to be a function of u, v, and w by Walters and Jones, while Jones and Ahn assume curvature change expressions are just a function of w. If, however, inextensible buckling is assumed, one can express the in-plane displacements, u and v as functions of the transverse displacement w only, and arrive at the expressions derived by Jones and Ahn. Thus, it is reasonable to assume that the transverse equilibrium equation of Walters and Jones must be modified by inclusion of the term

$$AB\left(\frac{M_2}{R_2{}^2} + \frac{M_1}{R_1{}^2}\right) \tag{5.9}$$

which is generated by the $\frac{w}{R^2}$ term.

Hence, the modified transverse perturbation equation becomes

$$\bar{N}_{\phi}\left(w'_{,\phi\phi} + \cot\phi w'_{,\phi} + \csc^2\phi w'_{,\theta\theta}\right) + M_{\phi,\phi\phi}$$

$$+ 2\cot\phi M'_{\phi,\phi} + 2M'_{\theta} + \csc^2\phi M'_{\theta,\theta\theta}$$

$$+ 2\cot\phi\csc\phi M'_{\phi\theta,\theta} + 2\csc\phi M'_{\phi\theta,\phi\theta} - \cot\phi M'_{\theta,\phi} = 0 \qquad (5.10a)$$

The in-plane perturbation equations, (5.6 b-c) are rewritten in terms of w as

$$\frac{3}{2}\dot{w}'_{,\phi} + w'_{,\phi\phi\phi} - \frac{5}{2}\csc^2\phi\cot\phi\dot{w}'_{,\theta\theta} + \frac{5}{2}\csc^2\phi\dot{w}'_{,\phi\theta\theta} = 0 \qquad (5.10b)$$

and

$$\cot\phi\dot{w}'_{,\phi\theta} + (\frac{5}{2} - 4\cot^2\phi)\bar{w}_{,\theta}$$

$$+ \csc^2\phi\dot{w}'_{,\theta\theta\theta} + \frac{5}{2}\csc\phi\cot\phi w_{,\theta\phi\phi} = 0 \qquad (5.10c)$$

To remain consistent, the preceding alteration is only valid if equations (5.10 b-c) are either equal to zero or nearly zero. The equations can be nearly zero since the transverse equation (5.10a) is considered the more dominant equation.

5.3.1 Linear Visco-elastic Case

The dominant transverse displacement rate is achieved by substituting the linear constitutive equation (3.3a) into the equilibrium equation (5.6a)

$$\dot{\bar{w}} = \frac{a^2 p_{\pi}}{3\alpha} \qquad (5.11)$$

Utilizing the following Legendre identities

$$Pn_{,\phi\phi} + \cot\phi Pn_{,\phi} + (\csc^2\phi + \lambda n)Pn = 0 \qquad (5.12a)$$

and

$$P^m n_{,\phi\phi} + \cot\phi P^m n_{,\phi} + (m^2\csc^2\phi + \lambda n)P^m n = 0 \qquad (5.12b)$$

where

$$\lambda n = n(n + 1)$$

The perturbation equation (5.10a) can be recast to

$$\Phi\nabla^2\dot{w}' - (\nabla^2 + \frac{3}{2})(\nabla^2 + 2)\dot{w}' = 0 \qquad (5.13a)$$

where

$$\nabla^2(\ ) = (\ )_{,\phi\phi} + \cot\phi(\ )_{,\phi} + \csc^2(\ )_{,\theta\theta} \qquad (5.13b)$$

and

$$\Phi = -\frac{3a\alpha\dot{\bar{w}}}{2\xi}$$

Substituting the assumed solution for the perturbation transverse displacement (5.1) uncouples the amplification function in the form of ordinary differential equations of constant coefficients

$$\Phi\lambda nB_{0n} + (\frac{3}{2} - \lambda n)(2 - \lambda n)\dot{B}_{0n} = 0 \qquad (5.14a)$$

$$\Phi\lambda nB_{mn} + (\frac{3}{2} - \lambda n)(2 - \lambda n)\dot{B}_{mn} = 0 \qquad (5.14b)$$

Equation (5.14b) is identical to equation (5.14a) if m is understood to include the case m equals zero.

Thus, providing p_z is constant

$$B_{mn} = D_{mn} \exp\left\{\frac{\Phi\lambda nt}{(\frac{3}{2} - \lambda n)(2 - \lambda n)}\right\} \qquad (5.15)$$

where D_{mn} is an arbitrary constant dependent on initial imperfections.

When $\hat{\tau}_s$ is defined as Φt a non-dimensional plot, Figure 9, can be constructed to exhibit that the critical mode is n equal to two.

If the function

$$\frac{w'}{D_{2m}} = \sum_{m=0}^{2} P^m_2(\cos\phi)\cos m\theta \qquad (5.16)$$

is calculated for a number of points of various ϕ and θ values using computer program A of Appendix (A), the two dimensional contour surface

of Figure 10 is generated. On the contour map, positive values indicate an outward elevation of the mid-surface from the mean radius, and a negative value indicates an inward depression of the mid-surface from the mean radius, due to the perturbation solution. Since the elliptical mode has been proven to be the most critical mode, it will be henceforth assumed that the initial imperfections are of the elliptical shape.

5.3.2 Non-linear Visco-elastic Case

Substituting the constitutive equation (3.8a) into (5.6a) produces a dominant transverse displacement rate of

$$\dot{\bar{w}} = \frac{a^2 p_z \sigma^{*(M-1)}}{3\Omega} \tag{5.17}$$

In a method similar to the linear case (eqn. 5.12a), the perturbation transverse equilibrium equation is transformed to

$$\Lambda \nabla^2 \dot{w}' - (\nabla^2 + \tfrac{3}{2})(\nabla^2 + 2)\dot{w}' = 0 \tag{5.18a}$$

with

$$\Lambda = -\frac{3}{2}\frac{a\Omega\dot{\bar{w}}}{} \tag{5.18b}$$

When the curvature change equations (5.4 d-f) are combined with constitutive equations (3.8 d-f) and then substituted into equation (5.10).

Using the proper Legendre identities (5.13 a-b), and assumed solution for w' (5.1), the uncoupled expressions for the amplification function become

$$\Lambda\lambda n B_{on} + (\tfrac{3}{2} - \lambda n)(2 - \lambda n)\dot{B}_{on} = 0 \tag{5.19a}$$

and

$$\Lambda\lambda n B_{mn} + (\tfrac{3}{2} - \lambda n)(2 - \lambda n)\dot{B}_{mn} = 0 \tag{5.19b}$$

Thus, providing p_z is constant

$$B_{mn} = D_{mn} \exp\left(\frac{\lambda n \tau_s}{(\frac{3}{2} - \lambda n)(2 - \lambda n)} \right) \tag{5.20}$$

where

D_{mn} is an arbitrary constant dependent on initial imperfections,

and

$$\tau_s = \Lambda t \quad .$$

The critical mode, as in the linear example, is n equal to two.

As with the infinitely long cylinder, the assumption that the effective stress remains constant must be modified. Effective stress is assumed to be piecewise constant. Time is divided into a finite number of segments within which the effective stress is assumed to remain constant. When the effective stress increases by a given percentage, the segment is terminated, and a new segment with an increased value of effective stress is initiated.

From equation (3.5b) the effective stress equals

$$\sigma^* = \frac{1}{\sqrt{2}} \left((\sigma_\phi - \sigma_\theta)^2 + \sigma_\phi^2 + \sigma_\theta^2 + 6\tau_{\phi\theta} \right)^{\frac{1}{2}} \tag{5.21a}$$

where, from equations (1.2 a-f and 3.8 a-f), the stresses are expressed as

$$\sigma_\phi = \bar{\sigma}_\phi + \sigma_\phi' \tag{5.21b}$$

$$\sigma_\theta = \bar{\sigma}_\theta + \sigma_\theta' \tag{5.21c}$$

$$\tau_{\phi\theta} = \tau'_{\phi\theta} \tag{5.21d}$$

From equations (5.7 a-f) and 5.8 a-c) expressions (5.21b - 5.21d) can be expressed as

$$\bar{\sigma}_{\phi} = \bar{\sigma}_{\theta} = \frac{p_z R}{2H} \tag{5.22a}$$

where H is the shell thickness of the sphere,

$$\sigma'_{\phi} = \frac{4}{3} K H \sigma^{*(1-M)} (\dot{\varepsilon}'_{\phi} + \frac{1}{2} \dot{\varepsilon}'_{\theta}) \tag{5.22b}$$

rewritten in terms of w

$$\sigma'_{\phi} = -\frac{2}{3} \frac{KH}{R^2} \sigma^{*(1-M)} (\frac{3}{2} \dot{w}' + \dot{w}'_{,\phi\phi} + \frac{\dot{w}'_{,\phi}}{2} \cot\phi + \frac{\dot{w}'_{,\theta\theta}}{2} \csc^2\phi) \tag{5.22c}$$

which can be further simplified using Legendre identities (5.12 a-b) to

$$\sigma'_{\phi} = \frac{KH}{3R^2} \sigma^{*(1-M)} (3\dot{w}' - \dot{w}'_{,\phi\phi}) \tag{5.22d}$$

and in a similar manner

$$\sigma'_{\theta} = -\frac{KH}{R^2} \sigma^{*(1-M)} (\frac{3}{2} \dot{w}' + \dot{w}_{,\phi} \cot\phi + \dot{w}'_{,\theta\theta} \csc^2\phi + \frac{1}{2} \dot{w}'_{,\phi\phi}) \tag{5.22e}$$

which is simplified to

$$\sigma'_{\theta} = \frac{KH}{3R^2} \sigma^{*(1-M)} (9\dot{w}' + \dot{w}_{,\phi\phi}) \tag{5.22f}$$

Finally the shear stress is written as

$$\tau'_{\phi\theta} = \frac{K}{3} \sigma^{*(1-M)} \dot{\gamma}_{12} \tag{5.22g}$$

which, by substituting equation (5.8c), is

$$\tau'_{\phi\theta} = \frac{2KH\sigma^{*(1-M)}}{3R^2} (\dot{w}'_{,\phi} \csc\phi\cot\phi - \dot{w}'_{,\phi\theta} \csc\phi) \tag{5.22h}$$

Since the perturbated strains depend only on curvature change rates (5.8 a-e), which are all expressed as functions of $\dot{w}'$, it is postulated that the spatial point on the sphere which exhibits the maximum perturbated transverse deflection rate will be the point of maximum strains, thus stresses. To locate the point of maximum curvature rate ($\dot{w}'$) one can utilize a precedure to study maxima and minima of functions of several variables outlined by Hilderbrand (1962).

(a) Evaluate $\dot{w}'_{,\phi}$ and $\dot{w}'_{,\theta}$ and then set equal to zero.

(b) Evaluate $\dot{w}'_{,\phi\phi}$, $\dot{w}'_{,\theta\theta}$ and $\dot{w}'_{,\phi\theta}$

(i) if $\dot{w}'_{,\phi\phi}\dot{w}'_{,\theta\theta} > \dot{w}'^{2}_{,\phi\theta}$, and $\dot{w}'_{,\phi\phi} > 0$, a relative minimum exists.

(ii) if $\dot{w}'_{,\phi\phi}\dot{w}'_{,\theta\theta} > \dot{w}'_{,\phi\theta}$, and $\dot{w}'_{,\phi\phi} < 0$, a relative maximum exists.

From equation (5.1) the critical value of $w'(n = 2)$ is

$$\dot{w}' = \dot{B}_{2m}(t)\left(P_2(\cos\phi) + \cos\theta P^1_2(\cos\phi) + \cos 2\theta P^2_2(\cos\phi)\right) \tag{5.23a}$$

with

$$P_2(\cos\phi) = \frac{1}{2}(3\cos^2\phi + 1) \tag{5.23b}$$

$$P^1_2(\cos\phi) = \sin\phi \frac{dP_2(\cos\phi)}{d(\cos\phi)} = 3\sin\phi\cos\phi \tag{5.23c}$$

$$P^2_2(\cos\phi) = \sin^2\phi \frac{d^2P_2(\cos\phi)}{d(\cos\phi)^2} = 3\sin^2\phi \quad . \tag{5.23d}$$

Thus,

$$\dot{w}',\phi = -3\cos\phi\sin\phi + 3\cos\theta(\cos^2\phi - \sin^2\phi) + 6\cos 2\theta\sin\phi\cos\phi \tag{5.23e}$$

$$\dot{w}'_{,\theta} = -3\sin\theta\sin\phi\cos\phi - 6\sin 2\theta\sin^2\phi \qquad (5.23f)$$

Both of these expressions (5.23 e-f) are zero when ϕ and θ equal $\pi/2$.

Evaluating the second derivatives

$$\dot{w}'_{,\phi\phi} = 3(\sin^2\phi - \cos^2\phi) - 12\cos\theta\sin\phi\cos\phi + 6\cos 2\theta(\cos^2\phi - \sin^2\phi) \qquad (5.23g)$$

$$\dot{w}'_{\theta\theta} = -3\cos\theta\sin\phi\cos\phi - 12\cos 2\theta\sin^2\phi \qquad (5.23h)$$

and

$$\dot{w}'_{,\phi\theta} = +3\sin\theta(\cos^2\phi - \sin^2\phi) - 12\sin 2\theta\cos\phi\sin\phi \qquad (5.23i)$$

at $\phi = \pi/2$ and $\theta = \pi/2$ one finds

$$\dot{w}'_{,\phi\phi} = 9 \qquad (5.24a)$$

$$\dot{w}'_{,\theta\theta} = 12 \qquad (5.24b)$$

$$\dot{w}'_{,\phi\theta} = -3 \qquad (5.24c)$$

Thus, $\dot{w}'_{,\phi\phi}\dot{w}'_{,\theta\theta} > \dot{w}'_{,\phi\theta}$ and a relative minimum exists at ϕ equal to $\pi/2$ and θ equal to $\pi/2$. Noting, however, that the deflections rates herein are of a negative sense ($\dot{B}_{2m}$ is always negative), the point $\phi = \pi/2$, $\theta = \pi/2$ is actually a relative maximum. Further, this conclusion is in agreement with the maximum of the deflection field illustrated in Figure 10, which was calculated numerically.

Substituting values (5.24 a-c) into equations (5.22 d, f, h) yields

$$\sigma'_{\phi} = -\frac{1}{2}\frac{K_H}{R^2}\sigma^{*(1-M)}\dot{B}_{2m}(t) \qquad (5.25a)$$

$$\sigma'_{\theta} = \frac{7}{2}\frac{KH}{R^2}\sigma^{*(1-M)}\dot{B}_{2m}(t) \qquad (5.25b)$$

$$\tau'_{\phi\theta} = 2\frac{KH}{R^2}\sigma^{*(1-M)}\dot{B}_{2m}(t) \qquad (5.25c)$$

From equation (5.15)

$$B'_{2m}(t) = \frac{C_2}{3}\frac{\tau_s}{t}\exp\frac{\tau_s}{3}$$

$$= \frac{3}{2}C_2\left(\frac{R}{H}\right)^3\frac{p_z}{k}\sigma^{*(M-1)}\exp\left(\frac{\tau_s}{3}\right) \qquad (5.25d)$$

the perturbated stresses simplify to

$$\sigma'_{\phi} = -\frac{3}{4}\left(\frac{R}{H}\right)^2 R^*\frac{p_z}{k}\exp\left(\frac{\tau_s}{3}\right) \qquad (5.25e)$$

$$\sigma'_{\theta} = \frac{21}{4}\left(\frac{R}{H}\right)^2 R^*\frac{p_z}{k}\exp\left(\frac{\tau_s}{3}\right) = -7\sigma'_{\phi} \qquad (5.25f)$$

$$\tau'_{\phi\theta} = 3\left(\frac{R}{H}\right)R^*\frac{p_z}{k}\exp\left(\frac{\tau_s}{3}\right) = -4\sigma'_{\phi} \qquad (5.25g)$$

where

$$R^* = \frac{\text{maximum deviation from radius of imperfections}}{\text{radius}}.$$

Hence equation (5.21a) becomes

$$\sigma^* = \frac{1}{\sqrt{2}}\left[(8\sigma'_{\phi})^2 + (\bar{\sigma}_{\phi} + \sigma'_{\phi})^2 + (\bar{\sigma}_{\phi} - 7\sigma'_{\phi})^2 + 6(-4\sigma_{\phi})^2\right]^{\frac{1}{2}} \qquad (5.26a)$$

simplified to

$$\sigma^* = \frac{1}{\sqrt{2}}\left[2\bar{\sigma}_{\phi}^2 - 12\bar{\sigma}_{\phi}\sigma'_{\phi} + 200\sigma'^2_{\phi}\right]^{\frac{1}{2}} . \qquad (5.26b)$$

Substituting expressions (5.22a and 5.25e), the effective stress equals

$$\sigma^* = \frac{1}{\sqrt{2}}\frac{PR}{H}\left[\frac{1}{2} - \frac{9}{2}\left(\frac{R}{H}\right)R^*\exp\left(\frac{\tau_s}{3}\right) + 112.5\left(\frac{R}{H}\right)^2 R^{*2}\exp^2\left(\frac{\tau_s}{3}\right)\right]^{\frac{1}{2}} . \qquad (5.26c)$$

The initial effective stress ($\tau_s = 0$) equals

$$\sigma_0^* = \frac{1}{\sqrt{2}} \frac{PR}{H} \left[\frac{1}{2} - \frac{9}{2} \frac{R}{H} R^* + 112.5 \left(\frac{R}{H}\right)^2 R^{*2} \right]^{\frac{1}{2}} \quad . \quad (5.26d)$$

Defining

$$\psi = \frac{\sigma^*}{\sigma_0} \quad (5.27a)$$

$$\tau_s = \Lambda_0 t \quad (5.27b)$$

and

$$\Lambda_0 = \text{initial value of } \Lambda \text{ (eqn. 5.18b)}$$

the effective stress can be recast as

$$\sigma^* = \frac{P_z R}{\sqrt{2}\, H} \left[\frac{1}{2} - \frac{9}{2} \left(\frac{R}{H}\right) R^* \psi^{M-1} \exp \frac{\tau_s \psi^{M-1}}{3} + 112 \left(\frac{R}{H}\right)^2 R^{*2} \psi^{(M-1)^2} \exp^2 \frac{\tau_s \psi^{M-1}}{3} \right]^{\frac{1}{2}} \quad . \quad (5.27c)$$

As an example, with R/H, R*, M, ψ_0 equal to 10, .005, 3, 1.1 respectively, the growth of the amplification function is as shown in Figure 11. Note that the amplification function stays relatively small until the last ten percent of the lifetime of the sphere. As expected, the time segment duration decreases as time increases.

It should be further noted that the in-plane equilibrium equations (5.10 b & c) are equal to zero at the point of maximum stress and transverse deflection ($\phi = \pi/2$, $\theta = \pi/2$).

6. DISCUSSION

6.1 Infinitely Long Cylinder

6.1.1 Comparison to Past Results

The most convenient basis of comparison of the analysis herein with past investigations is the predicted critical time of creep buckling. The time behavior of the initial imperfection growth is such that it will become large and grow rapidly only for time near to the critical time. As an aid for the reader, Appendix B has been provided to transform the notation of past analyses into the notation used herein.

Hoff et al (1959) predict a critical time of

$$t_{cr} = \frac{\log\left(1 + \frac{9}{2}\Big/\left(\frac{2a^*a}{h}\right)^2\right)}{8\frac{p_z^m}{k}\left(\frac{a}{h}\right)^{(M+2)}} \qquad (6.1)$$

It is at this critical time at which the amplification of the initial imperfections becomes indefinitely large. The herein results have been compared to Hoff in three ways by varying the values of a/h, a*, and M in Figures 12, 13, 14 respectively. The comparison reveals favorable agreement for smaller a/h ratios (a/h < 25) with a* and M equal to .005 and 3 respectively; and small imperfections (a* < .003) with a/h equal to 10 and M equal to 3. For large a/h ratios, the Hoff estimate of buckling time is approximately an order of magnitude greater than the presented analysis. The Hoff solution is less sensitive to larger, gross initial imperfections, predicting a collapse time of five times greater than the herein analysis when gross imperfections are assumed.

The plot of varying creep exponent, M, (Figure 14) shows excellent agreement for M equal to one and seven and an estimate five times less than

Hoff for M equal to three and five. In Figure 14, a* and a/h equal .005 and 10 respectively.

The actual time history of the two amplification curves are nearly identical, as exhibited in Figure 15. The amplification of imperfections remains very small until the last ten percent of the lifetime of the cylinder.

The discrepancy in predicted critical time of the two analyses do not seem too serious in the light of the fact that creep buckling times are of the order of 10^5 hours, so that excellent agreement is observed for the first 10^4 hours.

Berman et al (1974) presented the particular case of stainless steel 304, which has the material properties at $1050^{o}F$ listed in Appendix C. One finds a great overestimation of Berman when compared to both the analyses of Hoff and herein. Berman predicts a buckling time for cylinder of a/h equal to 10 and a* equal to .05 of $1.743 \times 10^{24} p_z^{-5.6789}$, while Hoff predicts $3.6852 \times 10^{20} p_z^{-5.6789}$, and the herein investigation estimates $1.826 \times 10^{20} p_z^{-5.6789}$. Both the Hoff and herein analysis predict a buckling time of approximately four orders of magnitude sooner than Berman. The author feels that the calculated time of Berman is in possible error, since he uses an out-of-roundness ratio of .05, a very gross out-of-roundness for any realistic engineering design. Further Berman fails to update the effective stress with time. The herein analysis does predict a buckling time of $8.3 \times 10^{22} p_z^{-5.6789}$ if a* is .005, (an order of magnitude less) and the effective stress is not updated with increasing time.

The numerical analysis of Samuelson (1970) deals with the creep response of finite length cylinders subject to both non-uniform and uniform loads. Thus, higher harmonics come into an influencial role in the creep process. Further the transverse deflection is dependent on the longitudinal, x, coordinate

$$w' = \sum_{n=0}^{\infty} A_n(t)\cos n\theta \sin \frac{\pi x}{L} \tag{6.2}$$

Samuelson predicts a buckling time of approximately 100 seconds for a cylinder with a/h, L/a equal to 27 and 2 respectively. A similar buckling time is found for the same cylinder by the herein analysis if M equals 3, a nominal a* .002, is assumed and $\frac{K}{p_z^3}$ is assumed to be of the order 10^8. Thus, it is possible to state that the herein analysis predicts a buckling time of the same order of magnitude as Samuelson.

6.1.2 Elastic Response

The elastic response of the cylinder can be obtained by substituting the elastic part of the constitutive relation (3.2a) into the transverse equilibrium equation (4.6a) to yield

$$w_e = \frac{a^2 p_z (1-\upsilon^2)}{Eh} \tag{6.3a}$$

The elastic transverse deflection from Roark (1965) is

$$w_{e_{Roark}} = \frac{a^2 p_z}{Eh}\left(1 - \frac{\upsilon}{2}\right) \tag{6.3b}$$

If Poisson's ratio, υ, equals .3, the ratio of the herein elastic displacement to that of Roark is 1.07.

6.1.3 Parametric Study

Due to the dependence of the time history of the transverse deflection on a multitude of independent variables, radius to thickness ratio (a/h), out-of-roundness ratio (a*), material constants (M, K) and loading (p_z); an indefinitely large number of parametric curves are required to adequately explore the creep response of cylinders under external pressure. This task is greatly simplified by the computing of transverse displacement (4.18a) using computer program B of Appendix A.

Figures 16, 17, and 18 are plots of non-dimensional critical time, $\left(\frac{t_{cr} p_z^m}{K}\right)$, versus a/h for creep exponent M equal to 3, 5, 7 respectively. In each case as a/h ratio for a given a* decreases, the non-dimensional critical time drastically increases. Further, as a* increases for a given a/h ratio, the non-dimensional critical time decreases. Of the two parameters, a/h and a*, a/h is the more dominant variable. That is, critical time is more sensitive to a/h than a*. The same conclusion was reached by Hoff (1959).

Figure 19 illustrates the effect of varying the initiation point of a new time segment of constant effective stress. If for example, M, a/h, a* equal 3, 10, .005 respectively, the value $\frac{t_{cr} p_z^3}{K}$ equals 3.5×10^{-6} for time segments which are initiated when the effective stress (4.19) increases by fifty percent ($\psi = 1.5$) compared to a value of 2.2×10^{-6} when the time segments are initiated when the effective stress increases by five percent ($\psi = 1.05$), a ratio of 1.6 difference.

From a practical ocean engineering point of view, a comparison of the two most common creep prone materials, aluminum and titanium, used

in the ocean is in order. The alloys used in the comparison are Aluminum 6061-T6 and Titanium 6Al-2cb-1Ta-.08Mo. The room temperature creep constants of these materials are listed in Appendix C. The titanium constants where experimentally found by Chu (1972), while the aluminum constants by the author.

The first comparison is non-dimensional critical time verses the initial elastic hoop stress, expressed as a percentage of yield stress. The yield stresses of Titanium 621/.08 and Aluminum 6061-T6 are 120 and 40 ksi respectively. The two materials are compared with two a/h ratios, 10 and 50; and two a* ratios, .01, and .001. A number of conclusions can be drawn. The lifetime increases for both materials, approximately five times for a/h equal to 10 and forty-five times for a/h equal to 50, with an order of magnitude decrease in initial out-of-roundness ratio (a*). Hence, it appears to be more important that cylinders of large a/h ratios to be constructed to closer tolerances than cylinders of a smaller a/h ratio. Titanium is the better performer at low stress levels, but is surpassed by aluminum at higher stress levels. Imperfections play a more important role at higher stress levels. Finally, for a stress level less than forty percent of yield, there is a dramatic increase in lifetime.

The influence the varying a/h at a given stress level, sixty percent of yield, has on the non-dimensional critical time is portrayed in Figure 21. Again, a crossover occurs. For small a/h ratios ($a/h < 20$) titanium is the optimum material, while for larger a/h ratios aluminum exceeds titanium.

Taking another tack, if a* is varyed for a constant a/h (10) and a constant stress level, fifty percent of yield, Figure 22 is generated, a crossover of performance is observed with titanium being surpassed by aluminum for grosser tolerances (a* > .007).

The most pertinent collation is the comparison of the two materials at equal pressure levels. As an example, with p_z, a*, a/h equal to 2000 psi, .001 and 10 respectively titanium out performs aluminum by four orders of magnitude, (Figure 23). Titanium, with its superior strength, is able to operate at a much lower percentage of yield stress.

6.2 Complete Sphere

6.2.1 Elastic Response

By substituting the elastic part of the constitutive equation (3.2a) into the transverse equilibrium equation (5.6a), an expression for the elastic response is developed

$$w_e = \frac{a^2 p_z (1 - \upsilon^2)}{3Eh} \tag{6.4a}$$

The elastic deflection given by Roark (1965) is

$$w_{e_{Roark}} = \frac{a^2 p_z (1 - \upsilon)}{2Eh} \tag{6.4b}$$

A ratio of the elastic deflection to that of Roark is .86 of υ is assumed to be .3.

6.2.2 Parametric Study

As with the infinitely long cylinder, the dependence if the time history of the transverse deflection on a large number of independent variables requires the generation of a large assemblage of parametric curves to adequately investigate creep response of the sphere.

Again, the task is simplified by numerically computing equation (5.1) using computer program C of Appendix A.

Figures 24, 25, and 26 are graphs of non-dimensional time $\left(t_c \frac{p_z}{K}^m\right)$ versus R/H for various creep exponents, (M equal to 3, 5, 7). The non-dimensional critical time decreases rapidly with both increasing R/H and R*, being most sensitive to R/H.

The non-dimensional critical time of the sphere is fairly non-sensitive to the duration of the time segments, as illustrated in Figure 27. If the updating of effective stress (5.26a) is carried out when effective stress is increased by fifty percent ($\psi = 1.5$) the value of $\frac{t_{cr} p_z^3}{K}$ is 1.6×10^{-5}. If, however, the effective is updated when it has increased by five percent, ($\psi = 1.05$) $\frac{t_{cr} p_z^3}{K}$ equals 1.05×10^{-5}, an increase of fifty percent.

When the non-dimensional critical time is calculated for various initial elastic loadings, expressed as percentage of yield stress, for the two alloys, Aluminum 6061-T6 and Titanium 621/.08, Figure 28 is manifested. Initial imperfections are quite influencial on the critical time, causing a two order of magnitude increase for a/h equal to 10 and six orders of magnitude increase for R/H equal to 50 with an order of magnitude decrease in initial imperfections. Thus, revealing that for spheres of large R/H ratios, close tolerances are a prerequisite. Except for the case of high R/H ratio and gross imperfections, titanium is the superior material, producing a longer lifetime. Rapid increase in lifetime is achieved if the stress level of the sphere is less than sixty percent of the yield stress.

When R/H is varied for a given stress level, sixty percent of yield, titanium, regardless of the R/H ratio, out-performs aluminum. This superiority is even more obvious, as demonstrated in Figure 29, for substantial R/H ratios (R/H > 30).

If for a constant R/H ratio and a loading of fifty percent of yield, the magnitude of initial imperfections is allowed to veer, Figure 30 is developed. Again, titanium is always the superior performer, especially with small initial imperfections. That is, one has much more to gain by machining a titanium sphere to exacting tolerances than an aluminum sphere.

At the same pressure level, the titanium is vastly superior than the aluminum, having a lifetime of approximately 7 orders of magnitude longer with p_z equaling 2000 psi and R* equaling .001. The obvious reason being that a titanium sphere will operate at one-fourth the percentage of its yield stress at a given ambient pressure.

6.3 Comparison of the Creep Performance of the Sphere and Cylinder

If the critical time of a cylinder and a sphere of the same material at equal pressure levels are compared by plotting the ratio of critical time of the sphere to the critical time of the cylinder for various a/h ratios, initial imperfections, and creep exponents, (Figures 31, 32, and 33) it is discovered that regardless of the initial conditions, the cylinder has the inferior creep resistant properties. This point is especially manifested in the case of titanium, M equals 7. The oscillations observed in Figures 31, 32, and 33 result from the variation of the ratio of the effective stresses with various a/h and a* combinations.

The sphere is more sensitive to variations in initial imperfections, which is to be expected since the cylinder is a developable surface and is less constrained than the sphere.

The sphere has excellent creep characteristics for stress levels less than sixty percent of yield stress. The cylinder, on the other hand, the stress level must be less than forty percent of yield stress for favorable creep properties.

Finally titanium, because of its high yield stress is in every instance the best material to be used in ocean engineering applications of both the sphere and the cylinder.

6.4 Design Criterion

The extensive analysis present suggests an assemblage of simple design guidelines to assist the engineer in developing a cost-effective, creep resistant design. In most ocean engineering shell designs, the major constraint in design is considered to be the minimization of the weight to displacement ratio of the structure, while maintaining a maximum stress level of approximately fifty to sixty percent of yield. It is this constraint which dictates the use of lightweight, but creep-prone materials in the first place. Fortunately, this criterion is satisfied if titanium is used rather than aluminum in pressure vessels, even though titanium is 1.5 times as dense as aluminum. The reason being, the aluminum shell would have to be four times as thick to achieve a stress field of equal percentages of yield stress. Hence, titanium will always give a longer lifetime.

While the sphere furnishes a vastly superior creep response than the cylinder, it is more expensive to construct and machine. Thus,

the engineer must weigh the merits of the costs of materials, construction and machining of both an appropriate sphere or cylinder for his particular situation (pressure level and time constraints) before he develops a final design.

Regardless, the shape of the amplification curves for both the shell shapes suggest a creep design limit. For approximately the first seventy percent of the lifetime imperfections remain small and grow in a linear manner. Thus, an arbitrary design limit can be established which states that as long as the imperfection growth becomes linear, the design will not creep buckle. The in-service monitoring of the creep deformation process is easily accomplished with a three element strain gage rossette placed at the point of greatest imperfection. When the effective stress approaches the magnitude of the yield stress, the active use of the structure should be terminated.

6.5 Example Calculations

6.5.1 DSRV ALVIN

The research submersible, ALVIN, owned by the Office of Naval Research and operated by Woods Hole Oceanographic Institution, has a spherical titanium 621/.08 alloy pressure hull. The 40.005 inch radius hull has a a/h ratio of 20 and a maximum out-of-roundness ratio (a*) of 0.002. The maximum operating depth is 12,000 feet (5280 psi) and a collapse depth of 18,000 feet (7920 psi).

The secondary creep law for Ti 6Al-2cb-1Ta-0.8Mo alloy at room temperature has been empirically measured by Chu (1972) (Appendix C). While the measurements were done in tension, it is believed that the

compressive creep behavior is similar to that of tension. The law is expressed as

$$\sigma^7 = \kappa \dot{\varepsilon} \qquad (6.2a)$$

where

$$\kappa = 8.3941934 \times 10^{40} \left(\frac{lb}{in^2}\right)^7 \text{ hr.} \qquad (6.2b)$$

With values of a/h, a*, M equal to 20, .002, and 7 respectively, the amplification curve of Figure 34 is manifested. If subjected to the maximum operating pressure, buckling occurs at a time equal to 9870 hours. If the submersible is operated at only half its operational depth it would not buckle until 1.85×10^6 hours had past.

6.5.2 SOFAR Floats

The Woods Hole Oceanographic Institution has employed a long cylinder which when released at sea sinks to a depth at which it becomes neutrally buoyant. The current measuring floats, first designed by Swallow (1963), will follow a water mass of a constant density due to the neutrally compressible, buoyant properties. Placed at a depth of approximately 5000 feet, (the axis of the SOFAR Channel, a horizontal channel, in which the convex shape of the sound velocity-depth profile allows sound to be transmitted with minimal attenuation over thousands of miles), the floats emit an acoustic tone at a given frequency. The float is then spatially fixed using acoustic triangulation from land based listening stations. The floats have been successful in tracking eddies in the WHOI MODE program. Unfortunately, after two to three months, these floats have been found to sink an additional 230 to 560 feet, with accelerating sinking velocity, (an apparent creep buckling

phenomenon). Mavor (1974) computed a linear strain rate of 0.9 μin/in/hr from the change of displacement and an assumed constant in situ seawater density gradient.

$$\frac{\Delta\rho}{\rho\Delta Z} = 1.371 \times 10^{-6}/\text{ft} \tag{6.3}$$

where

ρ = density

Z = depth .

The floats are standard ALCOA extruded 6061-T6 aluminum cylindrical stock with a mean radius of 5.625 inches, a a/h ratio of 7.5, an approximate out-of-roundness ratio of 0.005 and a length of 17 feet. They operate at a mean depth of 5000 feet (2200 psi). The 6061-T6 aluminum follows a cubic creep law as experimentally found by the author (Appendix C)

$$\sigma^3 = \kappa\dot{\varepsilon} \tag{6.4a}$$

where

$$\kappa = 4 \times 10^{19} \text{ (psi)}^3\text{hr}. \tag{6.4b}$$

Figure 35 displays the predicted creep response with a/h, a*, M equal to 7.5, 0.005, and 3, respectively.

Since the problem is concerned with only the first three months of the lifetime, the perturbation transverse displacement can be considered linear. From Figure 35

$$\dot{w}' = 1.13795 \text{ μin/hr}. \tag{6.5a}$$

From equation (4.1), the perturbation hoop strain rate is

$$\dot{e}'_\theta = \frac{2h\dot{w}'}{a^2} = 5.3947 \times 10^{-8} \text{ in/in/hr}. \tag{6.5b}$$

From equation (4.7b), the dominant hoop strain rate is

$$\dot{\bar{e}}_\theta = \frac{\dot{\bar{w}}}{a} \quad . \tag{6.5c}$$

Computing $\dot{\bar{w}}$ from equation (4.8) yields a dominant hoop strain rate of

$$\dot{\bar{e}}_\theta = 9.45 \times 10^{-7} \text{ in/in/hr.} \tag{6.5d}$$

Hence, the total predicted linear strain rate is

$$\dot{\bar{e}}_\theta = \dot{\bar{e}}_\theta + \dot{e}'_\theta = .998 \ \mu\text{in/in/hr,} \tag{6.5e}$$

ten percent greater than the estimate of Mavor.

This calculation shows that, in fact, creep deformation is most probably the cause of the unexpected sinking of the floats.

7. SUMMARY AND CONCLUSIONS

The theoretical investigation which has been undertaken into the creep instability of the infinitely long cylindrical and complete spherical thin shells has satisfied the original thesis objective of developing a relatively simple analytical method to predict the creep deformation process of these shells. It was found that in both shells the critical buckling mode is the second elliptical mode. The roles of shell radius to thickness ratio and initial out-of-roundness have been explored. The relative superiority of the spherical shell over the cylindrical shell has been discussed.

The investigation demonstrated that the single most important factor in creep design is designing the structure in a manner which maintains the stress field at the lowest possible level, thus extending the structure's lifetime. This one factor endorses the use of high strength titanium and the spherical shell in creep design.

In conclusion, while creep buckling can be a problem in long term ocean structures, the nature of the time history of imperfection growth, almost negligible until the last ten percent of the lifetime, allows the ocean engineer to develop a safe design resistant to creep buckling with little difficulty.

8. RECOMMENDATIONS

Two essential advances in creep design are required in the future. First, the establishment of accurate creep constants at ambient temperatures for common ocean engineering materials. Second, a more advanced theoretical investigation which encompasses the effects of boundary conditions of such shells as finite length cylinders, and partial spherical shells (end caps).

REFERENCES

1. Abrahamson, G.R., and Goodier, J.N. "Dynamic Plastic Flow Buckling of a Cylindrical Shell from Radial Impulse", Proc. 4th U.S. Nat. Congress App. Mech., pp 939-950, 1962.

2. Ahn, C.S. "Elastic-Plastic Buckling of Shells Under Dynamic Loadings", Ph.D. Thesis, M.I.T., Ocean Engineering, May 1972.

3. Ahn, C.S. "A Consistent Set of Non-linear Shell Equations", M.I.T., Ocean Engineering, Report No. 73-18.

4. Bargmann, H. "Effect of Time-Varying Temperature and Varying External Pressure on Creep Collapse of a Cylindrical Shell", Proceedings of the First Int. Conf. on Structural Mechanics in Reactor Technology, Berlin, Gr., Vol. 5, Part J., pp 145-153, 20-24 Sept. 1971.

5. Benoit, M., Sendelbuk, R., Hoff, N.J. "An Experimental Study of the Creep Buckling of Moderately Thin-Walled Circular Cylindrical Shells Subjected to Axial Compression", Dept. of Aero & Astro, Stanford Univ., Sept. 1970.

6. Benoit, M., and Hoff, N.J. "Creep Buckling of Flat Plates", Dept. of Aero & Astro, Stanford Univ., Tech. Report No. 27, SUDAAR No. 463, Aug. 1973.

7. Berman, I., Chern, J.M., Gupta, G.D. "A Parametric Study of Elastic-Plastic Creep Buckling of a Thin Cylindrical Shell", Journal of Pressure Vessel Tech., Aug. 1974.

8. Berman, I., Chern, J.M., Gupta, G.D. "A Parametric Study of Elastic-Plastic Creep Buckling of a Thin Cylindrical Shell", ASME paper 74-PVP-37.

9. Burt, Charles W. "Creep Tensile Instability in Pressurized Shells of Revolution", Mech. of Solid State, ed. by F.P.J. Rimroff, Univ. of Toronto Press, 1968.

10. Chapman, J.C., Erickson, B., Hoff, N.J., "A Theoretical and Experimental Investigation of Creep Buckling", Int. J. Mech. Sci., Pergamon Press, Vol. 1, pp 145-174, 1960.

11. Chu, H.P. "Room Temperature Creep of Titanium Alloy Ti-6Al-2Cb-1TA-0.8 Mo", NSRDC Report 2866, June, 1969.

12. Chu, H.P. "Room Temperature Creep of A Ti-6Al-2Cb-1TA-0.8 Mo Alloy Weldment", NSRDC Report 28175, April 1972.

REFERENCES (cont.)

13. Dickey, R.L. "Dynamic Buckling of Visco-plastic Spherical Shells", MIT O.E. Thesis, Dept. of O.E., May 1974.

14. Drucker, Daniel, Introduction to Mechanics of Deformable Solids, McGraw-Hill, New York, N.Y., 1967.

15. Finnie, I., and Heller, W.R. Creep of Engineering Materials, McGraw-Hill, London, 1959.

16. Flügge, W. Viscoelasticity, Blaiedell Pub. Co., Waltham, Ma, 1967.

17. Flügge, W. Stress in Shells, Springer-Verlag, New York, N.Y., 1967.

18. Griffin, D.S. "Inelastic and Creep Buckling of Circular Cylinders Due to Axial Compression, Bending and Twisting", ASME paper 74-PVP-46.

19. Hildebrand, Francis B. Advanced Calculus for Applications, Prentice Hall Inc., Englewood Cliffs, N.J., 1962.

20. Hoff, N.J. "The Effects of Geometric Non-Linearities on the Creep Buckling Time of Axially Compressed Circular Cylindrical Shells", Dept. of Aero, Sanford Univ. Tech. Report No. 29, April 1974.

21. Hoff, N.J. "Creep Buckling of Rectangular Plates Under Uniaxial Compression", Engineering Plasticity, Cambridge University Press, 1968.

22. Hoff, N.J. "A Survey of the Theories of Creep Buckling", Proc. 3rd U.S. Natl. Congr. Appl. Mech., pp 29-49, 1958.

23. Hoff, N.J., "Axially Symmetric Creep Buckling of Circular Cylindrical Shells in Axial Compression", ASME paper 68-APM-30.

24. Hoff, N.J. "Creep Buckling", Polytechnic Institute of Brooklyn, Aeronautical Quarterly, Vol. VII, February 1956.

25. Hoff, N.J., and Wang L., "Creep Buckling of Circular Cylindrical Shells in Pure Bending", Dept. of Aero, Sanford Univ. Tech. Report, December 1970.

26. Hoff, N.J., Berke, L., Honikman, T.C., and Levi. I.M. "Creep Buckling of Flat Rectangular Plates When the Creep Exponent Ranges from 3 to 7", Contract AF33(615)-5115, USAF Flight Dynamics Lab., Structures Division, 1970.

REFERENCES (cont.)

27. Hoff, N.J., Jahsman, W.E., and Nachbar, W., "A Study of Creep Collapse of a Long Circular Cylindrical Shell under Uniform External Pressure", J. of the Aero Space Sci., Vol. 26, No. 10, pp 663-669, October 1959.

28. Honikman, T.C., and Hoff, N.J. "The Effect of Variations in the Creep Exponent on the Buckling of Circular Cylindrical Shells", Int. J. of Solid Structures, Vol. 7, pp 1685-1695, Pergamon Press, 1971.

29. Jones, N. and Ahn, C.S., "Dynamic Elastic and Plastic Buckling of Complete Spherical Shells", Int. J. of Solid Structures, pp 609-613, September 1974.

30. Jones, N., and Ahn, C.S. "Dynamic Plastic Buckling of Complete Spherical Shells", MIT Dept. of O.E. Report No. 73-19, 1973.

31. Kraus, H., Thin Elastic Shells, Wiley and Sons, New York, N.Y., 1967.

32. Lempriere, B.M., "Comparison of Ranges of Applicability of Predictions of Creep Buckling Time", Creep in Structures, ed. N.J. Hoff, IUTAM Conf. Sanford, 1960.

33. Lubahn, J.D., and Felgar, R.P. Plasticity and Creep of Metals, Wiley and Sons, New York, N.Y. 1965.

34. Mendelson, Alexander, Plasticity: Theory and Application, MacMillian Co., New York, N.Y. 1970.

35. Nishida, K., and Charles, R.M. "The Behavior of 6Al-4V Titanium Spherical Shells Under Static, Cyclic and Creep Conditions" NSRDC Report 3513, November 1970.

36. Odqvist, F.K.G., Mathematical Theory of Creep and Creep Rupture, Oxford Univ. Press, London, 1966.

37. Penny, R.K. "The Creep of Pressurized Cylindrical Shells", Univ. of Liverpool, Dept. of M.E., July 1968.

38. Penny, R.K., and Marriott, D.L. Design for Creep, McGraw-Hill, London, 1971.

39. Penny, R.K., and Marriott, D.L. "Creep Buckling of Boss Loaded Spherical Shells", Univ. of Liverpool, Dept. of M.E., January 1969.

REFERENCES (cont.)

40. Pittner, E.V., and Hoff, N.J. "Creep Buckling of Simply Supported Moderately Thin Circular Shells", Acta Mechanica, Vol. 8, pp 116-125, 1969.

41. Rabotnov, Yu. N., Creep Problems in Structural Members, North-Holland Pub. Co., London, Wiley and Sons, New York, N.Y., 1969.

42. Rikards, R.B., and Teters, G.A. "Non Symmetric Creep Buckling of Cylindrical Shells under Axial Compression and External Pressure", IUTAM Sym. in Buckling of Structures, Harvard Univ., June 1974.

43. Roark, R.J., Formulas for Stress and Strain, McGraw-Hill, New York, N.Y., 1965.

44. Samuelson, L.A. "Creep Buckling of a Circular Cylindrical Shell", AIAA Journal, Vol. 7, No. 1, pp 42-49.

45. Samuelson, L.A., "Creep Buckling of Imperfect Circular Cylindrical Shells under Non-Uniform External Loads", Creep in Structures, ed. J. Hult, Springer-Verlag Pub. Co. IUTAM Symp., Gothenburg, Gr., 1970.

46. Samuelson, L.A. "Creep Buckling of a Cylindrical Shell under Non-Uniform External Loads", Int. J. Solids Structures, Vol. 6, No. 1, pp 91-116, 1970.

47. Sankavanarayan, R. "Steady Creep of Circular Cylindrical Shells under Combined Lateral and Axial Pressure", Int. J. Solids Structures, Vol. 5, pp 17-32, 1969.

48. Sundstrom, B. "Creep Buckling of Cylindrical Shells", Trans. of the Royal Inst. of Tech., Stockholm, No. 115, 1957.

49. Tarpguard, P.T., Jones, N. "The Influence of Finite-Deformations Upon the Creep Behavior of Circular Plates", Int. J. Mech. Sci., Pergamon Press, Vol. 14, pp 447-467, 1972.

50. Thein, Wan, "Creep Collapse of Cylindrical Shells", J. Franklin Inst. 272, No. 1, 1961.

51. Timoshenko, S.J., and Gere, J.M. Theory of Elastic Stability, McGraw-Hill, New York, N.Y., 1961.

52. Timoshenko, S.J., and Goodier, J.N., Theory of Elasticity, McGraw-Hill, New York, N.Y., 1970.

REFERENCES (cont.)

53. Timoshenko, S.J., and Woinowsky-Krieger, S., Theory of Plates and Shells, McGraw-Hill, New York, N.Y., 1959.

54. Timoshenko, S.J., and Young, D.H., Elements of Strength of Materials, Van Nostrand Reinhold Co., New York, N.Y., 1968.

55. Walters, R.M., "Dynamic Response of Thin, Rigid-Plastic Shells Subjected to Transverse Loads", Ph.D. Thesis, MIT, Ocean Engineering, May 1971.

56. Walters, R.M. and Jones, W. "An Approximate Theoretical Study of the Dynamic Plastic Behavior of Shells", Int. J. Non-Linear Mech., Vol. 7, pp 255-273, Pergamon Press, 1972.

57. Wylie, C.R. Jr., Advanced Engineering Mathematics, McGraw-Hill, New York, N.Y., 1966.

TITLES OF FIGURES

Figure 1 Coordinates of a Point P on the middle surface of a shell.

Figure 2 Forces, moments, and external loads which act on the middle surface of a typical shell element.

Figure 3 (a) Maxwell model.

(b) Response of Maxwell model to a step loading.

Figure 4 Forces, moments and external loads which act on the middle surface of a cylindrical shell element.

Figure 5 Growth of amplification function for a infinitely long cylinder.

Figure 6 Growth of critical amplification function for a linear visco-elastic infinitely long cylinder.

Figure 7 Growth of critical amplification function for a non-linear visco-elastic infinitely long cylinder.

Figure 8 Forces, moments, and external loads which act on the middle surface of a spherical shell element.

Figure 9 Growth of amplification function for a complete sphere.

Figure 10 Contour plots of the spatial function of the perturbation transverse displacement

$$w'/B_{m2} = \sum_{m=0}^{2} P^{m}_{2} (\cos\phi)(\cos m\theta) .$$

Positive values indicate outward displacements from the mean radius, negative values indicate inward displacements.

Figure 11 Growth of critical amplification function for a non-linear visco-elastic complete sphere.

Figure 12 Comparison of Hoff solution with herein solution with varying a/h ($m = 3$, $a^* = .005$).

Figure 13 Comparison of Hoff solution to herein solution for various a^* ($a/h = 10$, $m = 3$).

TITLES OF FIGURES (cont.)

Figure 14 Comparison of Hoff solution to herein solution for various m ($a^* = .005$, $a/h = 10$).

Figure 15 Comparison of time histories of Hoff solution to herein solution ($m = 3$, $a/h = 10$, $a^* = .005$).

Figure 16 Non-dimensional critical time for creep exponent equal to 3 for various a^* and a/h for an infinitely long cylinder.

Figure 17 Non-dimensional critical time for creep exponent equal to 5 for various a^* and a/h for an infinitely long cylinder.

Figure 18 Non-dimensional critical time for creep exponent equal to 7 for various a^* and a/h for an infinitely long cylinder.

Figure 19 Non-dimensional critical time with various initiation points of time segments of constant effective stress (ψ) ($m = 3$, $a/h = 10$, $a^* = .005$).

Figure 20 Critical time for various initial elastic loadings, expressed as a percentage of yield stress, for cylinders of $a^* = .001, .01$, $a/h = 10, 50$; and constructed of Titanium 621/.08 and Aluminum 6061-T6.

Figure 21 Critical time for various a/h ratios at sixty percent of yield stress for Titanium 621/.08 and Aluminum 6061-T6 cylinders ($a^* = .001$).

Figure 22 Critical time for various a^* at fifty percent yield for Titanium 621/.08 and Aluminum 6061-T6 cylinders ($a/h = 10$).

Figure 23 Critical time at equal external pressure for various a/h ratios for Titanium 626/.08 and Aluminum 6061-T6 ($a^* = .001$) ($P_z = 2000$ psi).

Figure 24 Non-dimensional critical time for creep exponent equal to 3 for various R^* and R/H for a complete sphere.

Figure 25 Non-dimensional critical time for creep exponent equal to 5 for various R^* and R/H for a complete sphere.

Figure 26 Non-dimensional critical time for creep exponent equal to 7 for various R^* and R/H for a complete sphere.

TITLES OF FIGURES (cont.)

Figure 27 Non-dimensional critical time with various initiation points of time segments of constant effective stress (ψ) (m = 3, R/H = 10, R* = .005).

Figure 28 Critical time for various initial elastic loadings, expressed as a percentage of yield stress, for spheres of R* = .001, .01, R/H = 10, 50; and constructed of Titanium 621/.08 and Aluminum 6061-T6.

Figure 29 Critical time for various R/H ratios at sixty percent of yield stress for Titanium 621/.08 and Aluminum 6061-T6 spheres (R* = .001).

Figure 30 Critical time for various R* at fifty percent yield for Titanium 621/.08 and Aluminum 6061-T6 spheres (R/H = 10).

Figure 31 Ratio of critical time of the complete sphere to critical time of the cylinder for various a/h ratios (m = 3).

Figure 32 Ratio of critical time of the complete sphere to critical time of the cylinder for various a/h ratios (m = 5).

Figure 33 Ratio of critical time of the complete sphere to critical time of the cylinder for various a/h ratios (m = 7).

Figure 34 Creep response of the titanium spherical hull of DSRV ALVIN.

Figure 35 Creep response of the aluminum cylindrical SOFAR float.

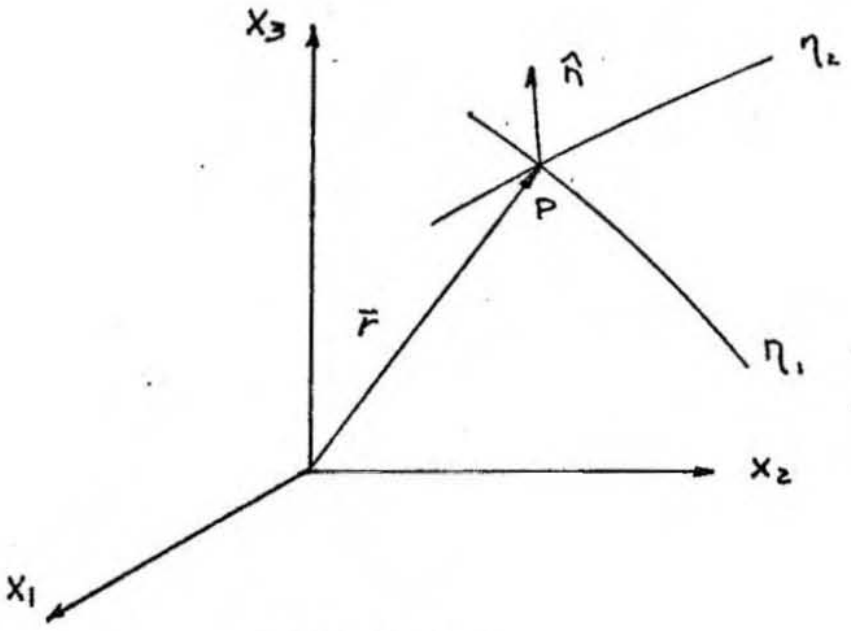

FIGURE 1

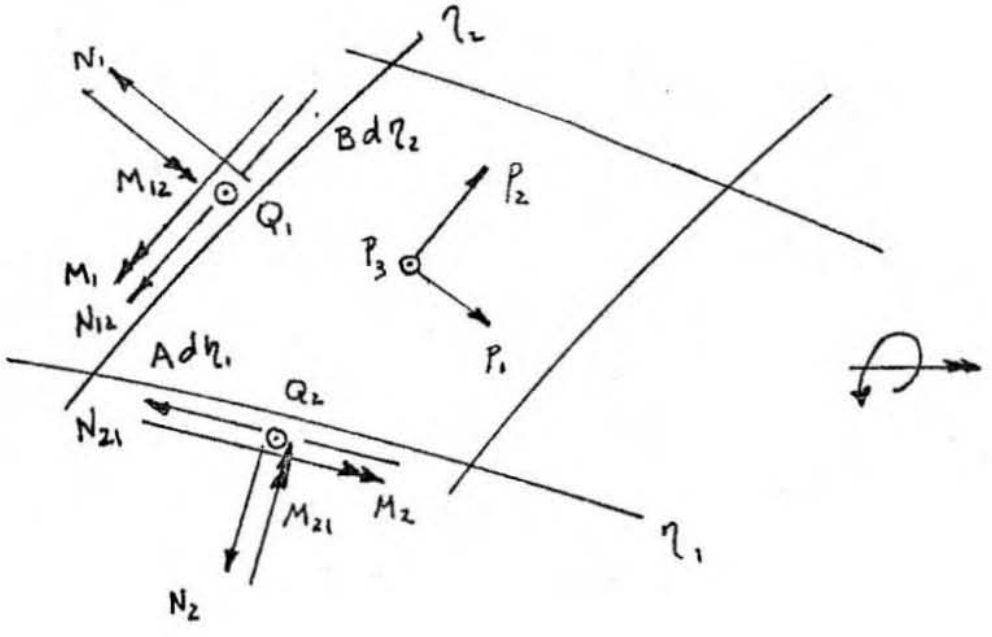

FIGURE 2

(a)

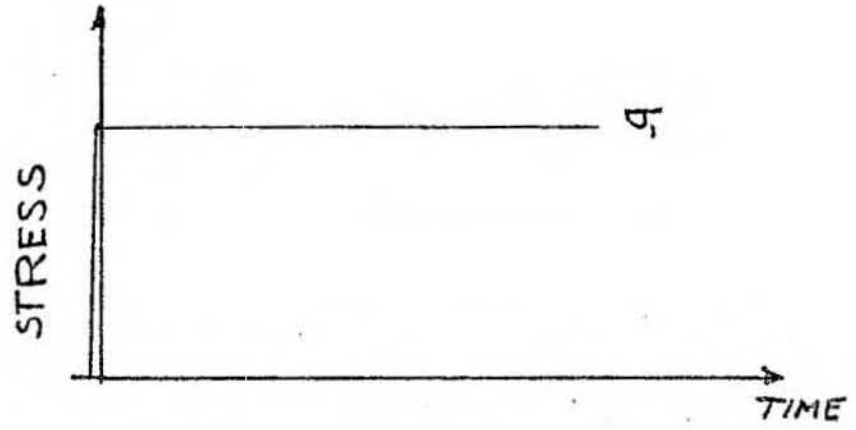

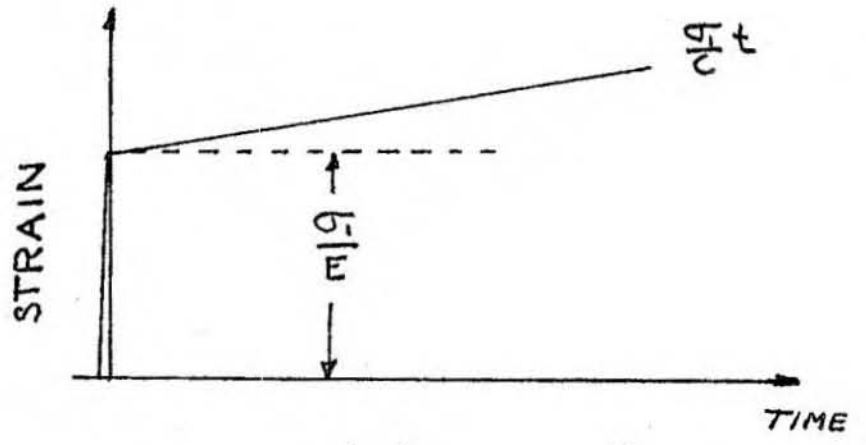

(b)

FIGURE 3

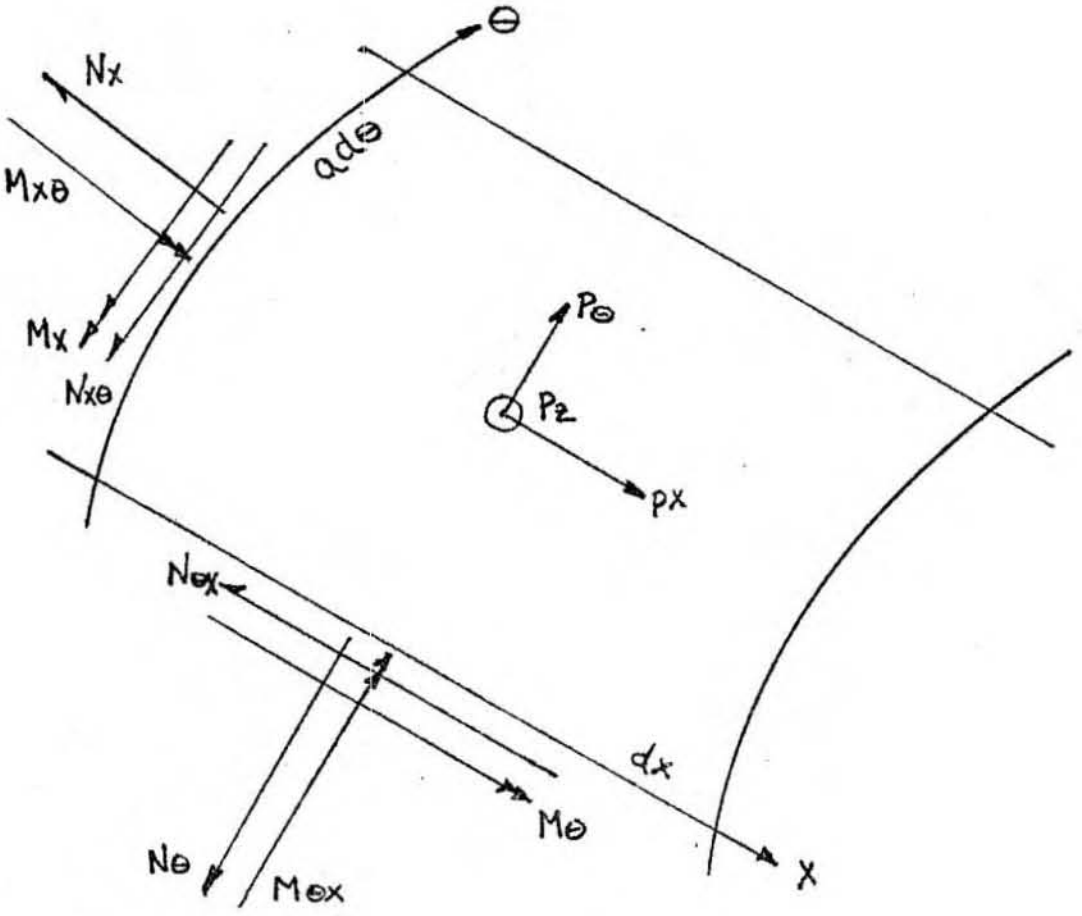

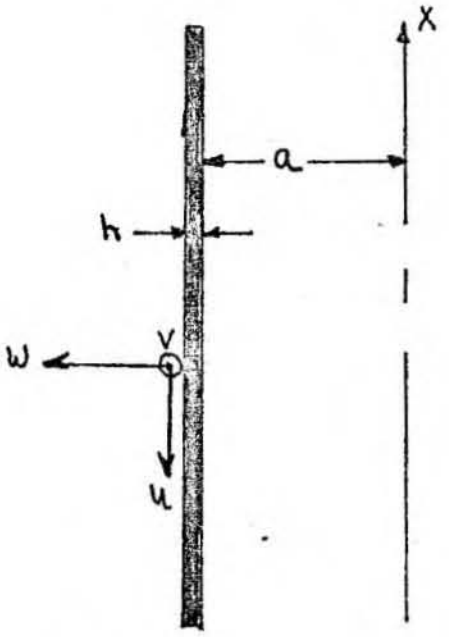

FIGURE 4

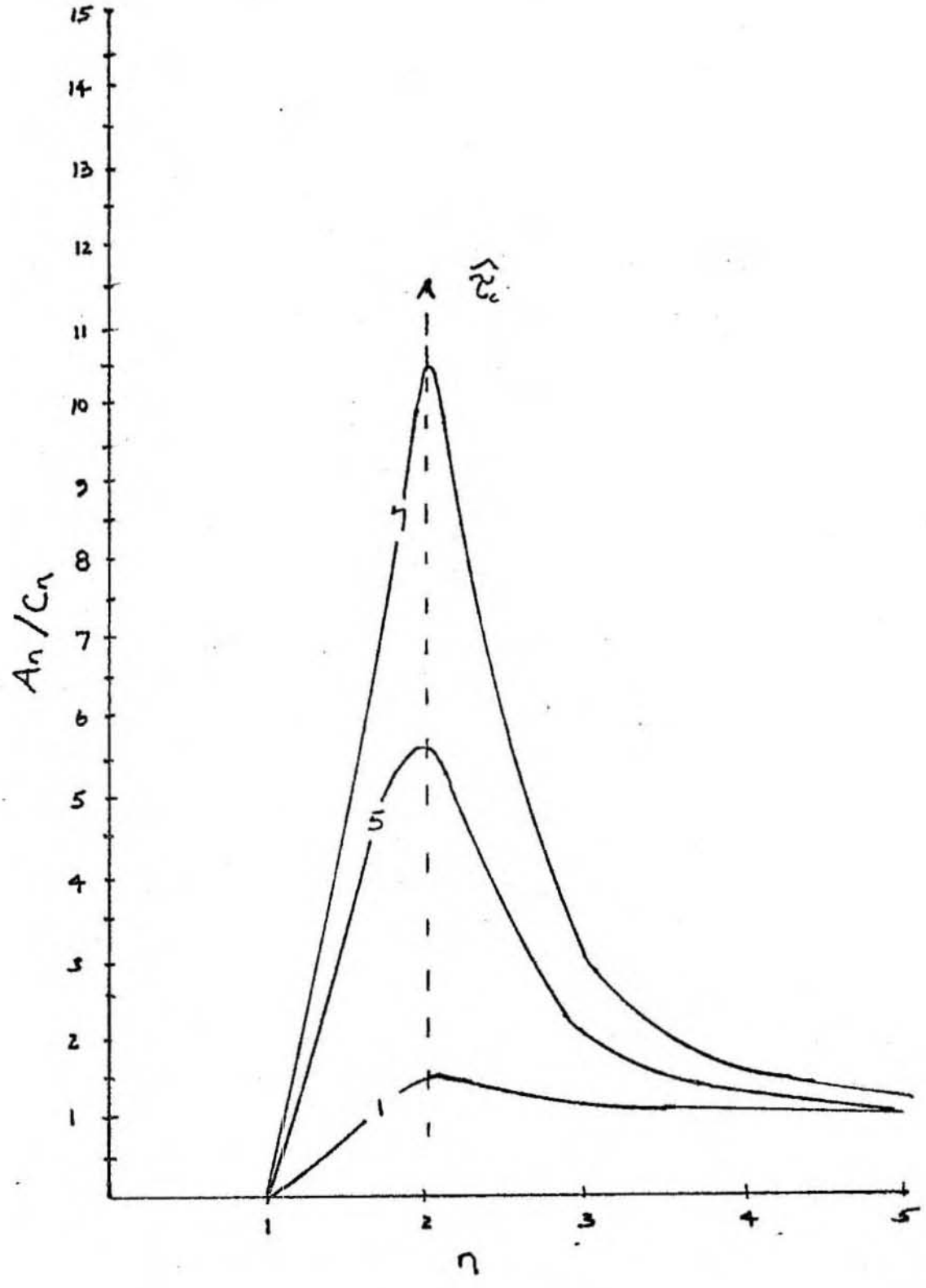

FIGURE 5

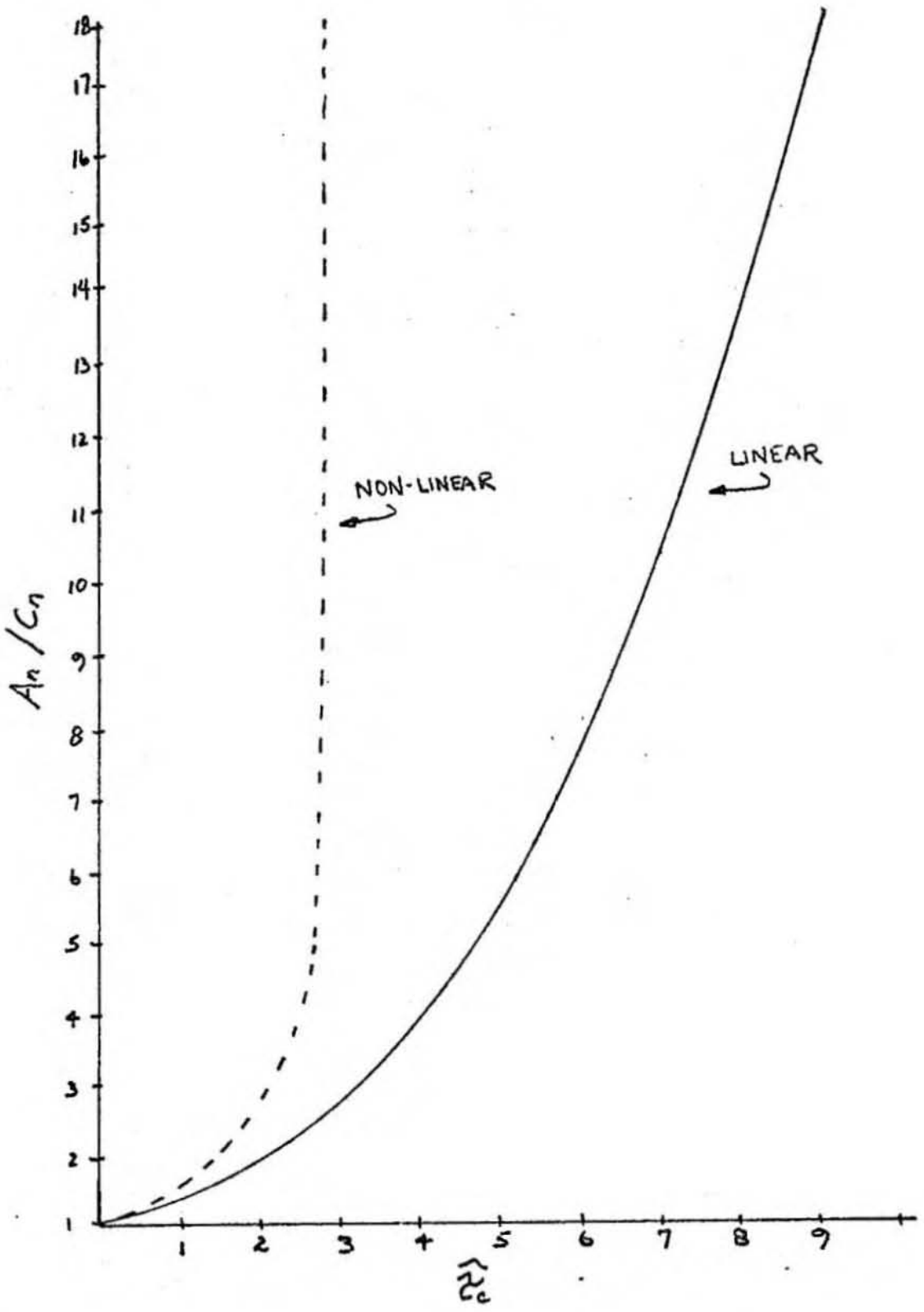
NON-LINEAR
LINEAR
A_n / C_n
$\hat{R}_c$
1
2
3
4
5
6
7
8
9
10
11
12
13
14
15
16
17
18

FIGURE 6

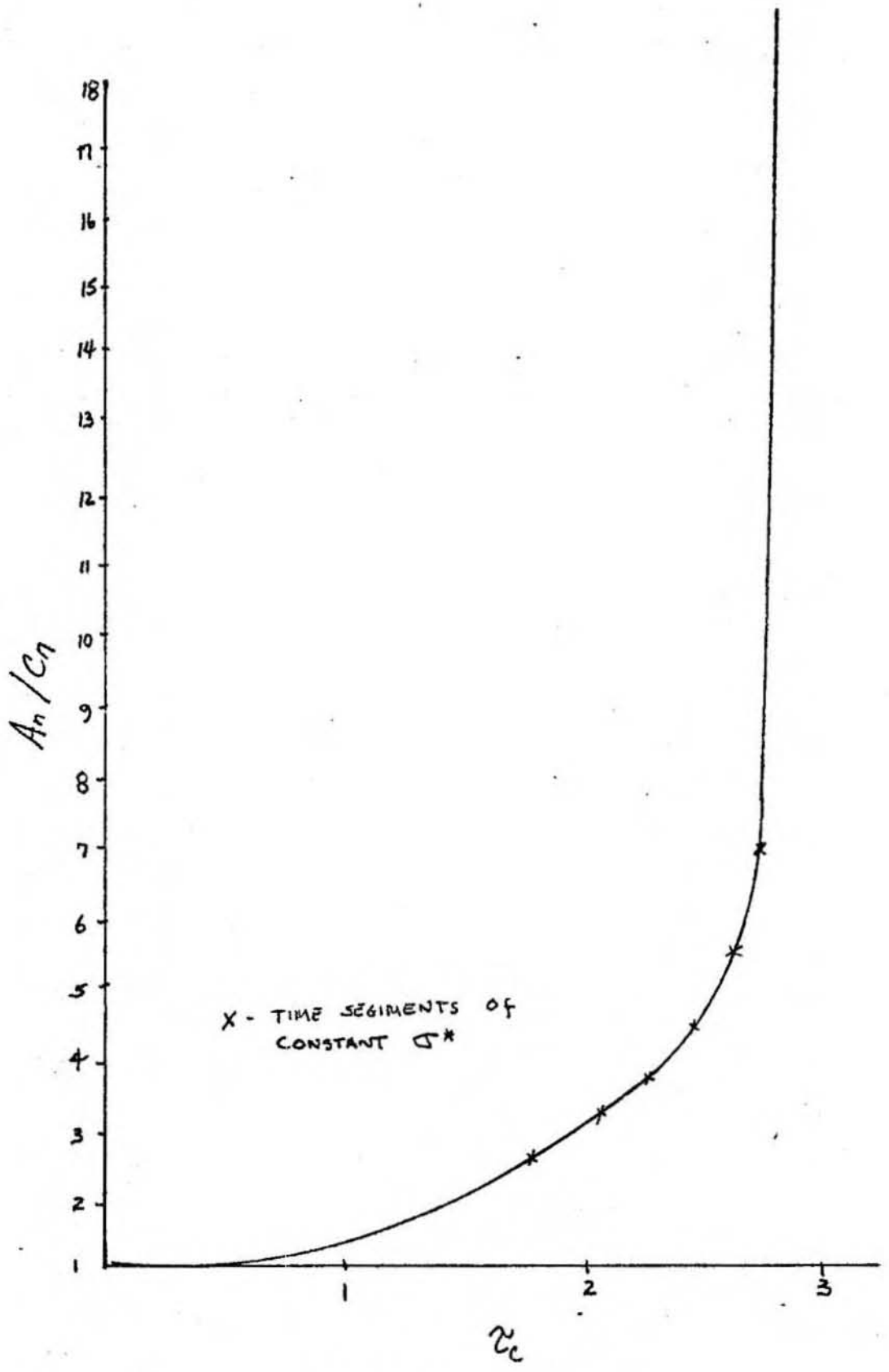
18
17
16
15
14
13
12
11
10
9
8
7
6
5
4
3
2
1
A_n / C_n
X - TIME SEGIMENTS OF CONSTANT σ^*
1
2
3
τ_c

FIGURE 7

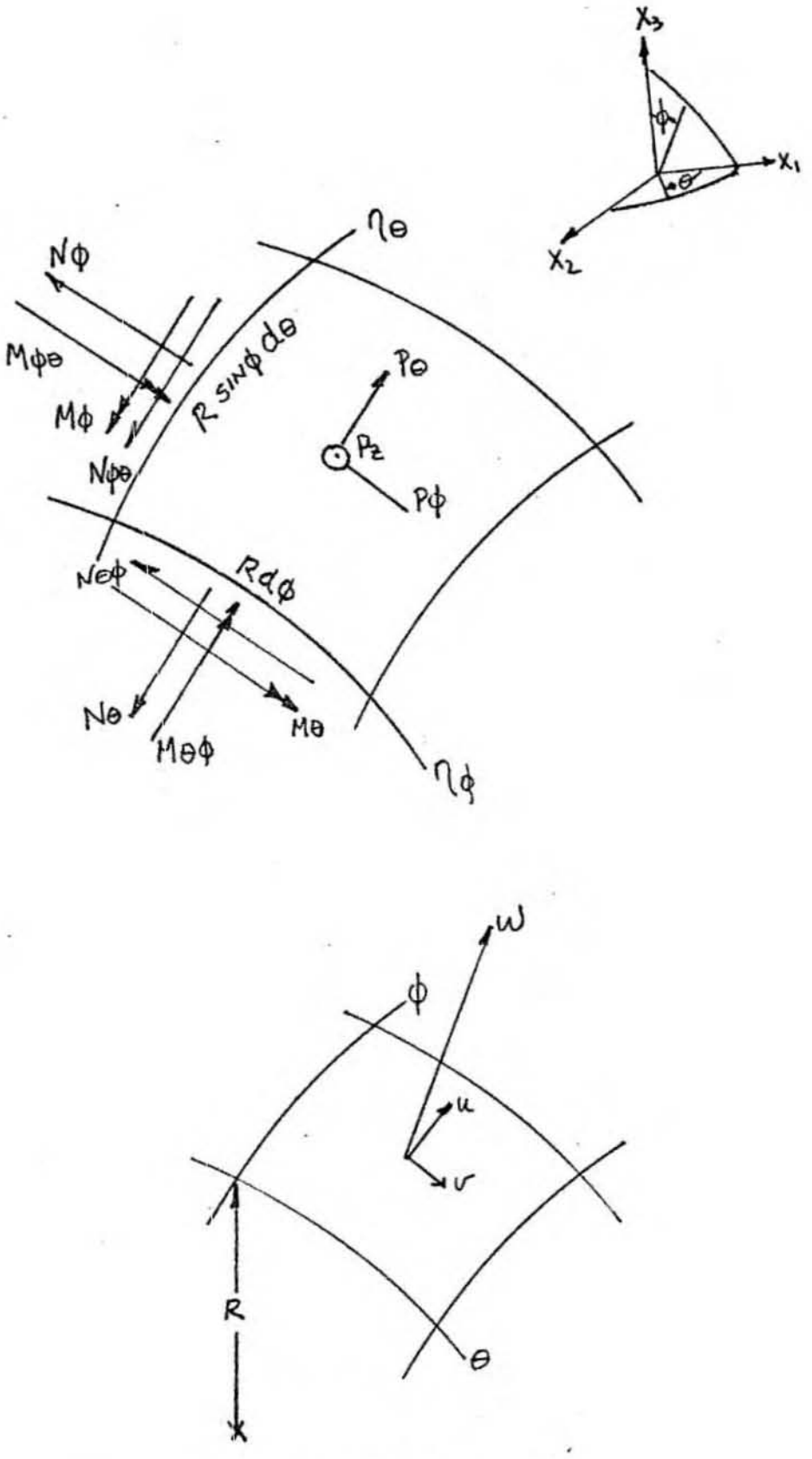
X3
X1
X2
ϕ1
θ
ηθ
Nϕ
Mϕθ
Mϕ
Nϕθ
R sinϕ dθ
Pθ
Pz
Pϕ
Nθϕ
Rdϕ
Nθ
Mθϕ
Mθ
ηϕ
w
ϕ
u
v
R
θ

FIGURE 8

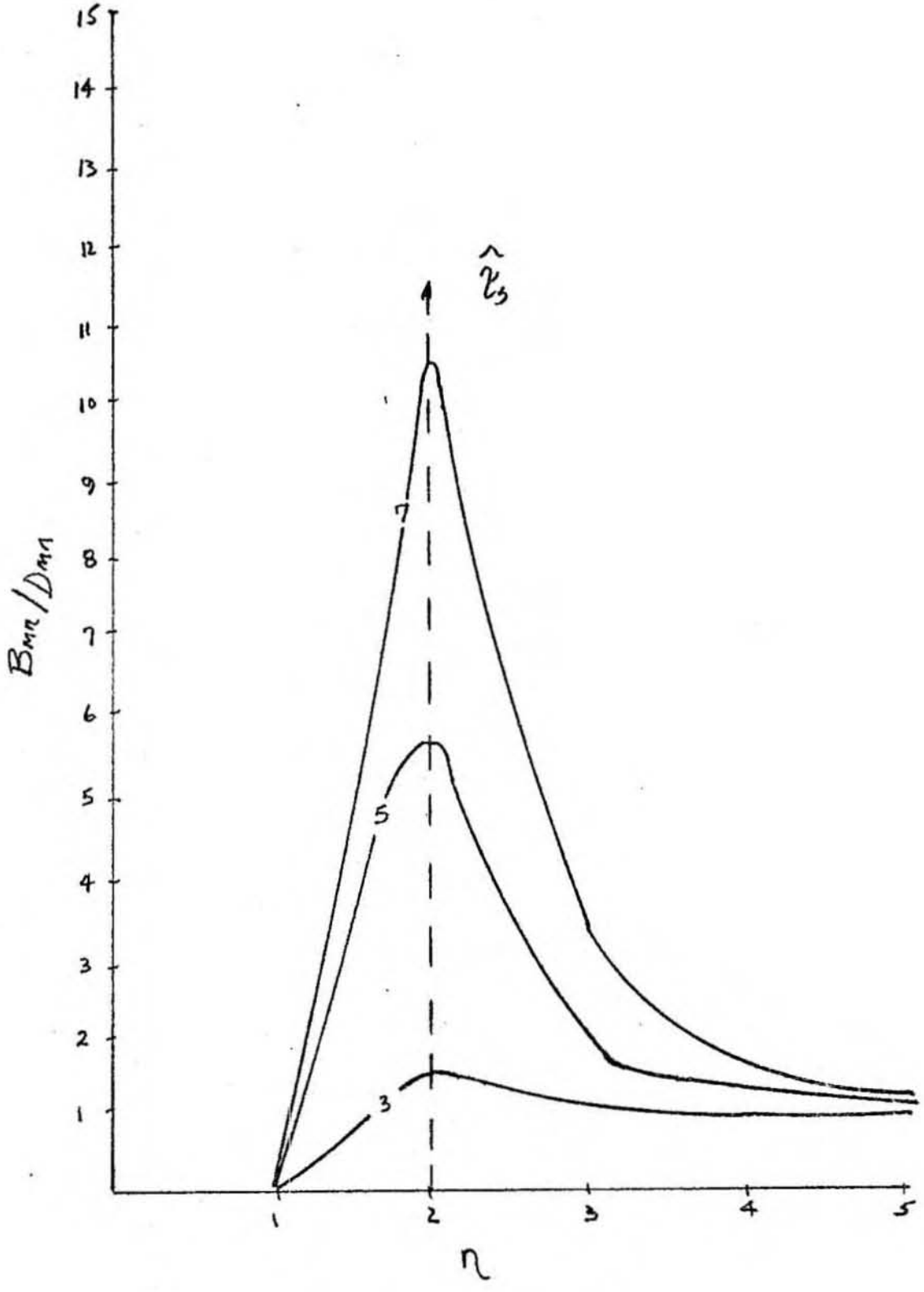

FIGURE 9

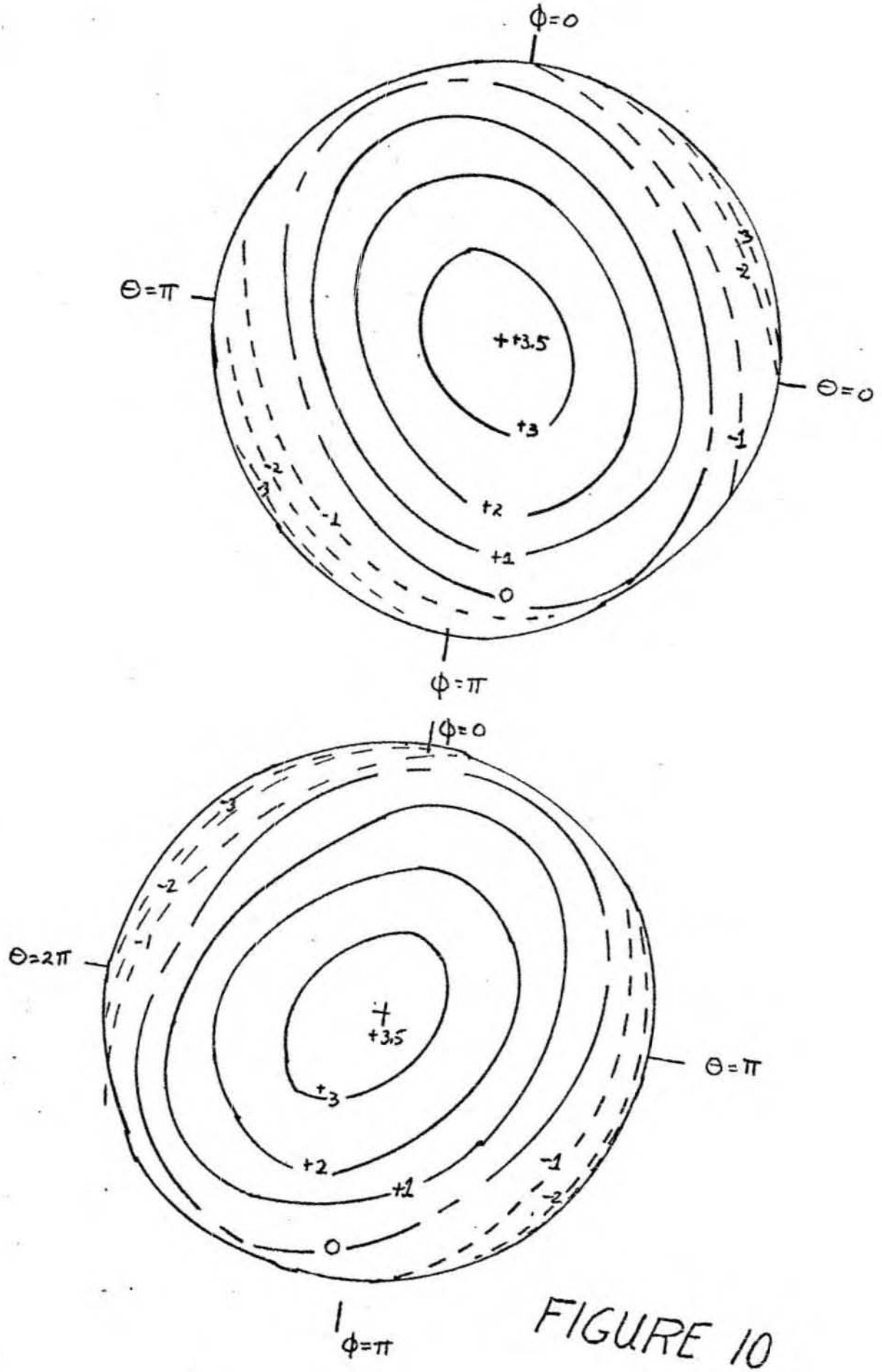

FIGURE 10

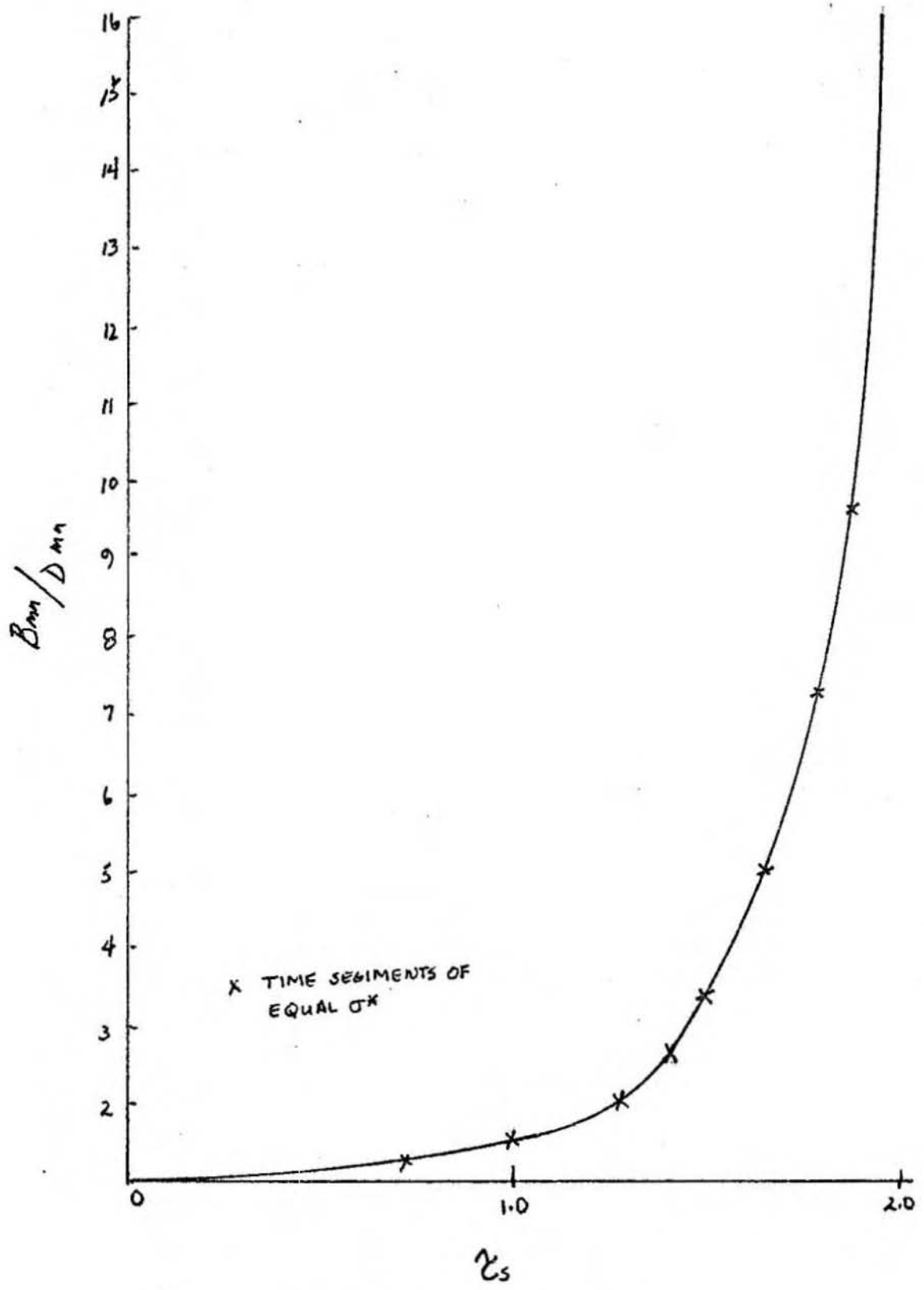
16
15
14
13
12
11
10
9
8
7
6
5
4
3
2
B_{mn}/D_{mn}
X TIME SEGIMENTS OF EQUAL σ^*
0
1.0
2.0
τ_s

FIGURE 11

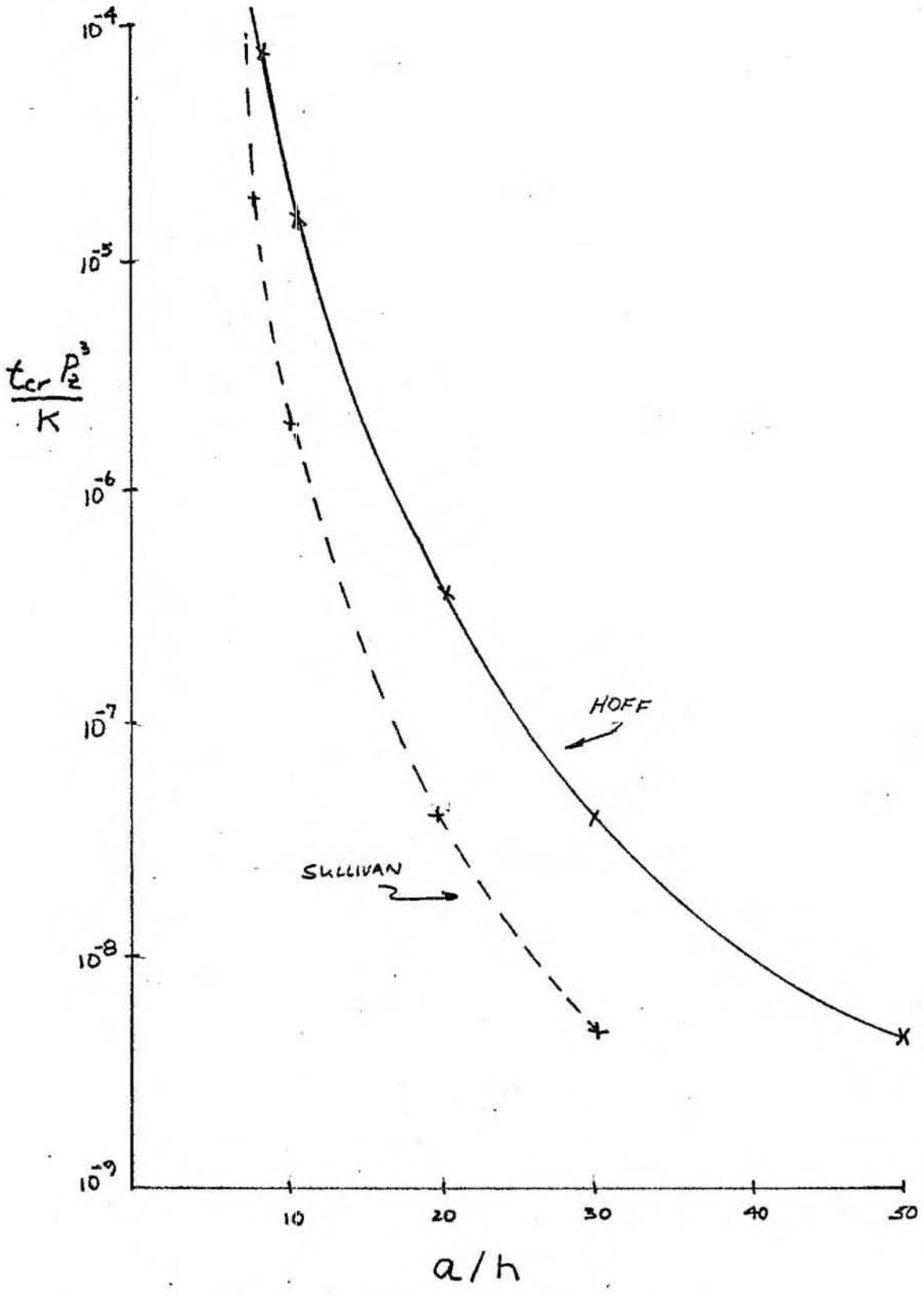
10^{-4}
10^{-5}
10^{-6}
10^{-7}
10^{-8}
10^{-9}
$\frac{t_{cr} P_z^3}{K}$
HOFF
SULLIVAN
10
20
30
40
50
a/h

FIGURE 12

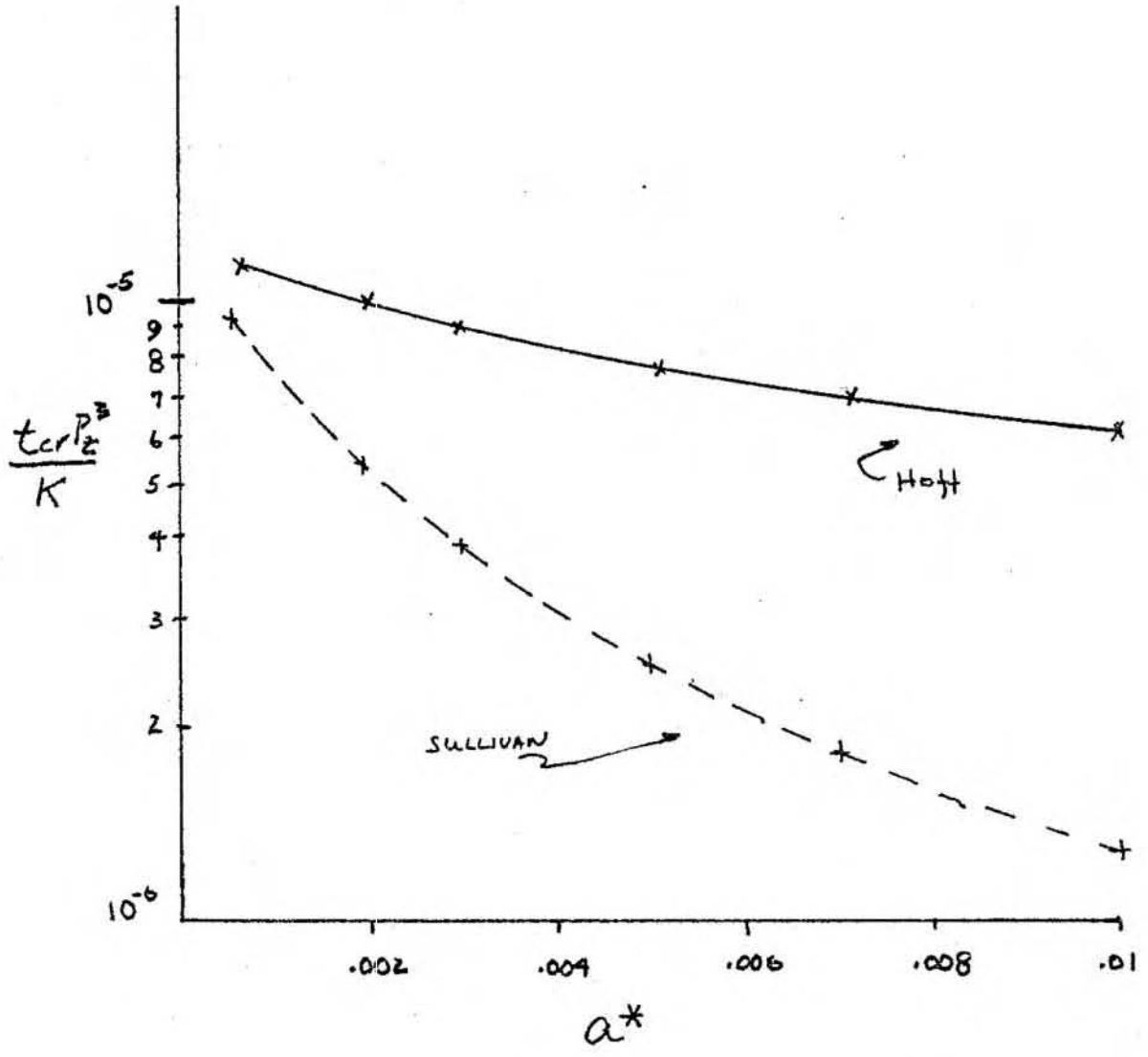
10^{-5}
9
8
7
6
5
4
3
2
10^{-6}
$\frac{t_{cr} P_z^3}{K}$
HOFF
SULLIVAN
.002
.004
.006
.008
.01
a^*

FIGURE 13

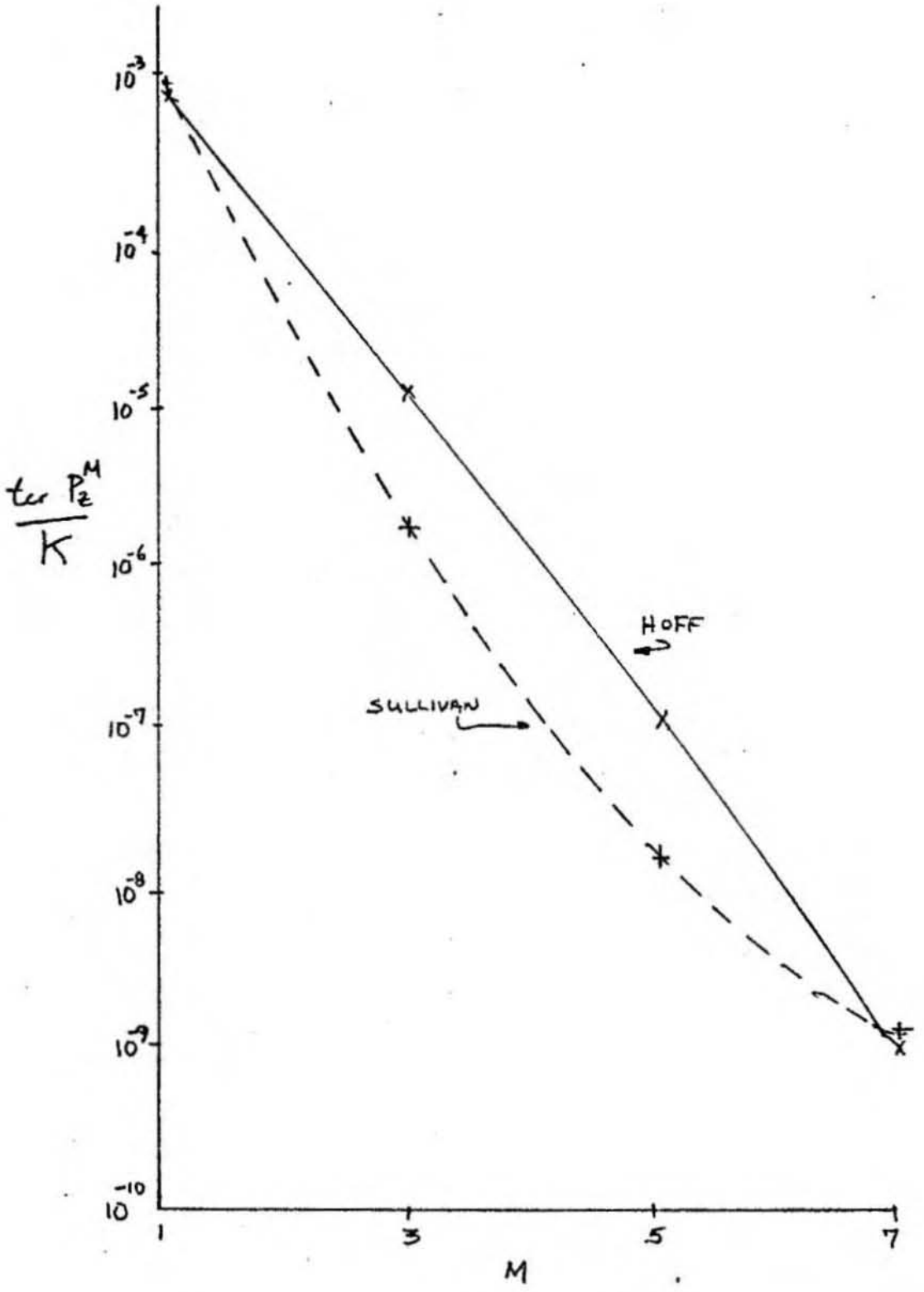
$\frac{t_{cr} P_z^M}{K}$
10^{-3}
10^{-4}
10^{-5}
10^{-6}
10^{-7}
10^{-8}
10^{-9}
10^{-10}
HOFF
SULLIVAN
1
3
5
7
M

FIGURE 14

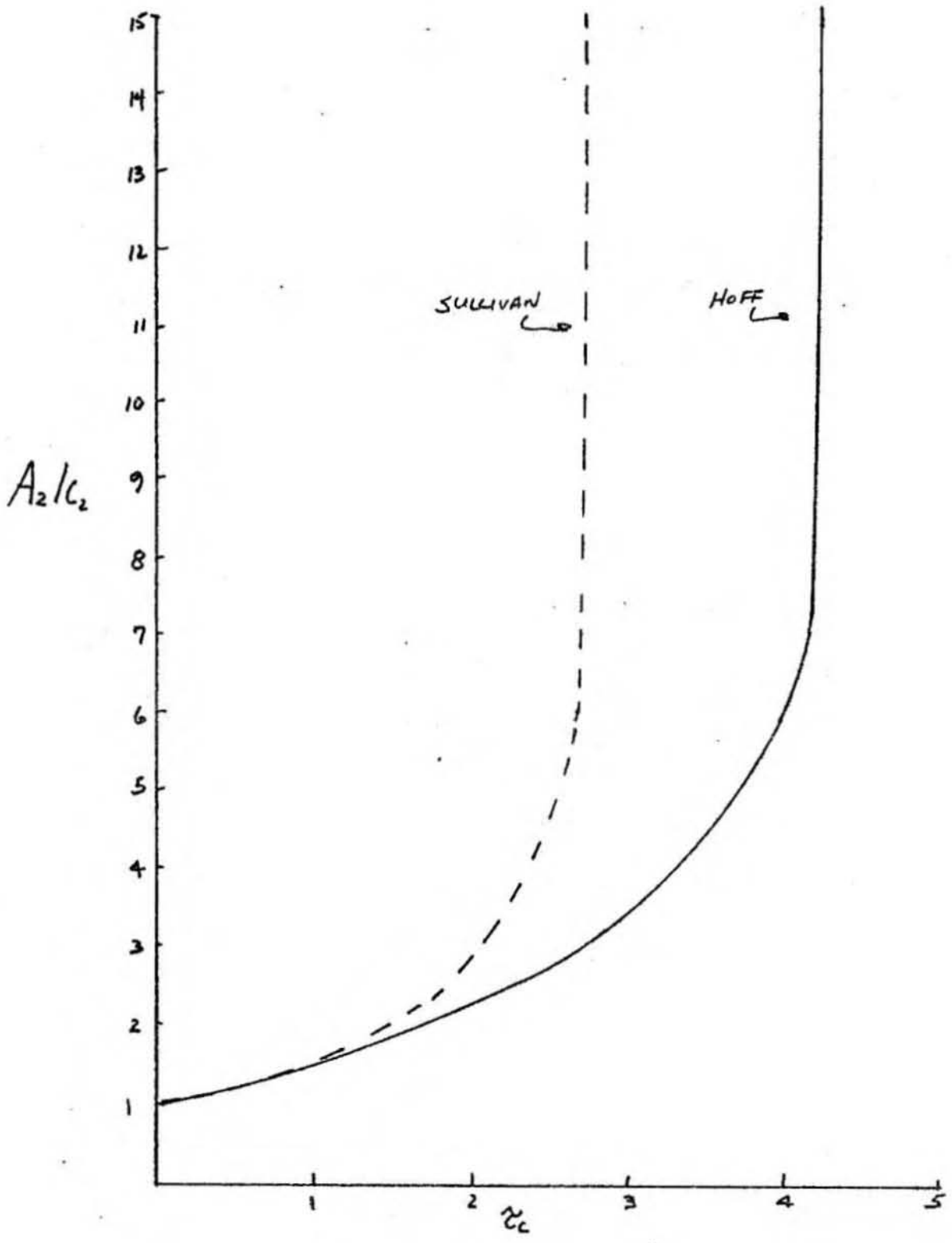

FIGURE 15

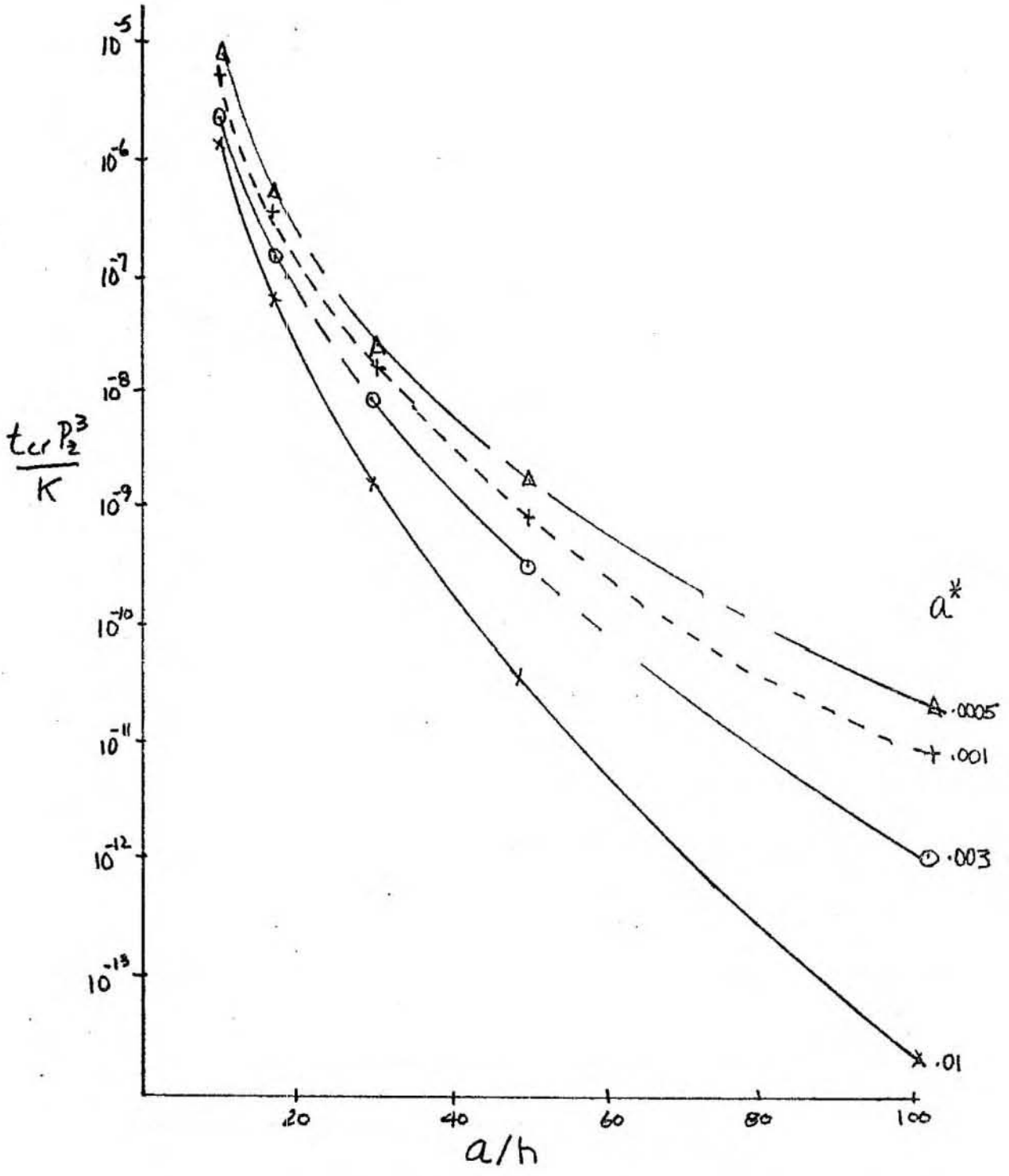
$\frac{t_{cr} P_z^3}{K}$
10^{-5}
10^{-6}
10^{-7}
10^{-8}
10^{-9}
10^{-10}
10^{-11}
10^{-12}
10^{-13}
20
40
60
80
100
a/h
a*
.0005
.001
.003
.01

FIGURE 16

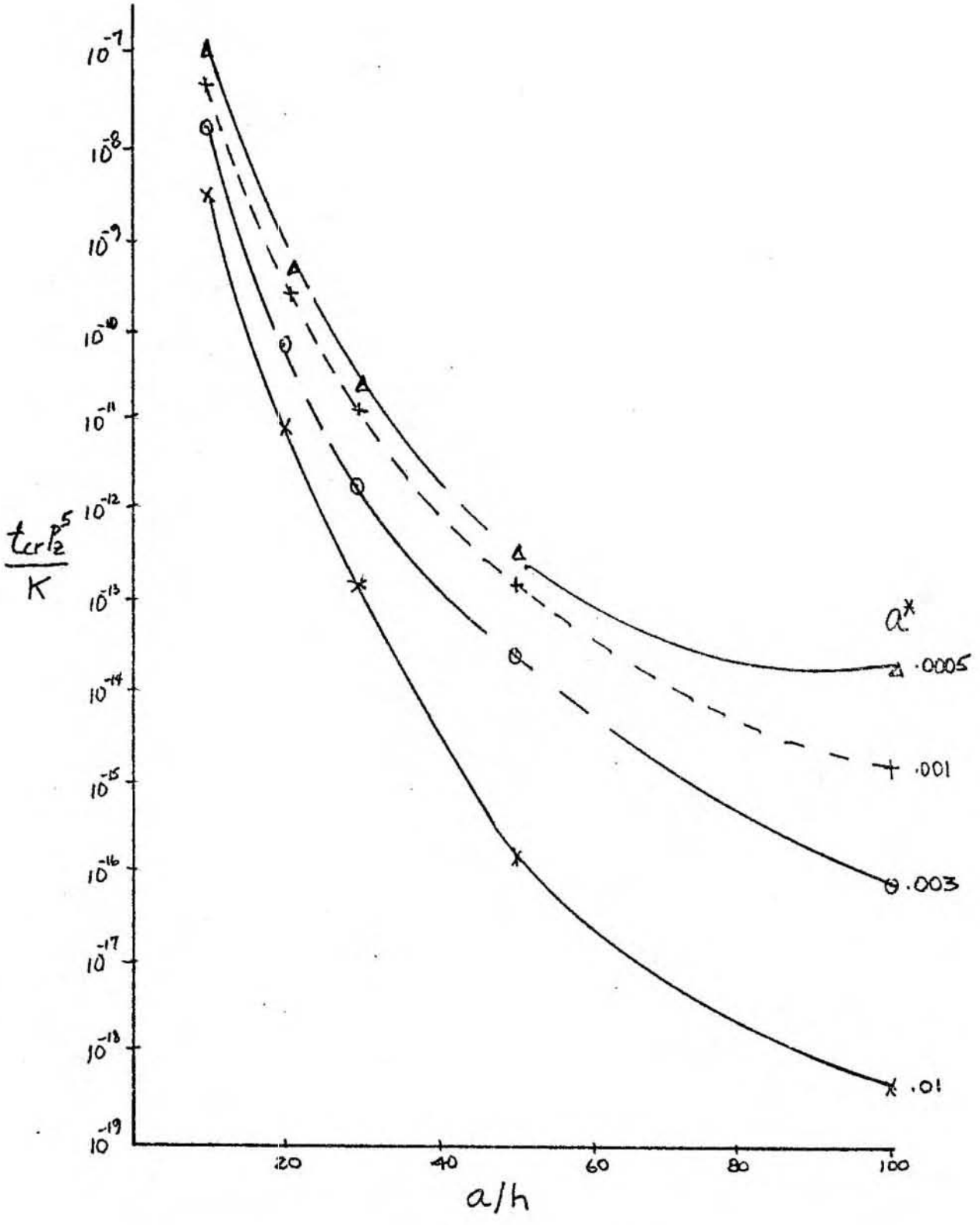
$\frac{t_{cr} P_2^5}{K}$
10^{-7}
10^{-8}
10^{-9}
10^{-10}
10^{-11}
10^{-12}
10^{-13}
10^{-14}
10^{-15}
10^{-16}
10^{-17}
10^{-18}
10^{-19}
20
40
60
80
100
a/h
a*
.0005
.001
.003
.01

FIGURE 17

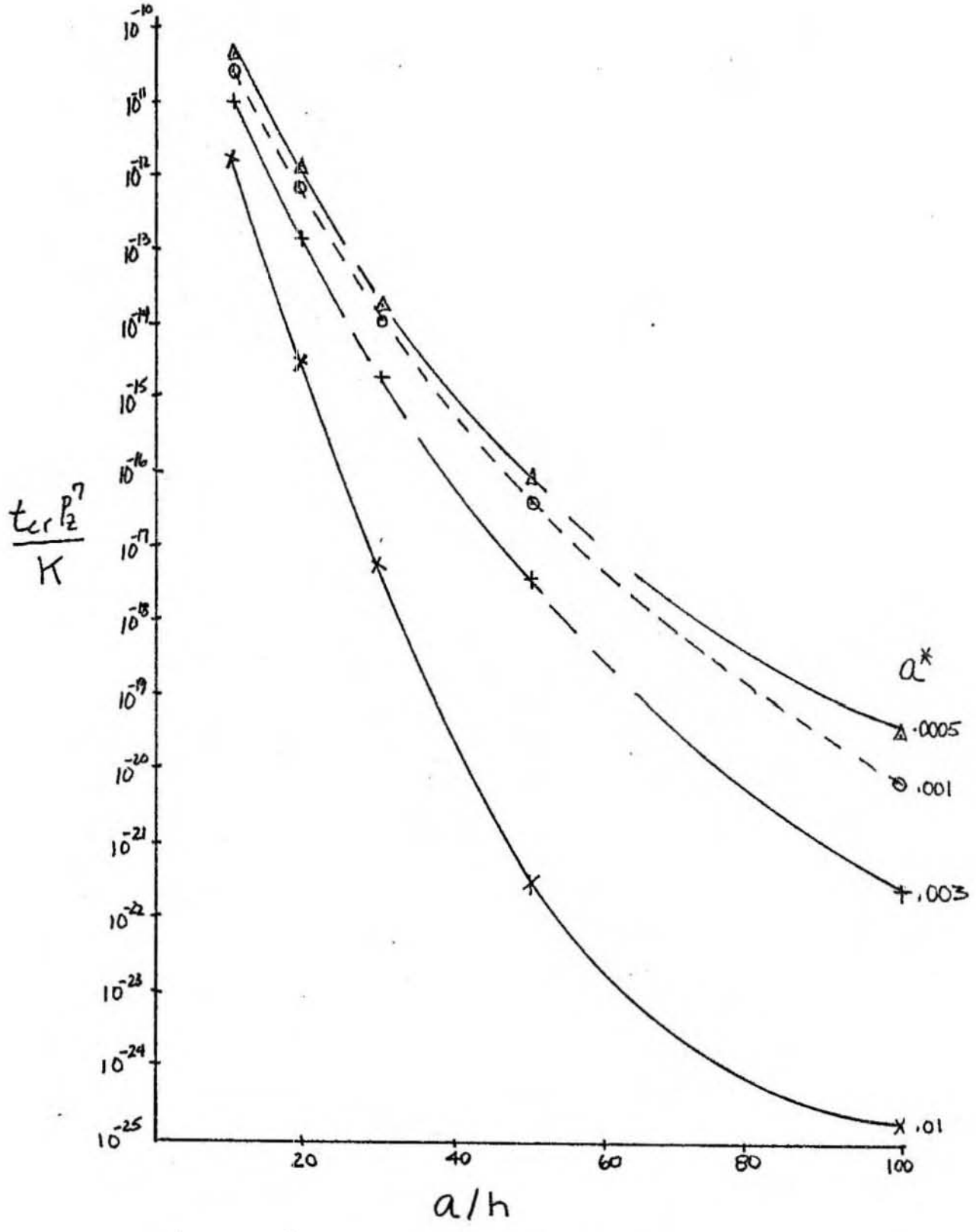
$\frac{t_{cr} P_z^7}{K}$
10^{-10}
10^{-11}
10^{-12}
10^{-13}
10^{-14}
10^{-15}
10^{-16}
10^{-17}
10^{-18}
10^{-19}
10^{-20}
10^{-21}
10^{-22}
10^{-23}
10^{-24}
10^{-25}
20
40
60
80
100
a/h
a*
.0005
.001
.003
.01

FIGURE 18

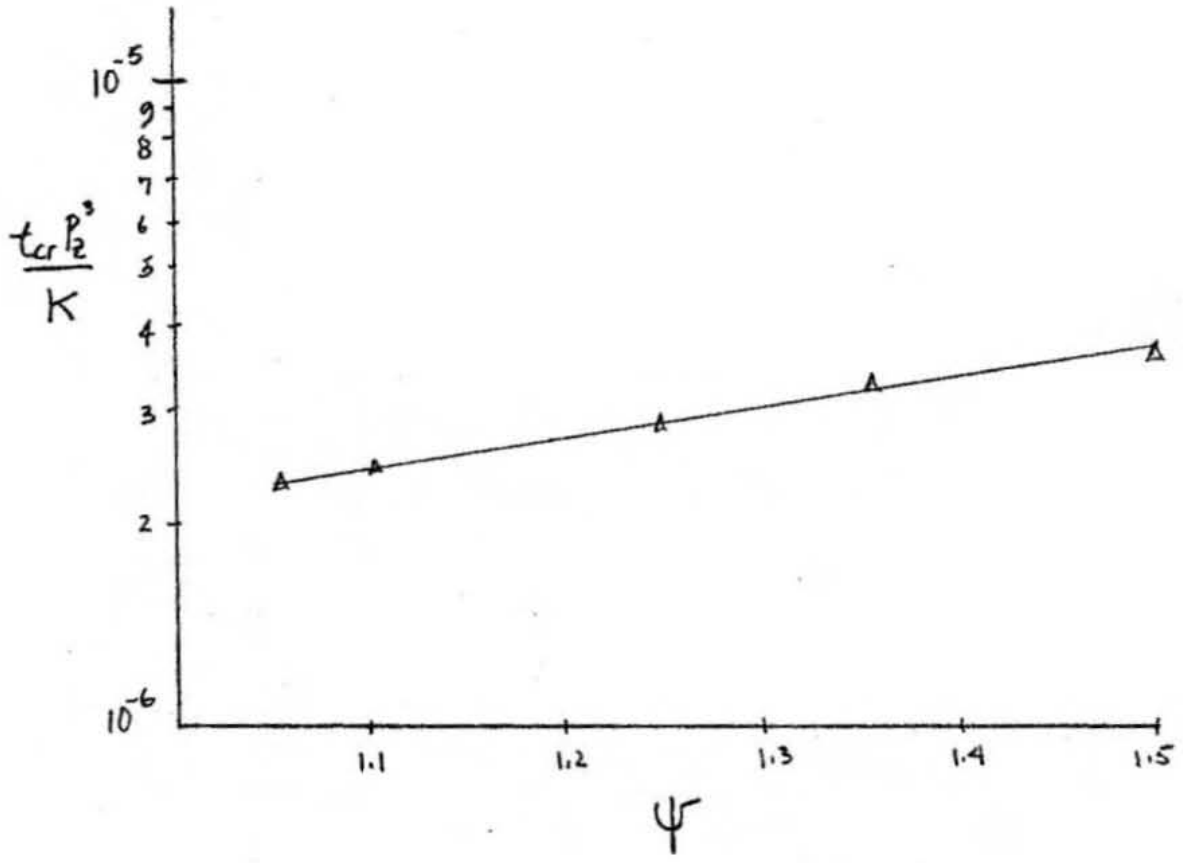

FIGURE 19

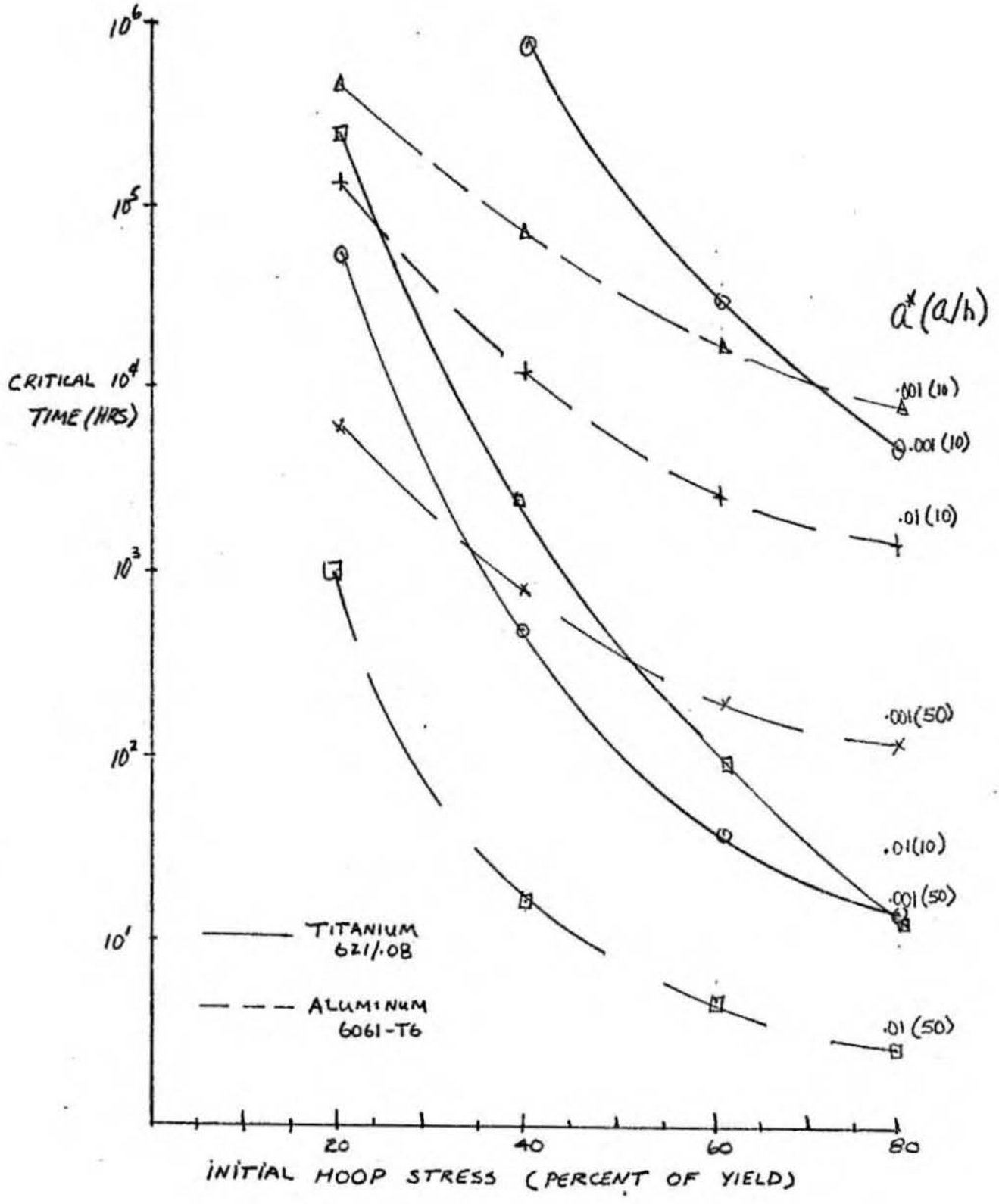
10^6
10^5
10^4
10^3
10^2
10^1
CRITICAL TIME (HRS)
a^* (a/h)
.001 (10)
.001 (10)
.01 (10)
.001 (50)
.01 (10)
.001 (50)
.01 (50)
TITANIUM 6Z1/.08
ALUMINUM 6061-T6
20
40
60
80
INITIAL HOOP STRESS (PERCENT OF YIELD)

FIGURE 20

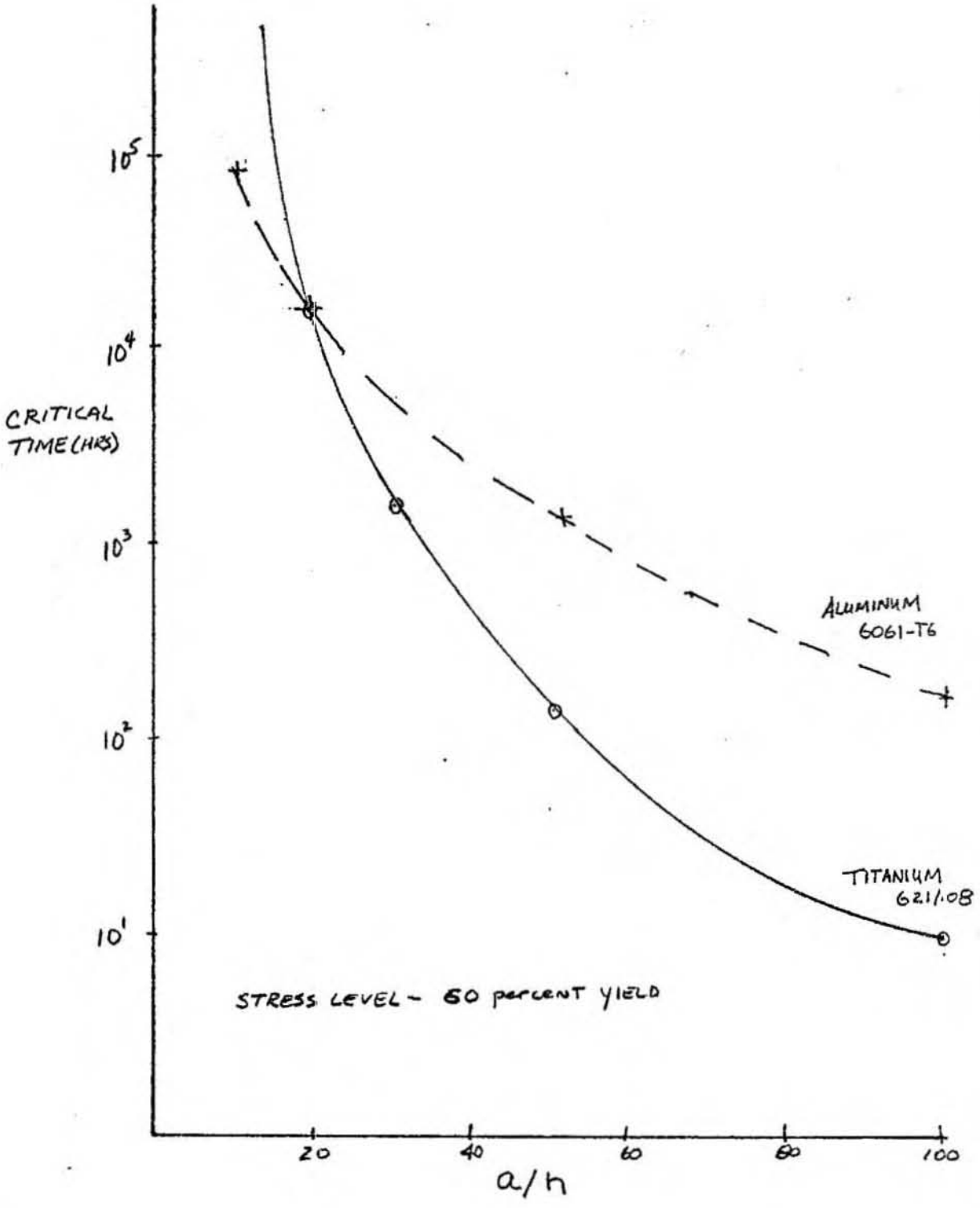
10^5
10^4
10^3
10^2
10^1
CRITICAL TIME (HRS)
ALUMINUM 6061-T6
TITANIUM 6211.08
STRESS LEVEL - 60 percent YIELD
20
40
60
80
100
a/h

FIGURE 21

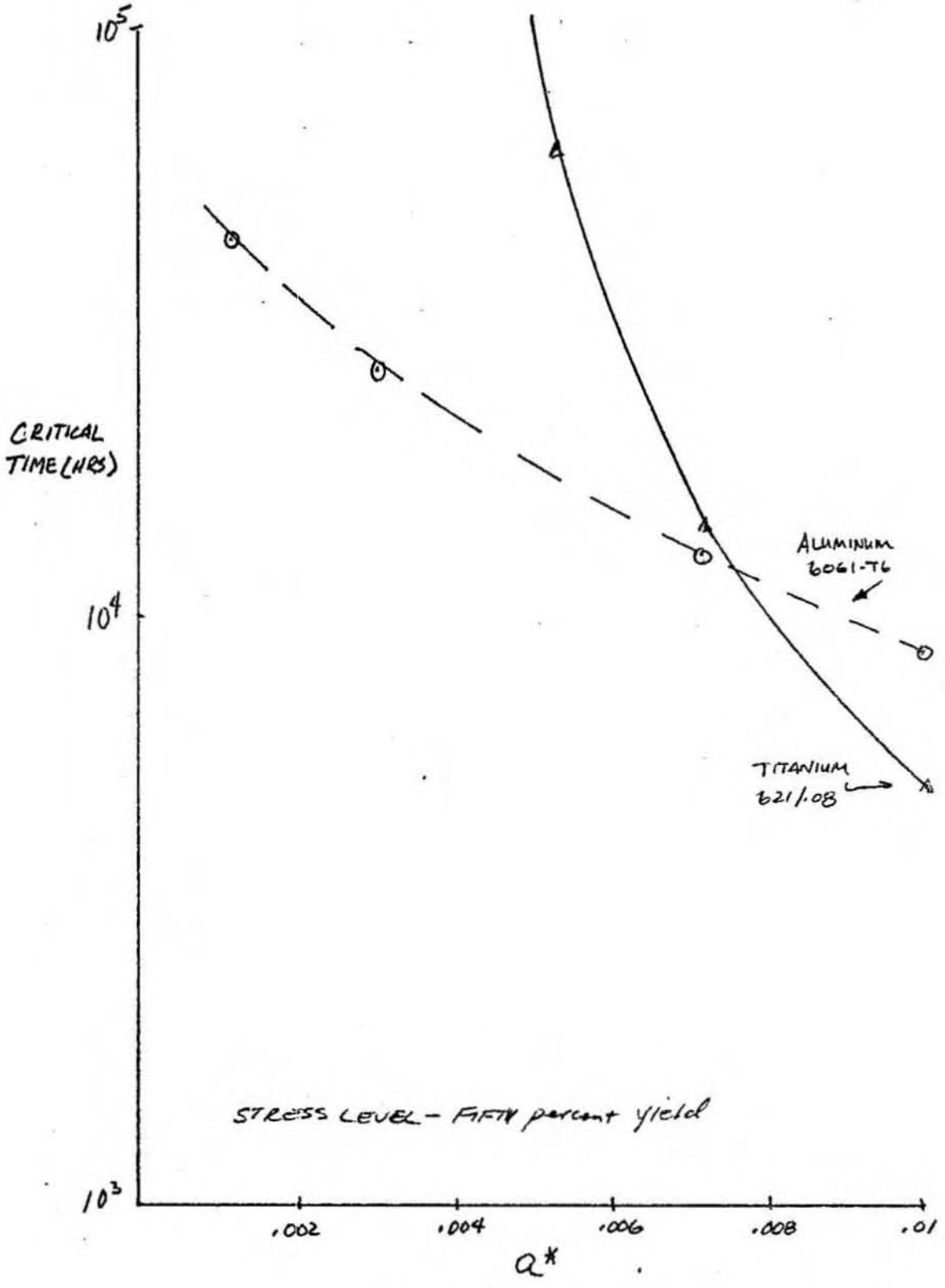
10^5
10^4
10^3
CRITICAL TIME (HRS)
ALUMINUM 6061-T6
TITANIUM 621/.08
STRESS LEVEL - FIFTY percent yield
.002
.004
.006
.008
.01
Q*

FIGURE 22

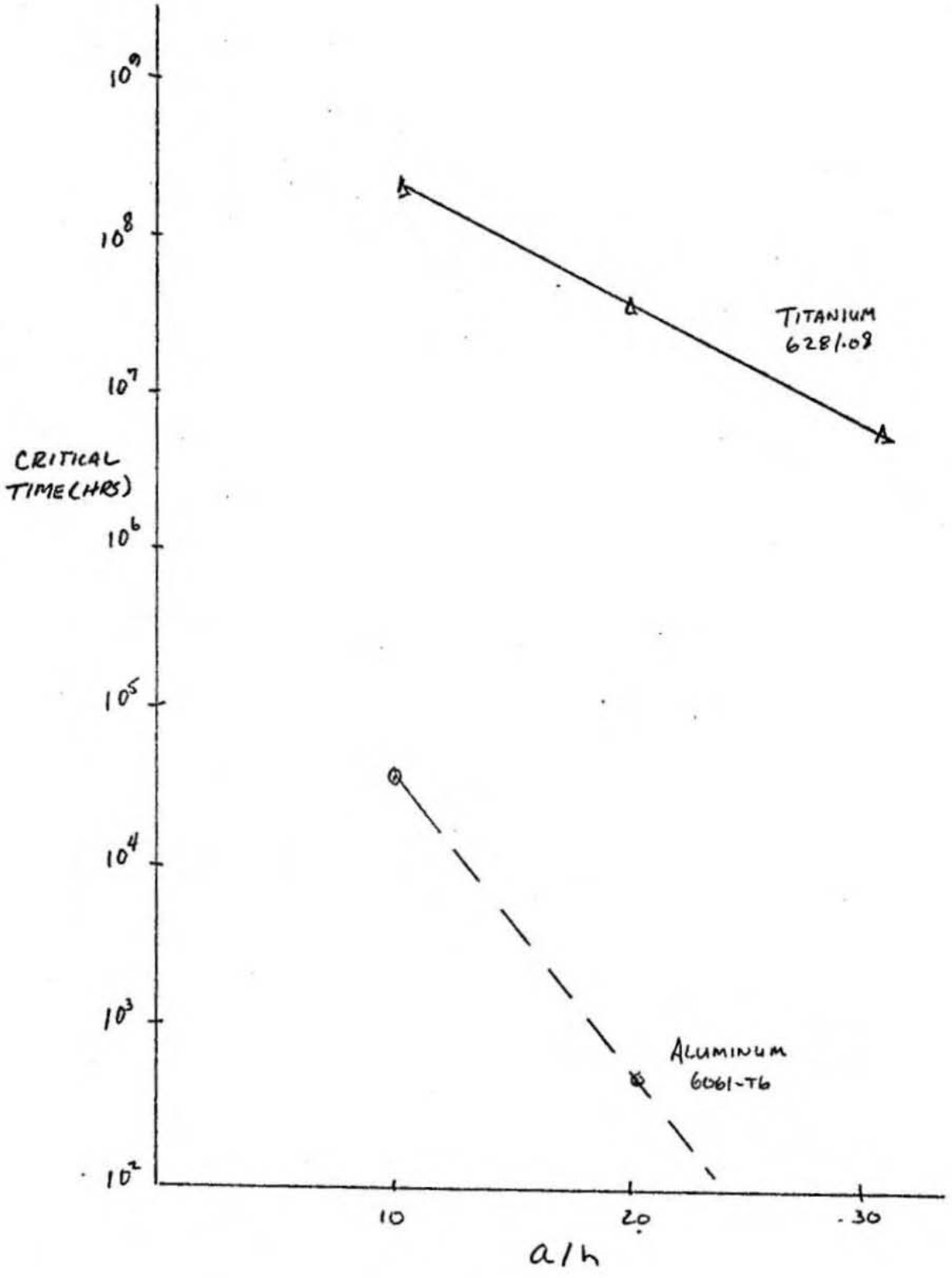
10^9
10^8
10^7
CRITICAL TIME (HRS)
10^6
10^5
10^4
10^3
10^2
TITANIUM 6281.08
ALUMINUM 6061-T6
10
20
30
a/h

FIGURE 23

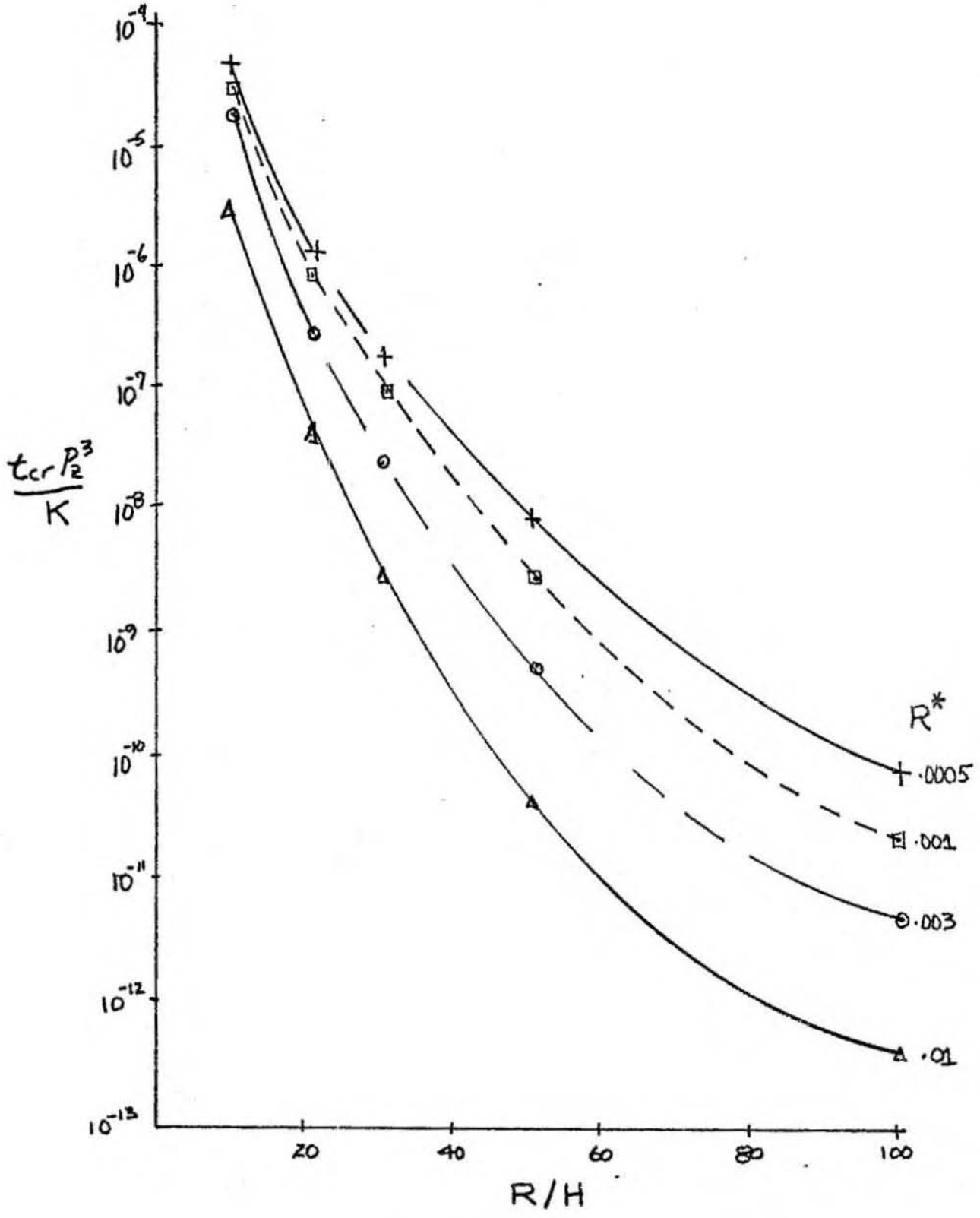
10^{-4}
10^{-5}
10^{-6}
10^{-7}
10^{-8}
10^{-9}
10^{-10}
10^{-11}
10^{-12}
10^{-13}
$\frac{t_{cr} P_2^3}{K}$
20
40
60
80
100
R/H
R*
.0005
.001
.003
.01

FIGURE 24

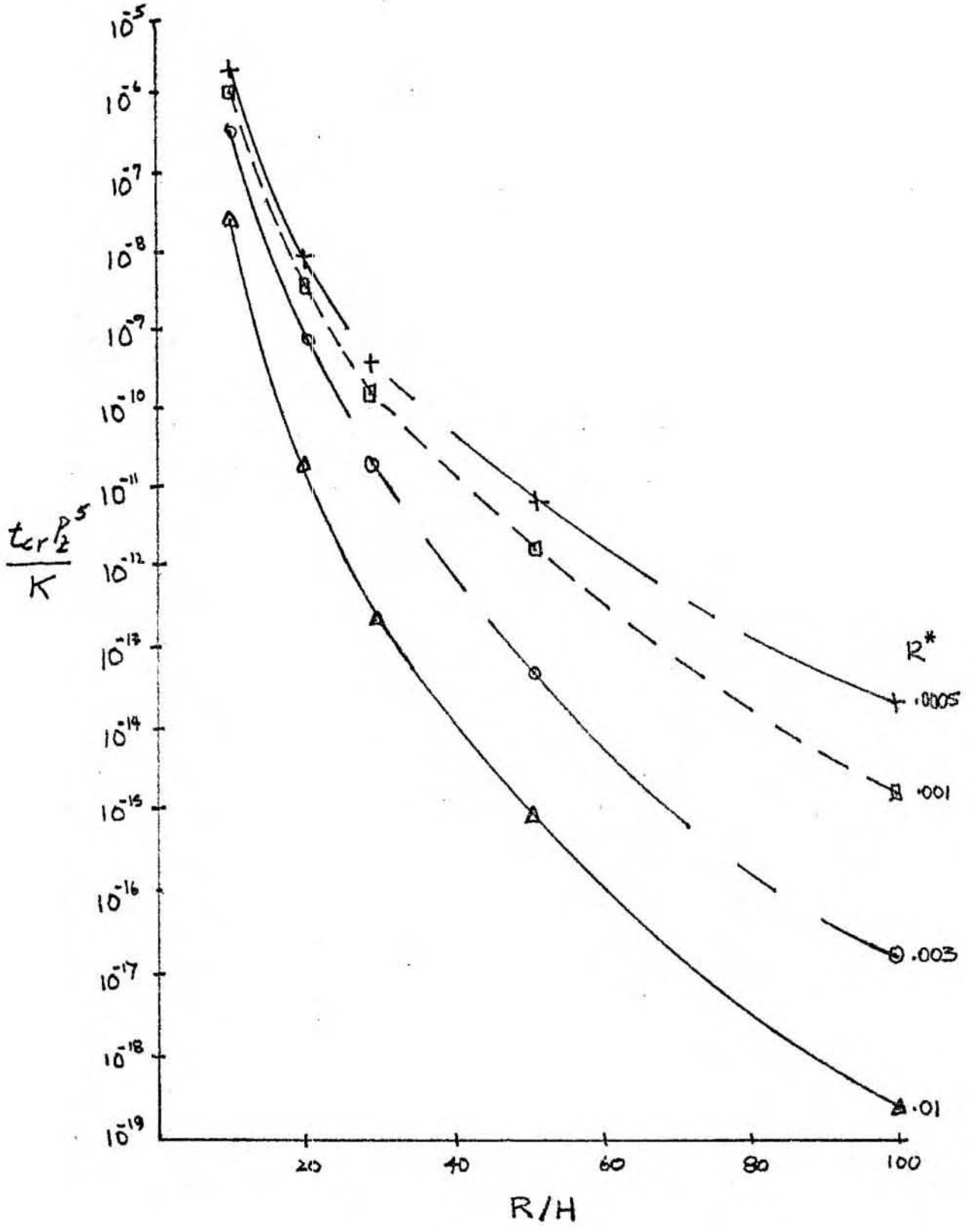
$\frac{t_{cr} P_2^5}{K}$
10^{-5}
10^{-6}
10^{-7}
10^{-8}
10^{-9}
10^{-10}
10^{-11}
10^{-12}
10^{-13}
10^{-14}
10^{-15}
10^{-16}
10^{-17}
10^{-18}
10^{-19}
20
40
60
80
100
R/H
R*
.0005
.001
.003
.01

FIGURE 25

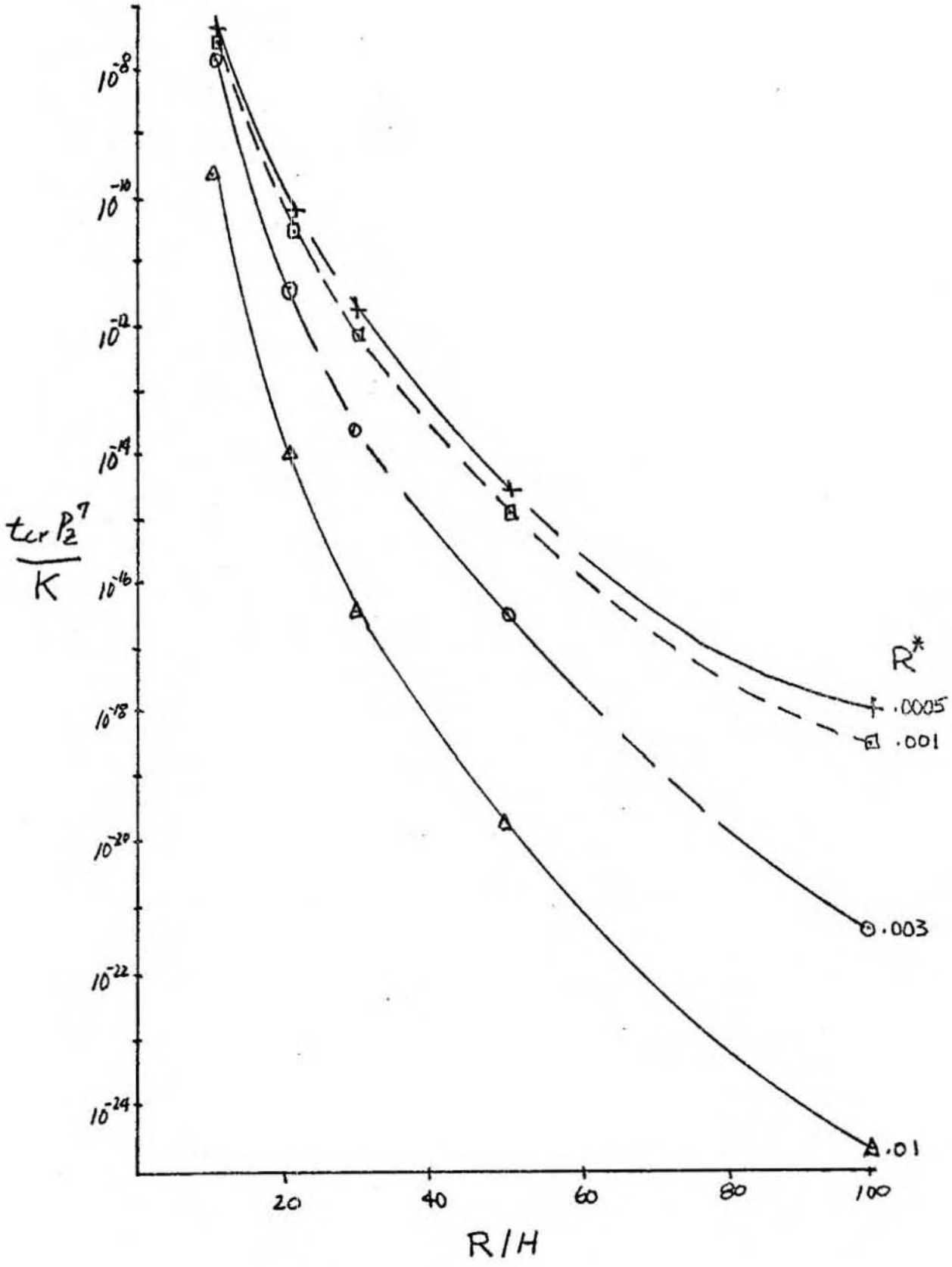
10^{-8}
10^{-10}
10^{-12}
10^{-14}
10^{-16}
10^{-18}
10^{-20}
10^{-22}
10^{-24}
$\frac{t_{cr} P_2^7}{K}$
20
40
60
80
100
R/H
R*
.0005
.001
.003
.01

FIGURE 26

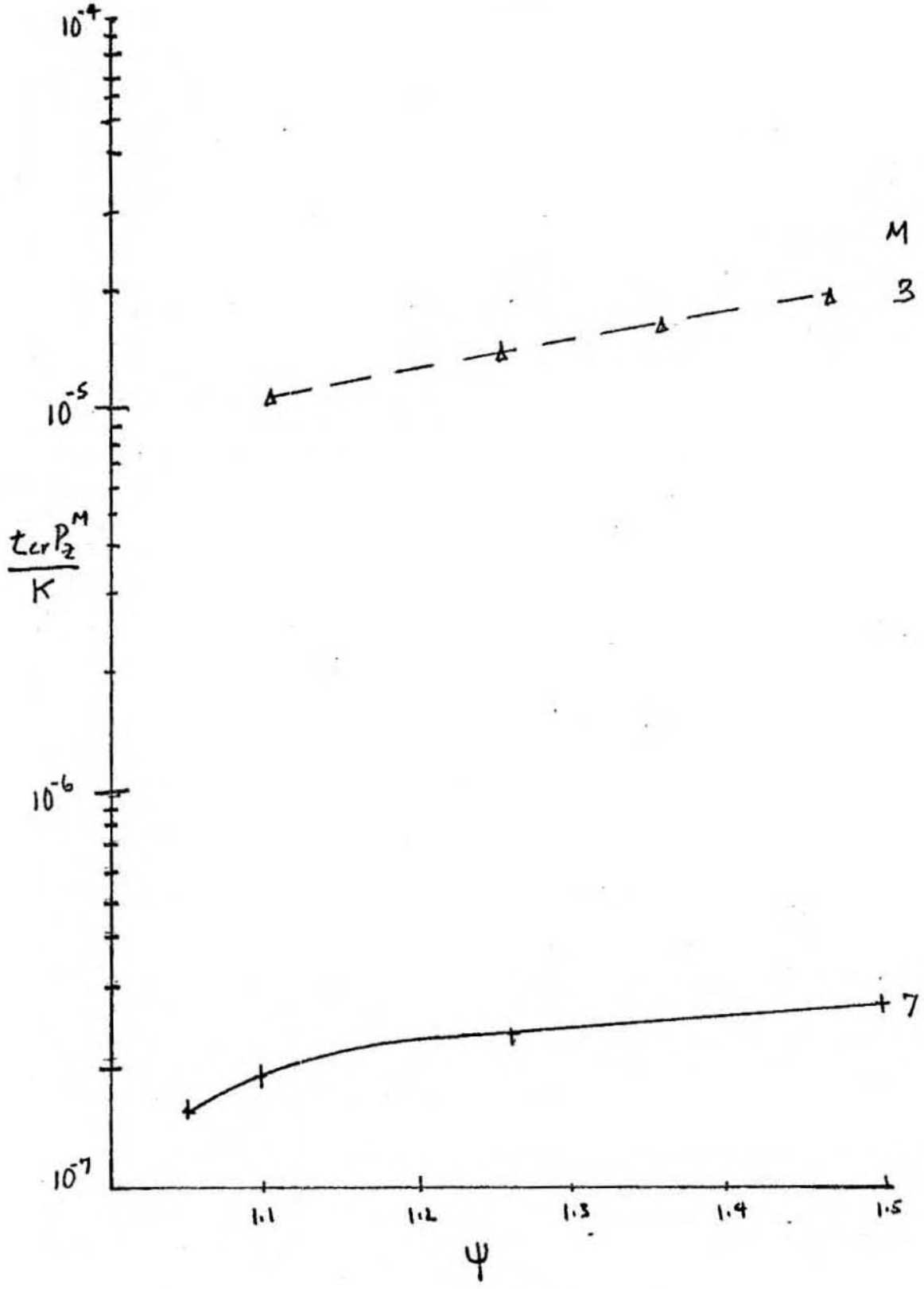

FIGURE 27

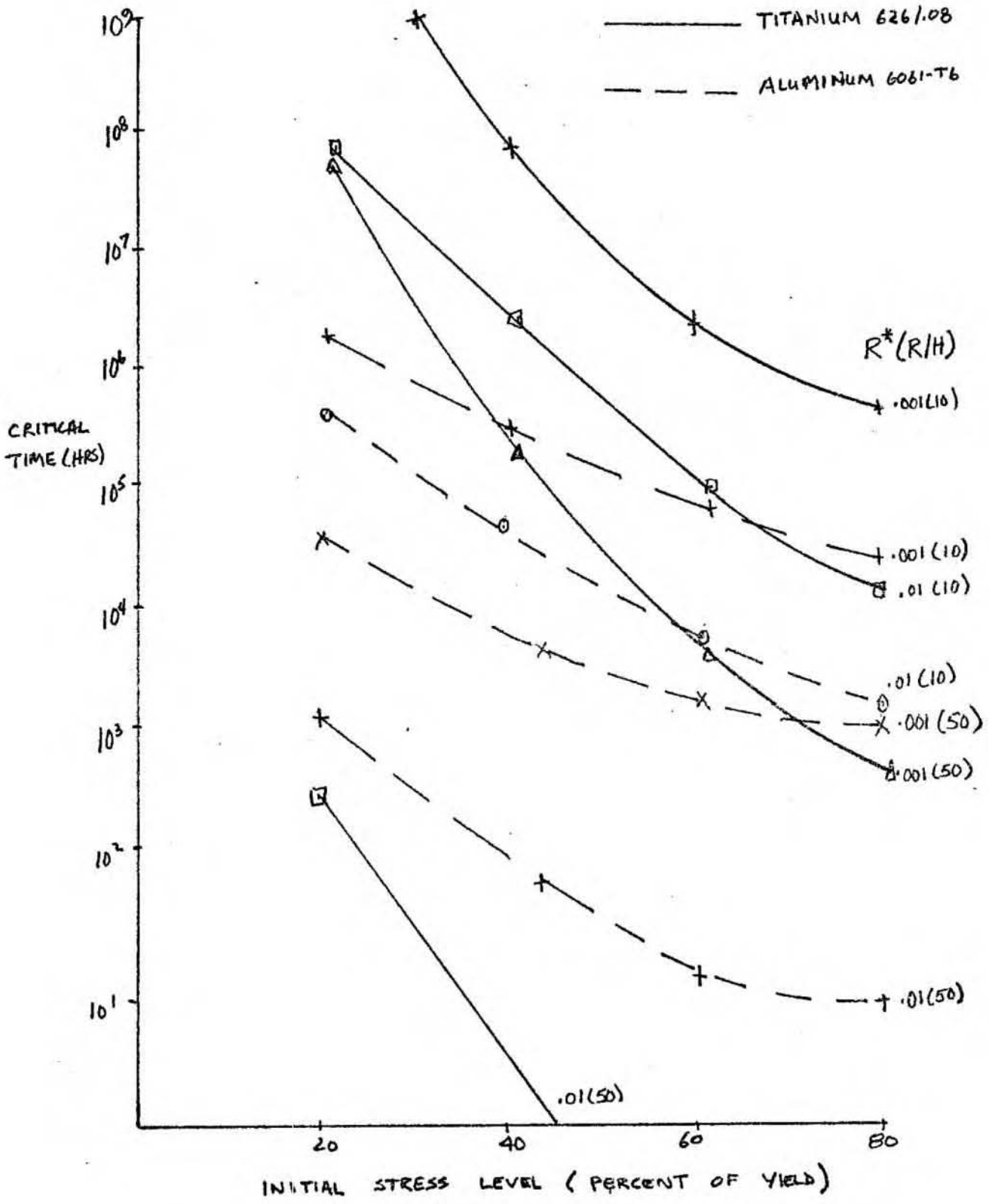
TITANIUM 6261.08
ALUMINUM 6061-T6
R*(R/H)
.001(10)
.001 (10)
.01 (10)
.01 (10)
.001 (50)
.001(50)
.01(50)
.01(50)
CRITICAL TIME (HRS)
10^9
10^8
10^7
10^6
10^5
10^4
10^3
10^2
10^1
20
40
60
80
INITIAL STRESS LEVEL (PERCENT OF YIELD)

FIGURE 28

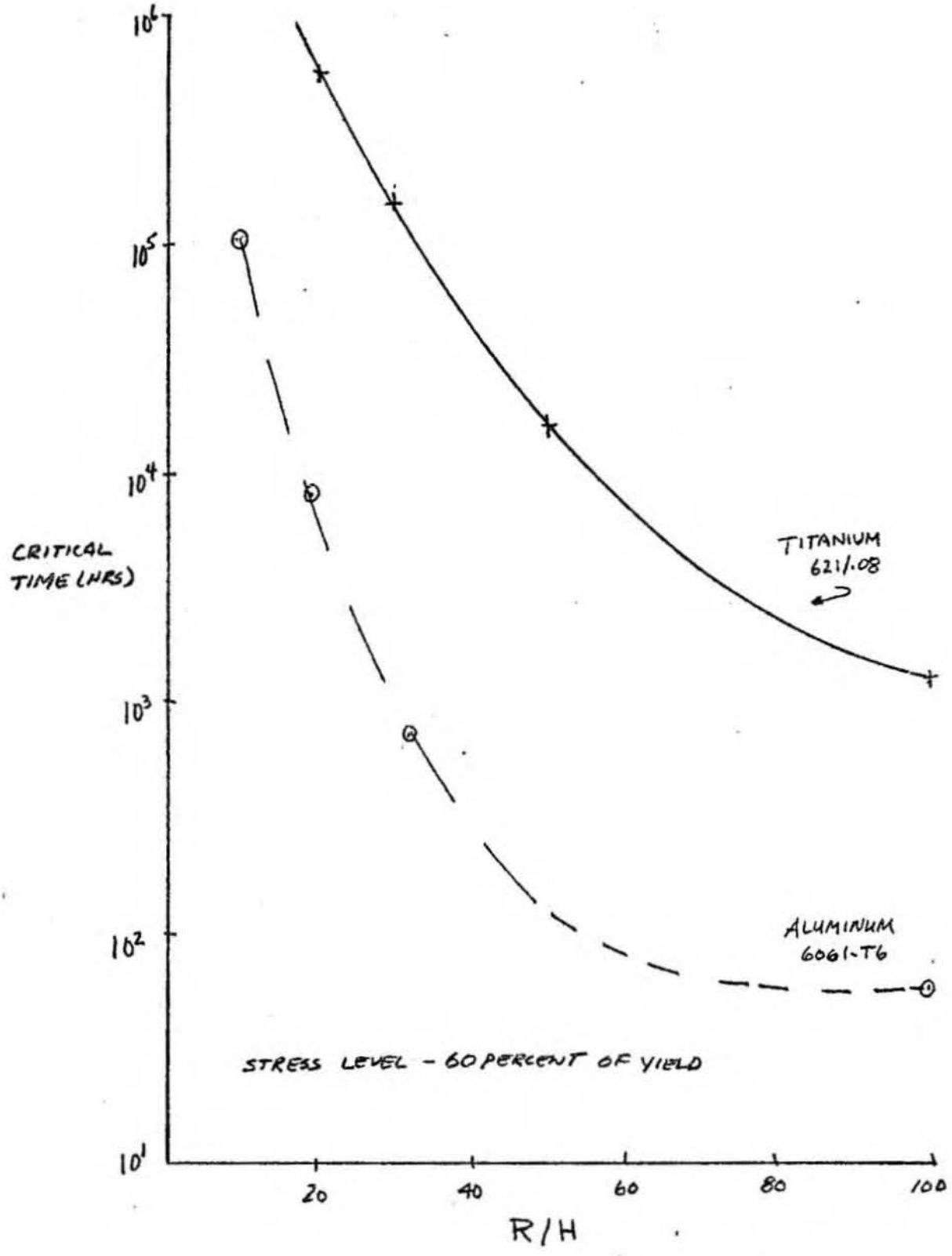
10^6
10^5
10^4
10^3
10^2
10^1
CRITICAL TIME (HRS)
TITANIUM 621/.08
ALUMINUM 6061-T6
STRESS LEVEL - 60 PERCENT OF YIELD
20
40
60
80
100
R/H

FIGURE 29

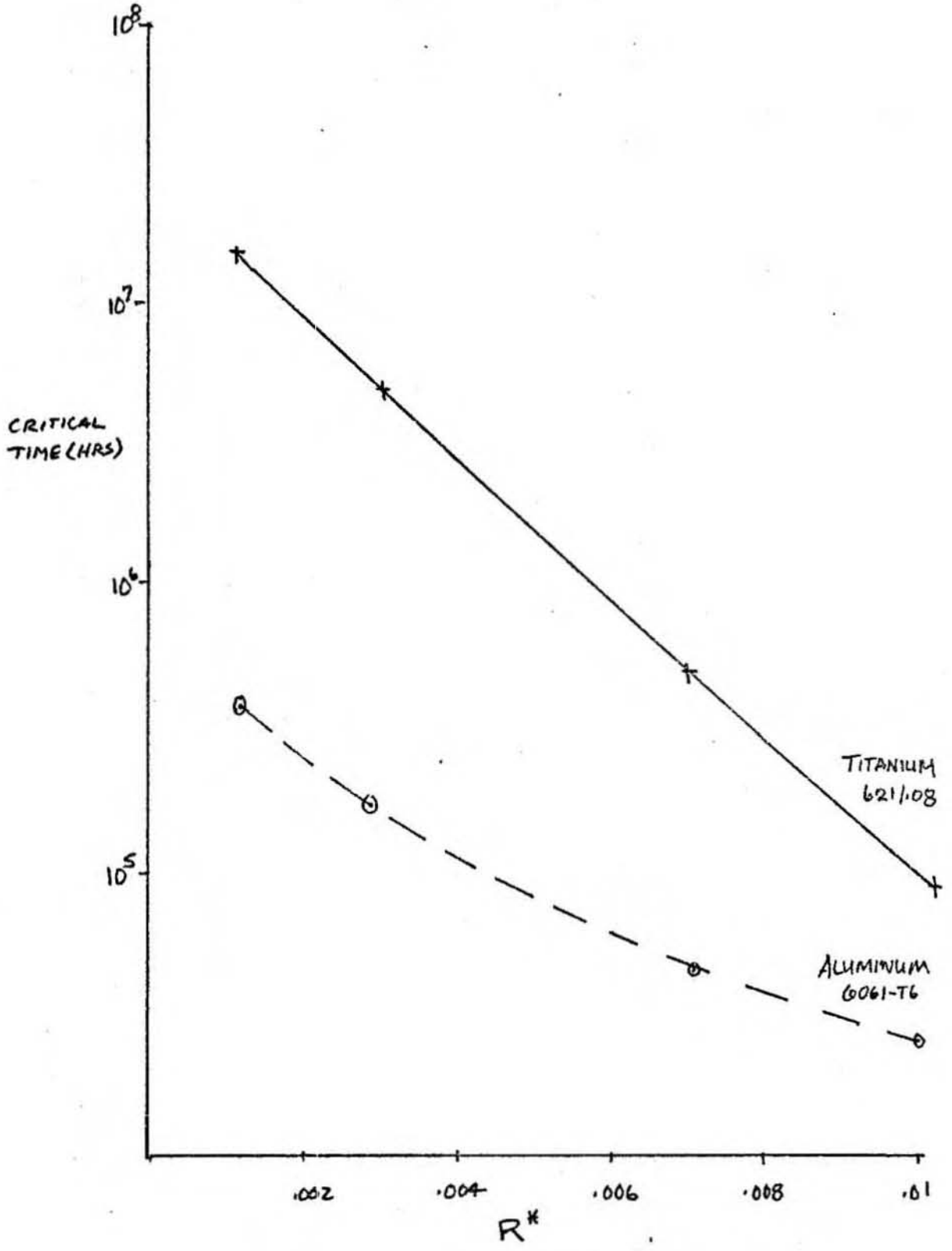
10^8
10^7
10^6
10^5
CRITICAL TIME (HRS)
TITANIUM 6211.08
ALUMINUM 6061-T6
.002
.004
.006
.008
.01
R*

FIGURE 30

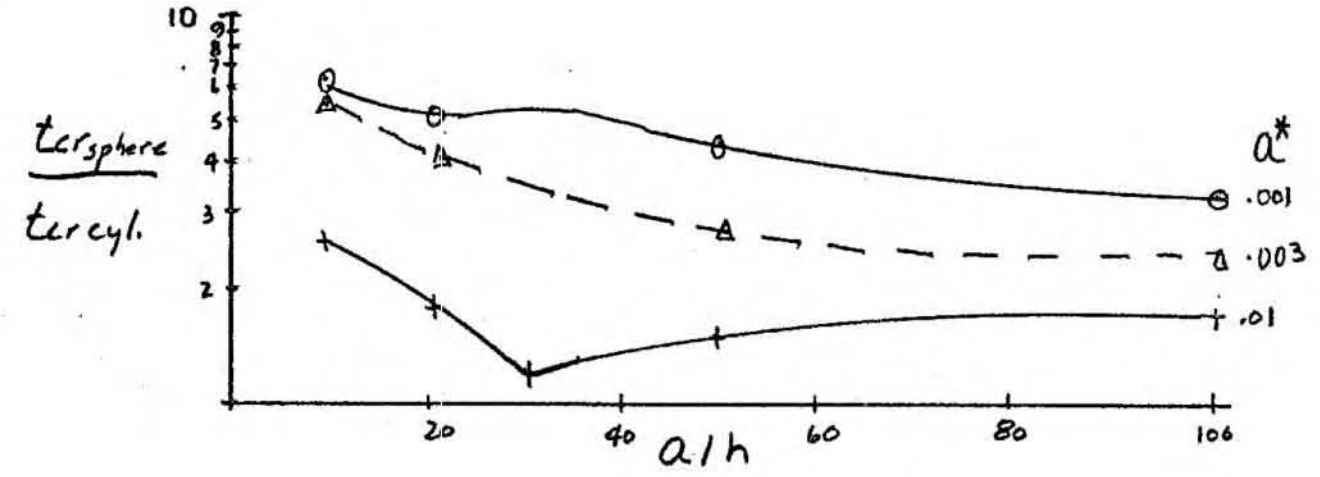

FIGURE 31

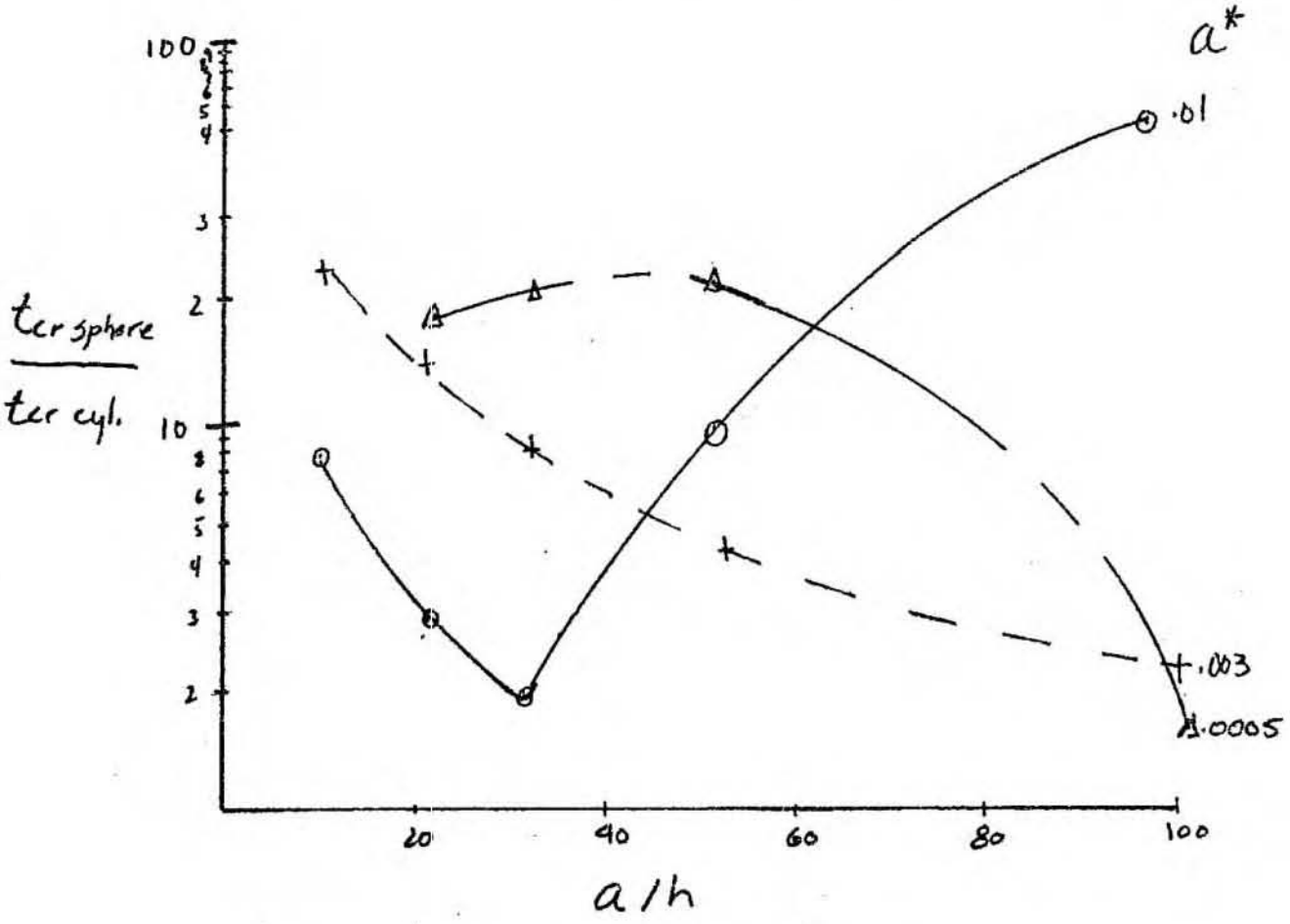

FIGURE 32

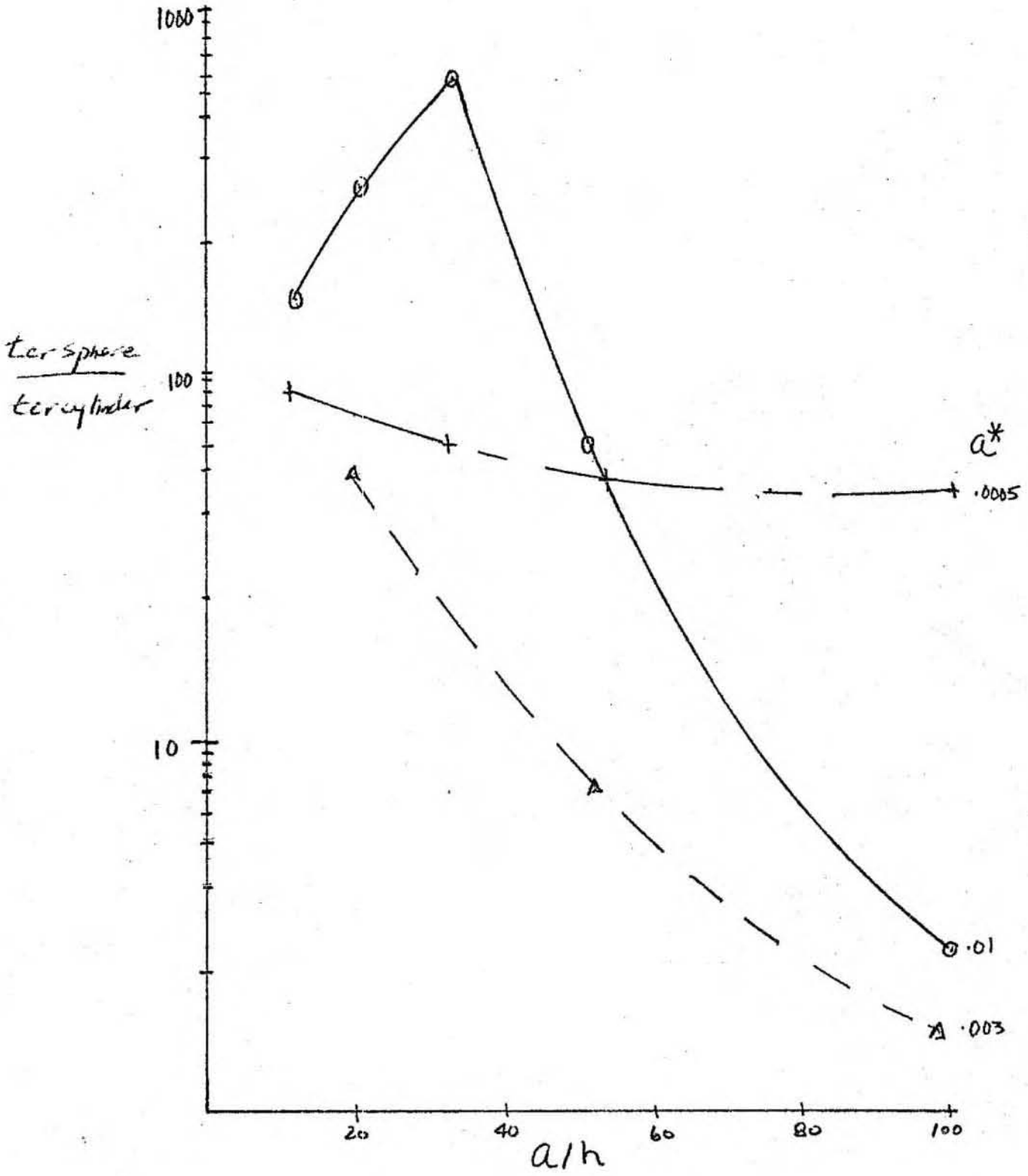
1000
100
10
ter sphere / ter cylinder
a*
.0005
.01
.003
20
40
60
80
100
a/h

FIGURE 33

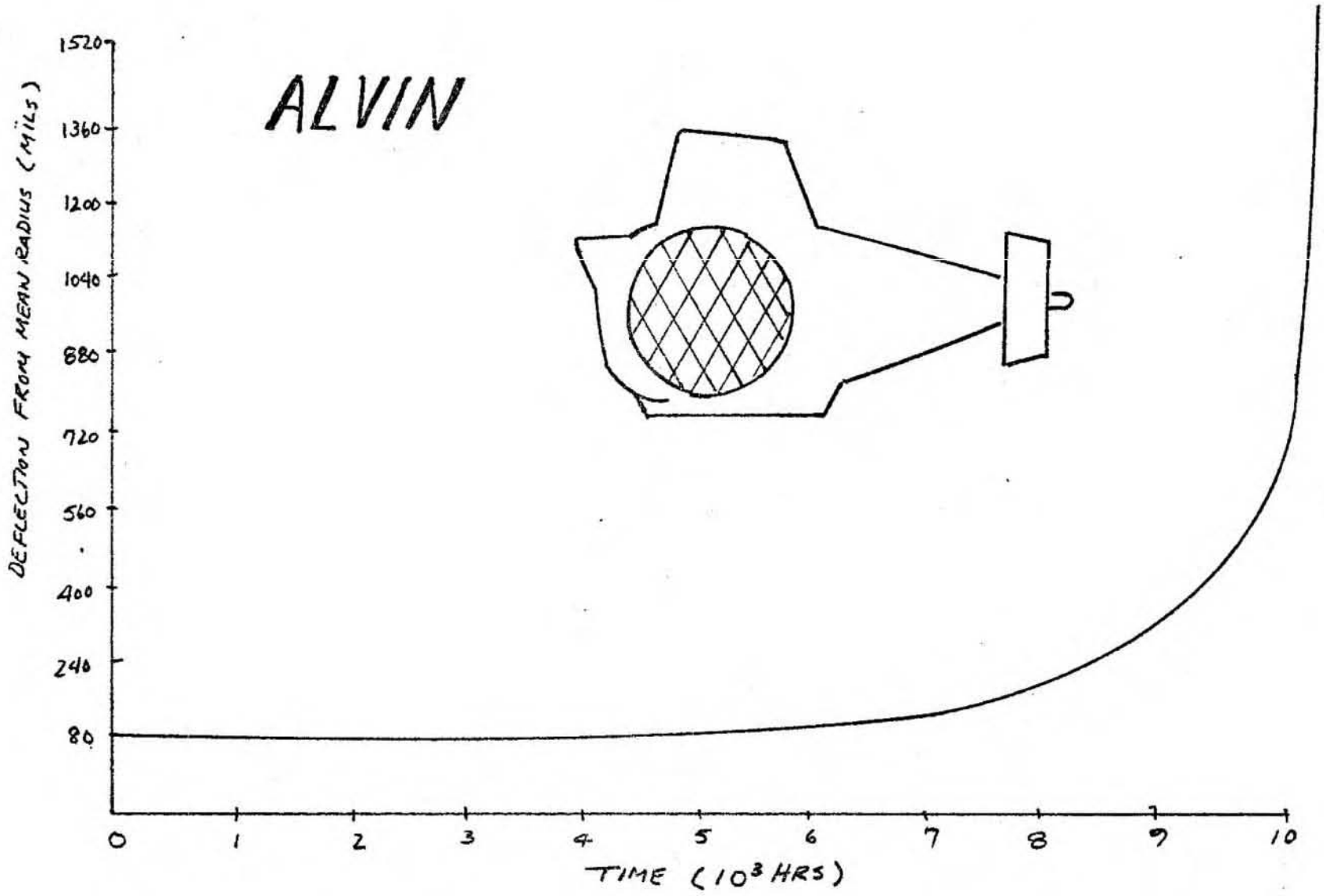
ALVIN
DEFLECTION FROM MEAN RADIUS (MILS)
1520
1360
1200
1040
880
720
560
400
240
80
0
1
2
3
4
5
6
7
8
9
10
TIME (10³ HRS)

FIGURE 34

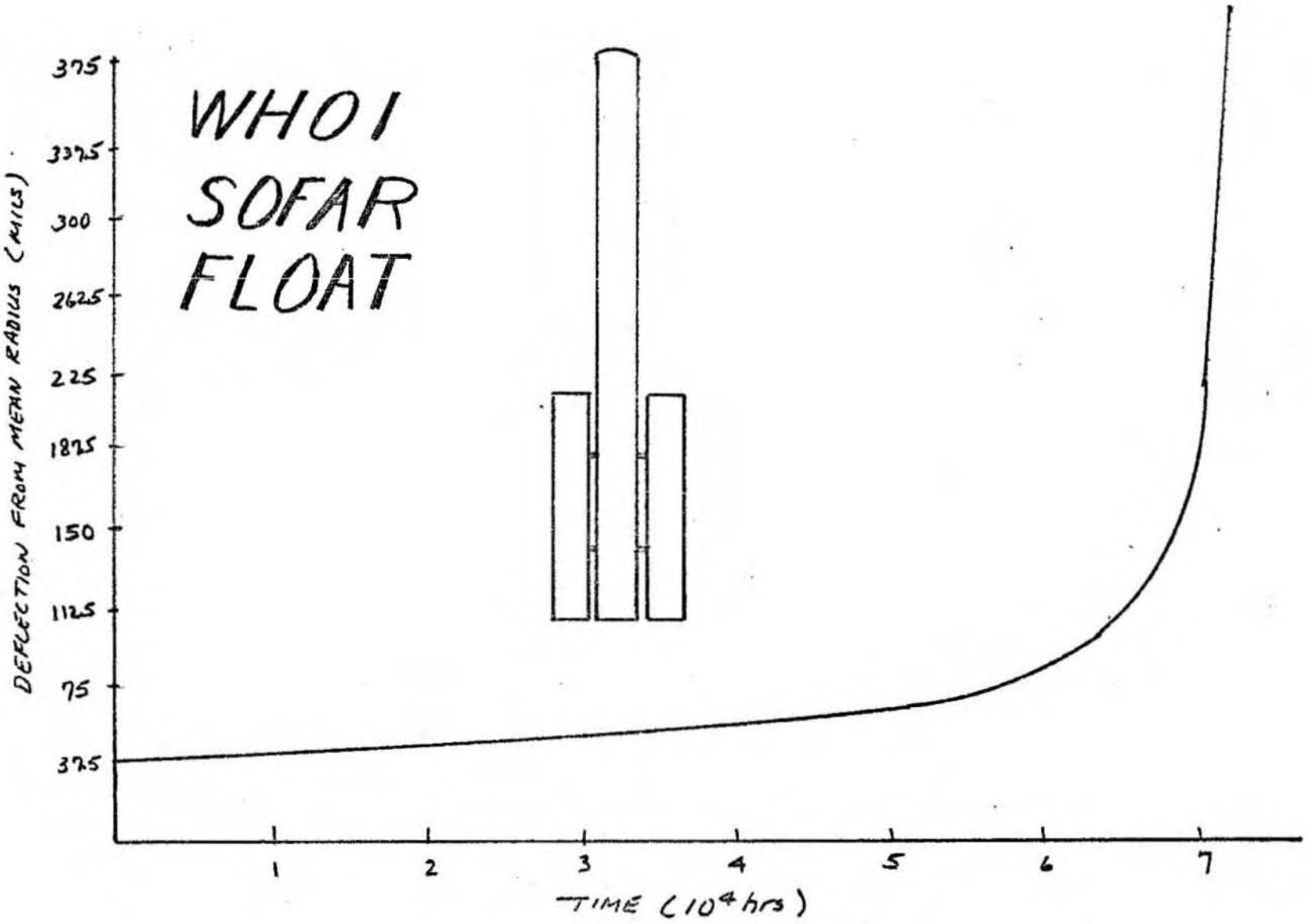
WHOI
SOFAR
FLOAT
DEFLECTION FROM MEAN RADIUS (MILES)
375
3375
300
2625
225
1875
150
1125
75
375
1
2
3
4
5
6
7
TIME (10⁴ hrs)

FIGURE 35

APPENDIX A - COMPUTER UTILIZATION

(i) Computer Program A - Perturbation contour map of the complete sphere.

The following FORTRAN program was developed to compute w'/B_{2m} for a discrete number of points, (5^o by 5^o grid) in a given quadrant. One needs only to input the initial values of ϕ and θ of a given quadrant to receive the x-y position and value of w'/B_{2m} of the before mentioned grid.

$$x = \sin\phi\cos\theta \tag{1}$$

$$y = \cos\phi \tag{2}$$

$$\frac{w'}{B_{2m}} = \sum_{m=0}^{2} P^{m}{}_{2}(\cos\phi)\cos m\theta \tag{3}$$

PERTURBATION CONTOUR MAP OF THE COMPLETE SPHERE

```
      DIMENSION T(19), P(19), W(19), E(19), F(19), P2(3)
      DO 51 M=1, 4
      READ(8,200) U,V
  200 FORMAT (2F10.6)
      DO 52 N=1, 19
      A=N-1
     T (N)=.0174•5.0•A+U
      DO 53 I=1, 19
      B=I-1
      P(I)=.0174•5.0•B+V
      S=SIN(P(I))
      C=COS(P(I))
```

```
      P2(1)=.5*(3.0*C**2.0-1.0)
      P2(2)=3.0*S*C
      P2(3)=3.0*S**2.0
      W(I)=0.0
      DO 54 J=1, 3
      R=J-1
      D=COS(T(N)*R)
      WZ=D*P2(J)
   54 W(I)=W(I)+WZ
      E(I)=S*COS(T(N))
      F(I)=C
      WRITE(5,202) E(I), F(I), W(I)
  202 FORMAT('', 3F15.5)
   53 CONTINUE
   52 CONTINUE
   51 CONTINUE
      END
```

Notation of Program A:

T	θ
P	ϕ
P2(1)	$P_2(\cos\phi)$
P2(2)	$P^1_2(\cos\phi)$
P2(3)	$P^2_2(\cos\phi)$
W	transverse displacement/amplification function
E	x

F	y
U	initial θ value
V	initial ϕ value

(ii) Computer Program B - Growth of the amplification function of the infinitely long cylinder.

This program was devised so that one inputs a/h, a*, M and ψ_2/ψ_1 and equation (4.19) is computed. The output consists of non-dimensional time (τ_c), normalized amplification function (A_2/C_2) and a second non-dimensional time which is a better indicator of real time $\left(\frac{tP_z^m}{k}\right)$

```
      INFINITELY LONG CYLINDER

      MS=3

      JS=15

      DO 1 M=1, MS

      READ(8,100) B,D,E,XM

  100 FORMAT(4F10.6)

      T=0.0

      Y=1.0

      WRITE(5,101) B,D,E,XM

  101 FORMAT('1',5X,'A/H=',F10.6,'A = ',F10.6,10X,'PHI=',F10.6,10X,'M

      1=',F10.6,//,15X,'TIME',20X,'AMP FN',10X,'REAL TIME',//)

      DO 2 J=1,JS
      IF (J.GT.1) GO TO 7
      F=1.0

      GO TO 8

    7 Y=E*X

      F=Y**(XM-1.0)
```

```
      8 S=EXP(T•F/3.0)
        A=E•(1.0+6.0•E•B•D•EXP(T•F/3.0))
        T=3.0/F•ALOG((A-1.0)/(B•D•F•6.0))
        T1=T/(9.0 B••(XM+2.0)•(.866•(1.+6. B D))• •(XM-1.))
        WRITE(5,103) T,A,T1
    103 FORMAT('',7X,F10.3,17X,F10.3,15X,E20.5)
      2 X=Y
      1 CONTINUE
        END
```

The number of input statements is controlled by the variable MS, while the number of cycles for a given set of inputs is controlled by the variable JS.

Notation of Program B:

T	τ_c
A	A_2/C_2
T1	$\frac{tP_z^m}{k}$
Y	ψ
XM	M
B	a/h
D	a*
E	ψ_2/ψ_1

(iii) Computer Program C - Growth of the normalized spherical amplification function with time.

This program is structured exactly as the cylindrical use. Equation (5.1) is computed from the inputs R/H, R* M and ψ_1/ψ_2. The output received is non-dimensional time (τ_s), amplification function (B_{2m}/D_{2m}) and a second non-dimensional time which is a better indicator of real time $\left(\frac{tP_m}{k}\right)$. Again, the number of input statements and number of cycles for a given set of input is controlled by the variables MS, JS respectively.

COMPLETE SPHERE

```
      MS=8
      JS=50
      DO 1 M=1,MS
      READ(8,100) B,D,E,XM
  100 FORMAT(4F10.6)
      T=0.0
      Y=1.0
      WRITE(5,101) B,D,E,XM
  101 FORMAT('1',5X,'A/H=',F10.6,'A= ',F10.6,10X,'PHI=',F10.6,10X,'M
     1=',F10.6,//,15X,'TIME',20X,'AMP FN',10X,'REAL TIME',//)
      DO 2 J=1,JS
      IF (J.GT. 1) GO TO 7
      F=1.0
      GO TO 8
    7 Y=E*X
      F=Y**(XM-1.0)
    8 S=EXP(T*F/3.0)
```

```
      R1=4.5*B*D*F*S
      R2=112.5*(B*D*F*S)** 2.0
      G=E**2.0*(0.5+R1+R2)-0.5
      A=((-R1/S)+((R1/S)** 2.0+4.0*G*R2/S**2.0)** 0.5)/(2.0*R2/S** 2.0)
      T=3.0/F*ALOG(A)
      T1=T*2./(9.*B**(XM+2.)*(1./2.** .5*(.5-4.5*B*D+112.5*(B*D)** 2.))
      0.5*(XM-1.)
      WRITE(5,103) T,A,T1
  103 FORMAT('',7X,F10.3,17X,F10.3,15X,E20.5)
    2 X=Y
    1 CONTINUE
      END
```

Notation of Program C:

T	τ_s
Y	ψ
A	B_{2m}/D_{2m}
T1	$\frac{tP_z^m}{k}$
XM	M
B	R/H
D	R*
E	ψ_2/ψ_1

APPENDIX B - EQUIVALENT NOTATION FROM PAST INVESTIGATIONS

(i) Hoff, N.J., Jahsman, W.E. and Nachbar, W. "A Study of Creep Collapse of a Long Circular Cylindrical Shell Under Uniform External Pressure", J. of Aero Space Science, Vol. 20, No. 10, 1959.

Notation of Paper	Equivalent Notation
α	a^*
$X = \frac{\alpha\bar{R}}{\rho}$	$2a^*(\frac{a}{h})$
$\bar{\tau}' = (\frac{nk}{3})(\frac{P\bar{R}}{A\lambda})^n(\frac{R}{\rho})^{-2}$	$\frac{1}{k}(\frac{Pa}{h})^m(\frac{2a}{h})^2$
$t_{cr} = \frac{1}{2}\log(1 + \frac{9}{2}/X_0^2)$	$\frac{\log\left(1 + \frac{9}{8}(\frac{h}{a})\frac{1}{a^*}^2\right)}{2\tau^{-1}}$
A	h/l
$\frac{k}{\lambda^n}$	K
n	M

where $\rho = \frac{h}{2}$ radius of gyration

$\bar{R}$ = average radius

α = shape factor

X = weighted shape factor

(ii) Berman, I., Chern, J.M. and Gupta, G.D. "A Parametric Study of Elastic-Plastic Creep Buckling of a Thin Cylindrical Shell", J. of Pressure Vessel Technology, August 1974.

Notation of Paper	Equivalent Notation
$\delta_0 = \frac{w^+ - w-}{2a}$	a*
a	a
h	h
q	P_z

(iii) Samuelson, L.A. "Creep Buckling of a Cylindrical Shell Under Non-Uniform External Loads", Int. J. Solids Structures, Vol. 6, 1970.

Notation of Paper	Equivalent Notation
ϕ	θ
B	K
R	a

The remainder of the notation is consistent.

APPENDIX C - CREEP CONSTANTS OF COMMON OCEAN ENGINEERING MATERIALS

(i) Titanium 621/.08 (Ti-6AL-1Ta-.8 Mo)

(σ_y = 120 ksi)

Chu (1972) found that the creep data of Ti 621/.08 at room temperature can be represented as

$$\varepsilon = \left(\frac{\sigma}{103.55}\right)^{13.890} t^{0.183} \qquad (1)$$

where

ε = creep strain, %

σ = stress, ksi

t = time, hours

If equation (1) is plotted at a given stress level, it is discovered that after an initial period of primary creep, the non-linear viscous behavior of secondary creep becomes apparent

as example: for σ = 103.55 ksi, $\dot{\varepsilon}$ = .1071 μin/in/hr.

By calculating the constant strain rates for a number of stress levels the following power law emerges

$$\sigma^7 = 8.3 \times 10^{40} \dot{\varepsilon} \qquad (2)$$

where σ = stress, psi

ε = creep strain rate, μin/in/hr

(ii) Titanium 6-4 (6AL-4V)

(σ_y = 135 ksi)

Chu has found the emperical equation for titanium 6-4 at room temperature, but has not as yet published it.

(iii) Aluminum 6061-T6 (wrought alloy - magnesium and silicon alloy solution treated and artifically aged)

(σ_y = 40 ksi)

The author conducted a number of tests in which cylindrical columns of Aluminum 6061-T6 were loaded with a uniform load in compression by a lever system. Deformation was measured using two uniaxial strain gages mounted on opposite sides of the column in a series configuration. The series configuration allowed bending effects to be internally cancelled out of the readings by the gages.

The Aluminum 6061-T6 was found to abhor to a cubic law at room temperature

$$\sigma^3 = 4 \times 10^{19} \dot{\varepsilon} \qquad (3)$$

where

σ = stress, psi

$\dot{\varepsilon}$ = creep strain rate, μin/in/hr.

All tests were conducted at high load levels, greater than 65 percent of yield, at room temperature. The strain rates computed are

σ(psi)	$\dot{\varepsilon}$(μin/in/hr)
34670	0.8504
33750	0.8420
31450	0.7768
27615	0.0569

(iv) Stainless Steel 304 (Austentic)

Berman (1974) expresses the secondary creep behavior of Stainless Steel 304 at 1050°F as

$$\sigma^{5.6789} = 8.035 \times 10^{28} \dot{\varepsilon}$$

where

σ = stress, psi

$\dot{\varepsilon}$ = creep strain, μin/in/hr.